General Disclaimer

One or more of the Following Statements may affect this Document

- This document has been reproduced from the best copy furnished by the organizational source. It is being released in the interest of making available as much information as possible.

- This document may contain data, which exceeds the sheet parameters. It was furnished in this condition by the organizational source and is the best copy available.

- This document may contain tone-on-tone or color graphs, charts and/or pictures, which have been reproduced in black and white.

- This document is paginated as submitted by the original source.

- Portions of this document are not fully legible due to the historical nature of some of the material. However, it is the best reproduction available from the original submission.

Produced by the NASA Center for Aerospace Information (CASI)

AN EVALUATION OF RANDOM ANALYSIS METHODS

FOR THE DETERMINATION OF PANEL DAMPING

By Waman V. Bhat and John F. Wilby

Distribution of this report is provided in the interest of information exchange. Responsibility for the contents resides in the authors or organization that prepared it.
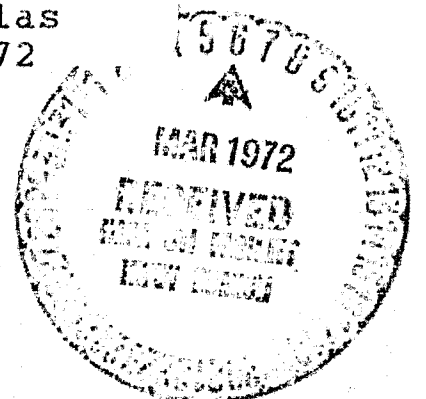
Prepared under contract NAS 2-6285
The Boeing Company
Seattle, Washington

for

NATIONAL AERONAUTICS AND SPACE ADMINISTRATION

AN EVALUATION OF RANDOM ANALYSIS METHODS

FOR THE DETERMINATION OF PANEL DAMPING

By Waman V. Bhat and John F. Wilby

Distribution of this report is provided in the interest of
information exchange. Responsibility for the contents
resides in the authors or organization that prepared it.

CONTENTS

CONTENTS—Concluded

AN EVALUATION OF RANDOM ANALYSIS METHODS

FOR THE DETERMINATION OF PANEL DAMPING

By Waman V. Bhat and John F. Wilby
The Boeing Company, Seattle, Washington

1.0 SUMMARY

An analytical study is made of steady-state and non-steady-state methods for the measurement of panel damping. Particular emphasis is placed on the use of random process techniques in conjunction with digital data reduction methods. The steady-state methods considered use the response power spectral density, response autocorrelation, excitation-response cross-power spectral density, or single-sided Fourier transform (SSFT) of the response autocorrelation function. Non-steady-state methods are associated mainly with the use of rapid frequency sweep excitation. Problems associated with the practical application of each method are evaluated with specific reference to the case of a panel exposed to a turbulent airflow, and two methods, the power spectral density and the single-sided Fourier transform methods, are selected as being the most suitable. These two methods are demonstrated experimentally, and it is shown that the power spectral density method is satisfactory under most conditions, provided that appropriate corrections are applied to account for filter bandwidth and background noise errors. Thus, the response power spectral density method is recommended for the measurement of the damping of panels exposed to a moving airflow.

2.0 INTRODUCTION

The amplitude of vibration of a structural system exposed to an exciting force is controlled, to a large extent, by the total damping present in the system. When predicting the response of a structure to a given excitation it is necessary to know the damping to a sufficient degree of accuracy. Equally important, when measuring the vibration of a model or full-scale structure under certain excitation conditions, measurements of the panel damping are required if the experimental data are to be extrapolated to other conditions with reasonable reliability.

Techniques for the measurement of the damping of a structure have been developed over the years, but, until recently, the methods have been limited to the use of steady-state, discrete frequency excitation (e.g., refs. 1 through 4). For a structural system whose damping does not vary with operating condition or environment, and where measurements can be made under specially controlled test conditions, the discrete frequency methods are usually adequate. However, when the damping is dependent on operating condition, for example where flutter or acoustic damping is important, alternative techniques for damping measurement have to be used. In response to this need, techniques using steady-state random excitation and transient excitation have been developed in recent years. These alternative methods can be used when the structure is exposed to random excitation or is exposed to the operating environment for only a short time or when noise interference occurs in the measured excitation or response.

The case of a structure exposed to a moving airstream is an important example of a test situation where the steady-state, discrete frequency methods are unreliable. It was for this reason that the present study of damping measurement methods was undertaken. Results of the study, which considers steady-state random excitation and transient excitation methods, are contained in this report. Essentially, the discussion can be separated into two parts, the first of which is an analytical survey of available methods. The second part describes an experimental demonstration of two techniques that, on the basis of the analytical study, are judged to be the most suitable for the application under consideration, namely, the measurement of panel damping in the presence of a moving airstream. Throughout the discussion, emphasis is placed on the accuracy and reliability of each method in practical situations. Digital techniques for data reduction will be required for several of the damping measurement methods. Therefore, special attention is given to problems associated with these digital techniques.

As a final result of the study, techniques will be recommended for the measurement of panel damping in the presence of an airflow. In principle, the methods will be applicable to structures of greater complexity than a simple panel in a wind tunnel wall. However, it may be necessary to assume that there is some knowledge of the natural frequencies and mode shapes of the system so that the measuring tranducers can be placed at optimum locations.

The program was carried out at The Boeing Company, Seattle, Washington and was monitored by Dr. Wei J. Chyu, NASA Ames Research Center.

SYMBOLS

A	area of structure, for panel $A = L_1 L_3$
A, B	see equation (29)
A_α, A_β	defined by equations (43) and (83)
a_1, b_1	defined by equation (84)
C	Viscous damping rate
$C_p(\underline{x}', \underline{x}'', \omega)$	real part of cross-power spectral density function $S_p(\underline{x}', \underline{x}'', \omega)$
$C_{p1}(\underline{x}', \underline{x}'', \omega)$	real part of cross-power spectral density function $S_{p1}(\underline{x}', \underline{x}'', \omega)$
C_α	generalized damping coefficient in α^{th} mode
$C_{\alpha e}$	equivalent viscous damping coefficient in terms of the hysteretic damping, $(\kappa_\alpha \nu_\alpha)/\omega$
D	flexural rigidity of a plate
$D(\tau)$	weighting function, lag window
$D_{\alpha\beta}, D_{\alpha\beta}^r, D_{\alpha\beta}^i$	see equation (39)
$F_w(\omega)$	single-sided Fourier transform of the response autocorrelation function, $R_w(\tau)$, defined by equation (71)
f	frequency
f_F	center frequency of analyzing filter
$f_\alpha \equiv f_{m,n}$	natural frequency of mode ($\alpha \equiv m,n$)
f_{max}	upper frequency of interest
$\Delta f_\alpha, \Delta f_A$	ideal half-power bandwidth of a resonance peak
Δf_F	filter bandwidth at the half-power point
Δf_M	measured bandwidth of a resonance peak
$\Delta f'$	frequency interval at which frequency-dependent functions are calculated, $1/\Delta T'$
$|H|$	modulus of vector H
$H_\alpha(\omega)$	complex frequency response function for mode of order α, defined by equations (4) and (5)

3

$H_\alpha^*(\omega)$	complex conjugate of $H_\alpha(\omega)$
$H_\alpha(\omega, t)$	time-varying frequency response function
$\overline{\|H_\alpha(\omega)\|^2}$	time-averaged square of frequency response function
$h_\alpha(t)$, $h_\alpha(\tau)$	impulse response function for mode of order α, defined by equation (5)
$I_{\alpha\beta}(\omega)$	defined by equation (18)
i	$\sqrt{-1}$
j	positive integer
$J_{\alpha\alpha}(\omega)$	displacement joint acceptance for mode α
$J_{\alpha\beta}(\omega)$	displacement cross acceptance for modes α, β
$K, K', K'', K_\alpha, K_\beta$	miscellaneous constants or functions, defined in text
k	time constant in $\omega'(t)$
L	number of degrees of freedom in section 4.1.7
L	number of data points used for calculating finite discrete transforms, 2^j
L_1	panel length in x_1 direction
L_3	panel length in x_3 direction
L_α	generalized external force in mode of order α
M	mass per unit area
M_α	generalized mass in mode of order α
m	mode order in x_1 direction denoting the number of modal half-wavelengths
N	number of measurement locations in section 4.1.7
N	number of data points
n	mode order in x_3 direction, denoting the number of modal half-wavelengths
$n(t)$	noise in response (see fig. 1)
n	ratio of ideal bandwidth of resonance peak to filter bandwidth, $\Delta f_\alpha / \Delta f_F$

$P(\underline{x},\omega)$	Fourier transform of $p(\underline{x},t)$, defined by equation (10)
$P^*(\underline{x},\omega)$	complex conjugate of $P(\underline{x},\omega)$
$P_1(\omega)$, $P_2(\omega)$	Fourier transform of $p_1(t)$ and $p_2(t)$, respectively
$P(\omega)$	Fourier transform of $p(t)$
$p = p(\underline{x}, t)$	pressure at point $\underline{x}$ and time t
$p_1(\underline{x}',t)$, $p_2(\underline{x}'',t)$	excitation and noise in excitation (see fig. 1)
$p_n = p(n,\Delta\tau)$	pressure at time $n \cdot \Delta\tau$
$Q_p(\underline{x}', \underline{x}'', \omega)$	complex part of $S_p^*(\underline{x}', \underline{x}'', \omega)$
$Q_{p1}(\underline{x}', \underline{x}'', \omega)$	complex part of $S_{p1}^*(\underline{x}', \underline{x}'', \omega)$
$Q_\alpha(\omega)$	Fourier transform of $q_\alpha(t)$
$q_\alpha(t)$	generalized coordinate of mode of order α
$R(\tau)$	autocorrelation function
$R_p(\underline{x}', \underline{x}'', \tau)$	excitation pressure cross-correlation function
$R_w(\underline{x}, \tau)$	displacement autocorrelation function
$R_w(\tau;\Delta\omega)$	narrow band autocorrelation function
R_{p1}, R_{p2}	defined by equation (49)
$R_w(\tau)$, $R_n(\tau)$	defined by equation (51)
$R_{w,p}(\underline{x}, \underline{x}', \tau)$	cross-correlation function, equation (62)
$R_n(n, \Delta\tau)$	autocorrelation at time delay $n \cdot \Delta\tau$
r	mode order in x_1 direction
S_α^r, S_α^i	defined by equation (39)
S_n	white noise power spectral density
$S(\omega)$	power spectral density function
$S_p(\omega)$	power spectral density function of excitation $p(\underline{x}, t)$
$S_{p1}(\omega)$, $S_{p2}(\omega)$	power spectral density functions of excitations $p_1(\underline{x}, t)$ and $p_2(\underline{x}, t)$, respectively

$S_w(\underline{x}, \omega)$	power spectral density function of the displacement $w(\underline{x}, t)$
$S_w(\underline{x}, \omega)_\alpha$	displacement power spectral density function in mode α
$S_{w,p}(\underline{x}, \underline{x}', \omega)$	cross-power spectral density function relating the excitation $p(\underline{x}', t)$ and response $w(\underline{x}, t)$, equations (54) and (55)
$S_{w,p}(\underline{x}, \underline{x}', \omega)_\alpha$	contribution of α mode to $S_{w,p}(\underline{x}, \underline{x}', \omega)$
$S_k(k, \Delta f_F)$	power spectral density at a frequency of $k \cdot \Delta f_F$
s	digitizing or sampling rate, $1/\Delta\tau$
s	mode order in x_3 direction
ds/df	rate of change of arc length with frequency
t, T	time parameters
T	total sample length
ΔT	length of sample subinterval, $N \cdot \Delta\tau$
$\Delta T'$	length of subinterval after addition of zeros
$U_\alpha(\omega)$	Fourier transform of $L_\alpha(t)$
V	number of subspectra, $T/\Delta T$
$W(\underline{x}, \omega)$	Fourier transform of the displacement $w(\underline{x}, t)$
$w(\underline{x}, t)$	displacement at point $\underline{x}$, and time t
X_a	see equation (35)
$\underline{x} \equiv (x_1, x_3)$	distance vector in (x_1, x_3) plane
$\alpha \equiv (m, n)$	two-dimensional mode order
$\beta \equiv (r, s)$	two-dimensional mode order
β_{pn}	defined by equation (34)
β_{pn}^*	complex conjugate of β_{pn}
$\Gamma_{mn}(\omega)$	defined by equation (31)
$\Gamma_{w,p}(\underline{x}, \underline{x}', \omega)$	nondimensional cross-power spectral density function relating the excitation and response, defined by equation (56)
δ_{pq}	1 for $p = q$, 0 for $p \neq q$

$\delta(\underline{x}' - \underline{x}_0)$	delta function 1 for $\underline{x}' = \underline{x}_0$, 0 for $\underline{x}' \neq \underline{x}_0$
$\delta(\tau)$	delta function, 1 for $\tau = 0$, 0 for $\tau \neq 0$
ϵ	normalized standard error, equation (92)
ϵ_1	error in the frequency response function due to the drift in natural frequency
ζ_α	viscous damping factor in mode of order α
$\zeta_{\alpha e}$	equivalent viscous damping factor
η	see equation (25)
η_{pp}	sum of response power spectral densities at all measuring locations due to mode of order p, defined by equation (36)
$\theta_{\alpha\alpha}, \theta_{\alpha\beta}$	see equation (39)
κ	stiffness
κ_α	stiffness in the mode of order α
λ_{pi}	unitary matrix, defined by equation (32)
λ_{pi}^*	complex conjugate of λ_{pi}
$\mu(\underline{x})$	panel mass per unit area
ν_α	hysteretic damping factor for mode of order α
ρ	radius of curvature of the cross-power spectral density curve
σ	ratio of background noise power spectral density to the true response power spectral density at resonance
τ	time delay
τ_m	maximum time delay in autocorrelation function
$\Delta\tau$	sampling interval, $1/s$
$\Phi(\omega)$	spectral window, filter frequency response function
$\phi(\tau)$	time-varying phase angle
$\Psi(n)$	defined by equation (69)
$\psi_\alpha(\underline{x}), \psi_\beta(\underline{x})$	panel mode shapes of order α and β

$\psi_\alpha^*, \psi_\beta^*$ complex conjugate of ψ_α and ψ_β, respectively, $\psi_\alpha^* \equiv \psi_\alpha$ and $\psi_\beta^* \equiv \psi_\beta$

ω angular frequency

ω_α angular frequency of mode of order α

ω_d natural frequency for damped free vibrations, $\omega_\alpha (1 - \zeta_\alpha^2)^{1/2}$

$\omega'(t)$ drift in the natural frequency

ω_0 maximum value of the drift in natural frequency

ω_α' time-independent part of resonance frequency of a system with a time-varying frequency response function

$\Delta\omega$ angular frequency bandwidth

$\Delta\omega_\alpha$ angular frequency half-power bandwidth of a resonance peak for mode of order α

3.0 DAMPING OF STRUCTURES

3.1 GENERAL DISCUSSION

Two important sources of damping in typical aerospace structures are structural hysteresis and acoustic radiation. For structures with no special damping treatments, hysteretic damping is mainly due to the joints in the structure, although there is some contribution from the damping of the material itself. The hysteretic damping force is proportional to displacement and is in counterphase with velocity. Acoustic radiation damping arises from the dissipation of energy in the surrounding air and is viscous controlled. Viscous damping forces are proportional to, and in counterphase with, the structural velocity.

From available literature it is possible to determine typical values of the damping ratios of structures ranging from single rectangular plates to stiffened airplane structures. Maestrello (ref. 5) and Wilby (ref. 6) show damping ratios in the range $0.001 < \zeta < 0.008$ for single rectangular panels with clamped boundaries. In some cases (ref. 6), the damping is seen to be dependent on the environment, presumably when the acoustic radiation damping forms a significant fraction of the total damping. Laboratory measurements on stiffened panels by Mead (refs. 7 and 8) give damping ratios in the range 0.002 to 0.013. Higher damping ratios, 0.014 to 0.020, have been measured on aircraft structures by Clarkson and Ford (ref. 9), although Mead (ref. 7) has placed some doubt on the accuracy of these values because the method of data anlaysis could cause overestimation of the damping.

The damping of structures can be increased greatly by the addition of special treatments such as damping tape. Mead (ref. 8) lists damping ratios up to 0.07 for a rectangular aluminum plate with one layer of damping tape, and Maestrello (ref. 5) measures damping ratios as high as 0.1 for a plate with two layers of tape. These results show a more than ten-fold increase in the damping with respect to the untreated case. The damping introduced by the treatment, using either unconstrained or constrained layers, is hysteretic in nature (ref. 8), with the result that the damping of the treated structure will be mainly hysteretic.

The above data show that, for untreated structures of the type likely to be found in aerospace construction, the damping will be low. Thus, in the mathematical analysis, the damping can be represented for simplicity as either solely hysteretic or solely viscous. As will be seen later, this is particularly useful for random vibration where the concept of hysteretic damping is not strictly valid. When damping treatment is added and the damping is mainly hysteretic, the assumption that the damping is solely viscous will still be made, although it will introduce some error.

Several methods for measuring the damping of structures are available—discrete frequency or random, steady-state or transient—and the choice of method for a particular test will depend on the experimental conditions present. Discrete frequency methods are suitable for conditions where there is no noise present in either the excitation or response. These methods have been discussed extensively by several authors (see refs. 1, 2, 4, and 10) and will not be included in this report. In the present case of interest, the steady-state, discrete frequency method is unsatisfactory because of the high level of "noise" introduced by the pressure fluctuations in the airflow, and the method has been excluded from consideration. Thus, the

analytical study in sections 4.0 through 6.0 will consider only steady-state random methods and transient methods. In some cases the turbulent airflow will provide the necessary excitation, but in other cases a second excitation will be introduced as a reference and the turbulent airflow regarded as noise in the system. The methods described will apply to any representation of the panel vibration (displacement, velocity, acceleration, etc.), but since the method chosen will be used with displacement probe instrumentation, the structural vibration will be described, without loss of generality, in terms of displacement.

Several of the measurement methods discussed will be suitable for either analog or digital data analysis techniques, but in other cases digital analysis procedures will be necessary. Thus, emphasis will be placed on the use of digital techniques for all methods, particularly when these techniques involve relatively new problem areas.

3.2 PANEL VIBRATION

At several stages in the analysis of the damping methods, reference will be made to the equation of motion for rectangular panels. Thus it is appropriate to outline the normal mode analysis of a rectangular plate exposed to random excitation, the resulting displacement power spectral density and autocorrelation equations being extensions of the corresponding equations for single-degree-of-freedom systems. Although the analysis is performed with specific reference to rectangular plates, the general conclusions will have wider application.

Assume that the displacement $w(\underline{x},t)$ of the vibrating structure obeys the thin-plate equation for small deflections

$$M\frac{d^2w}{dt^2} + C\frac{dw}{dt} + D\nabla^4 w = p(\underline{x},t), \tag{1}$$

where M is the mass per unit area, C is the viscous damping, D is the flexural rigidity, and $p(\underline{x},t)$ is the exciting force. D can be complex if hysteretic damping is included in the stiffness term. Assume further that the solution to equation (1) can be expressed in terms of a linear sum of normal modes, i.e.,

$$w(\underline{x},t) = \sum_{\alpha} q_{\alpha}(t)\, \psi_{\alpha}(x), \tag{2}$$

where $q_{\alpha}(t)$ is the generalized coordinate for the αth mode and $\psi_{\alpha}(\underline{x})$ is the mode shape function. Then the equation of motion for the αth mode is given by

$$M_{\alpha}\ddot{q}_{\alpha} + C_{\alpha}\dot{q}_{\alpha} + \kappa_{\alpha}(1 + i\nu_{\alpha})q_{\alpha} = L_{\alpha}, \tag{3}$$

where M_{α}, C_{α}, $\kappa_{\alpha}(1 + i\nu_{\alpha})$, and L_{α} are, respectively, the generalized mass, viscous damping, complex stiffness, and external force in the αth mode. The parameter ν_{α} represents the hysteretic damping of the system. If the panel surface density is denoted by $\mu(\underline{x})$, then

$$M_{\alpha} = \int_{A} \mu(\underline{x})\, \psi_{\alpha}^{2}(\underline{x})\, d\underline{x},$$

where the notation $\int_A d\underline{x}$ denotes the double integral $\int_0^{L_1} \int_0^{L_3} dx_3 dx_1$ over the panel area $A = L_1 L_3$.

For purely viscous damping the frequency response function for the mode is

$$H_\alpha(\omega) = \frac{1}{M_\alpha[(\omega_\alpha^2 - \omega^2) + 2i\zeta_\alpha\omega_\alpha\omega]}, \qquad (4)$$

where $\omega_\alpha = \sqrt{\kappa_\alpha/M_\alpha}$ is the undamped natural frequency and $\zeta_\alpha = C_\alpha/2\sqrt{M_\alpha\kappa_\alpha}$ is the damping ratio. The frequency response function $H_\alpha(\omega)$ and the impulse response function $h_\alpha(t)$ are related by Fourier transformation, such that

$$h_\alpha(t) = \frac{1}{2\pi} \int_{-\infty}^{\infty} H_\alpha(\omega) e^{i\omega t} d\omega$$

and $\qquad (5)$

$$H_\alpha(\omega) = \int_{-\infty}^{\infty} h_\alpha(t) e^{-i\omega t} dt,$$

it being noted that $h_\alpha(t) = 0$ for $t < 0$. It can be shown that $h_\alpha(t)$ is real, as is expected from physical reasoning.

For hysteretic damping alone,

$$H_\alpha(\omega) = \frac{1}{M_\alpha[(\omega_\alpha^2 - \omega^2) + i\nu_\alpha\omega_\alpha^2]}, \qquad (6)$$

but the Fourier transform of this function is complex and does not represent a physically realizable response. This inconsistency illustrates the difficulties encountered when the concept of hysteretic damping is used in the analysis of vibrations which are not of the deterministic sinusoidal type. It has been suggested (ref. 8) that, to overcome the problem, the hysteretic damping term be replaced by an equivalent viscous term $C_{\alpha e} = (\kappa_\alpha \nu_\alpha)/\omega$. The equation of motion would then be

$$M_\alpha\ddot{q}_\alpha + C_{\alpha e}\dot{q}_\alpha + \kappa_\alpha q_\alpha = L_\alpha. \qquad (7)$$

Then the analysis can be performed as for viscous damping and the hysteretic damping reinstated in the final result (replacing the term $\omega\zeta_{\alpha e}/\omega_\alpha$ with $\nu_\alpha/2$). This argument provides further justification for considering only viscous damping in the subsequent analyses.

If the equation of motion for viscous damping, similar to equation (7), is Fourier transformed with respect to time, the equation reduces to

$$Q_\alpha(\omega) = H_\alpha(\omega)U_\alpha(\omega), \qquad (8)$$

where $Q_\alpha(\omega)$ is the Fourier transform (or complex Fourier amplitude) of $q_\alpha(t)$, i.e.,

$$Q_\alpha(\omega) = \frac{1}{2\pi} \int_{-\infty}^{\infty} q_\alpha(t) e^{-i\omega t} dt,$$

and $U_\alpha(\omega)$ is the Fourier transform of $L_\alpha(t)$.

Also,

$$U_\alpha(\omega) = \frac{1}{2\pi} \int_{-\infty}^{\infty} e^{-i\omega t} \int_A p(\underline{x},t) \psi_\alpha(\underline{x}) d\underline{x} dt$$

$$= \int_A \psi_\alpha(\underline{x}) P(\underline{x},\omega) d\underline{x} \tag{9}$$

where

$$P(\underline{x},\omega) = \frac{1}{2\pi} \int_{-\infty}^{\infty} p(\underline{x},t) e^{-i\omega t} dt. \tag{10}$$

Thus, from equation (2) the Fourier transform of the displacement is

$$W(\underline{x},\omega) = \sum_\alpha Q_\alpha(\omega) \psi_\alpha(\underline{x}), \tag{11}$$

and the displacement power spectral density function at $\underline{x} = (x_1, x_3)$ is

$$S_W(\underline{x},\omega) = W(\underline{x},\omega) W^*(\underline{x},\omega), \tag{12}$$

where the asterisk denotes the complex conjugate. The parameter $\underline{x}$ in $S_W(\underline{x},\omega)$ is included to indicate that the displacement power spectral density function for a finite structure is inhomogeneous.

Substituting equations (8), (9), and (11) in equation (12),

$$S_W(\underline{x},\omega) = \sum_\alpha \sum_\beta \psi_\alpha(\underline{x}) \psi_\beta(\underline{x}) H_\alpha^*(\omega) H_\beta(\omega) \int_A \int_A \psi_\alpha(\underline{x}') \psi_\beta(\underline{x}'') S_p(\underline{x}',\underline{x}'',\omega) d\underline{x}' d\underline{x}'', \tag{13}$$

where $S_p(\underline{x}',\underline{x}'',\omega)$ is the excitation pressure cross-power spectral density function,

$$S_p(\underline{x}',\underline{x}'',\omega) = P(\underline{x}',\omega) P^*(\underline{x}'',\omega).$$

Using the relationships

$$R(\tau) = \int_{-\infty}^{\infty} S(\omega) e^{i\omega\tau} d\omega$$

and

$$S(\omega) = \frac{1}{2\pi} \int_{-\infty}^{\infty} R(\tau) e^{-i\omega\tau} d\tau,$$

the displacement autocorrelation function at $\underline{x}$ is

$$R_W(\underline{x},\tau) = \sum_\alpha \sum_\beta \psi_\alpha(\underline{x}) \psi_\beta(\underline{x}) \int_A \int_A \psi_\alpha(\underline{x}') \psi_\beta(\underline{x}'') \int_{-\infty}^{\infty} H_\alpha^*(\omega) H_\beta(\omega) S_p(\underline{x}',\underline{x}'',\omega) e^{i\omega\tau} d\omega d\underline{x}' d\underline{x}''$$

(14)

$$= \sum_\alpha \sum_\beta \psi_\alpha(\underline{x}) \psi_\beta(\underline{x}) \int_A \int_A \psi_\alpha(\underline{x}') \psi_\beta(\underline{x}'') \int_{-\infty}^{\infty} \int_{-\infty}^{\infty} h_\alpha(\tau_1) h_\beta(\tau_2)$$

$$R_p(\underline{x}',\underline{x}'',\tau + \tau_1 - \tau_2) d\tau_1 d\tau_2 d\underline{x}' d\underline{x}'',$$

where $R_p(\underline{x}', \underline{x}', \tau)$ is the excitation pressure cross-correlation function.

For a single-degree of freedom system such as a dashpot, the above equations (13) and (14) reduce to the much simpler forms

$$S_W(\omega) = |H(\omega)|^2 S_p(\omega)$$

(15)

and

$$R_W(\tau) = \int_{-\infty}^{\infty} \int_{-\infty}^{\infty} h(\tau_1) h(\tau_2) R_p(\tau + \tau_1 - \tau_2) d\tau_1 d\tau_2,$$

(16)

respectively.

3.3 FREQUENCY RESPONSE FUNCTIONS

In some of the methods discussed in the following sections, the procedure reduces to the plotting of the frequency response function $H_\alpha(\omega)$ in the complex plane. The damping ratio is estimated by fitting a circle to the data points in the neighborhood of the natural frequency, as a representation of the single-degree-of-freedom system. This technique is used to minimize effects which cause the measured function to deviate from the true frequency response function for a single mode.

Kennedy and Pancu (ref. 4) have shown that for a single-degree-of-freedom system with hysteretic damping, the plot of $H_\alpha^{-1}(\omega)$ is a straight line in the complex Argand plane and the plot of $H_\alpha(\omega)$ (equation (6)) is a circle. However, for viscous damping the locus of $H_\alpha^{-1}(\omega)$ is a parabola and can be considered as an approximation to a straight line only in the neighborhood of the natural frequency when the damping is small. Thus, the fitting of a circle to the experimental data for $H_\alpha(\omega)$ is, in itself, an approximation when the damping is considered to be viscous.

4.0 STEADY-STATE METHODS

In this section, four methods using steady-state random excitation will be discussed. The methods use:

a)   The response power spectral density function

b)   The response autocorrelation function

c)   The excitation-response cross-power spectral density function

d)   The single-sided Fourier transform of the response autocorrelation function

In three of the methods, a), b), and d), the pressure fluctuations in the turbulent airflow provide the random excitation forces. Method c) requires the introduction of a second excitation that is used as reference for the cross-power spectral density function, since it is not practical to use the airflow pressure fluctuations as a datum.

4.1 RESPONSE POWER SPECTRAL DENSITY

4.1.1 Introduction

The response power spectral density method is the stochastic equivalent of the response amplitude method for discrete frequency excitation. The response power spectrum will exhibit a series of peaks associated with the natural frequencies of the structure, and the damping, in common with the discrete frequency excitation case, can be estimated from measurements of the bandwidth of the resonant peaks. The response power spectral density method is conceptually simple since the damping factor is related to the bandwidth of the resonance peak. In principle, the method has the advantage that there are no requirements additional to those normally associated with the measurement of structural response (fig. 1a). However, for practical multimodal systems, the method suffers from a number of limitations that can be separated into two broad categories: first, the basic limitations inherent in the method and, second, the limitations imposed by the data analysis techniques and other peculiarities of the experimental procedure. The basic limitations include errors introduced by the closeness of natural frequencies and the effect of statistical coupling. Examples of the second category will include errors due to drift of the natural frequencies, the finite bandwidth of the filter system, contributions from the background noise, and the statistical scatter due to the finite data sample length. These limitations are often interdependent and occasionally impose somewhat severe requirements on the experiment, e.g., if a very small filter bandwidth is required due to very light damping, then very long data sample lengths will be required to ensure acceptable statistical scatter (or to ensure high statistical reliability).

Errors encountered in the practical use of the response power spectral density method are investigated analytically. The investigations are carried out with two questions in mind:

a) How can the error under investigation be minimized?

b) How can corrections be made to data acquired from a particular experiment?

Some of the errors encountered are not peculiar to the power spectral density method since they, or their equivalents, arise in other methods.

4.1.2 Basic Analysis

The displacement power spectral density function for a rectangular panel exposed to random excitation is given by equation (13). It can now be written in the form

$$S_w(\underline{x},\omega) = \sum_\alpha \sum_\beta \psi_\alpha(\underline{x})\psi_\beta(\underline{x})H_\alpha^*(\omega)H_\beta(\omega)I_{\alpha\beta}(\omega), \tag{17}$$

where

$$I_{\alpha\beta}(\omega) = \int_A \int_A \psi_\alpha(\underline{x}')\psi_\beta(\underline{x}'')S_p(\underline{x}',\underline{x}'',\omega)d\underline{x}'d\underline{x}'' \tag{18}$$

and $S_w(\underline{x},\omega)$ is evaluated at point $\underline{x} \equiv (x_1,x_3)$. Joint acceptances $J_{\alpha\alpha}(\omega)$ and cross acceptances $J_{\alpha\beta}(\omega)$ can be defined as

$$J_{\alpha\alpha}(\omega) = \frac{4}{A^2 S_p(\omega)} I_{\alpha\alpha}(\omega)$$

and

$$J_{\alpha\beta}(\omega) = \frac{4}{A^2 S_p(\omega)} I_{\alpha\beta}(\omega).$$

The joint acceptance term can be simplified slightly because if

$$S_p(\underline{x}',\underline{x}'',\omega) = C_p(\underline{x}',\underline{x}'',\omega) - iQ_p(\underline{x}',\underline{x}'',\omega)$$

it can be shown (ref. 6) that

$$\int_A \int_A \psi_\alpha(\underline{x}')\psi_\alpha(\underline{x}'')Q_p(\underline{x}',\underline{x}'',\omega)d\underline{x}'d\underline{x}'' = 0.$$

It should be noted that the excitation $p(\underline{x},t)$ will affect the response power spectral density $S_w(\underline{x},\omega)$ only through $I_{\alpha\beta}(\omega)$. When the excitation is homogeneously distributed over the

panel, the integrand in equation (18) is a function of separation distance only. For an inhomogeneous excitation, the integrand, and hence $I_{\alpha\beta}(\omega)$, will depend on the location of the excitation on the panel.

For a single mode, the displacement power spectral density is given by

$$S_w(\underline{x},\omega) = H_\alpha(\omega)H_\alpha^*(\omega)\psi_\alpha^2(\underline{x})J_{\alpha\alpha}(\omega)S_p(\omega)$$

$$= |H_\alpha(\omega)|^2\psi_\alpha^2(\underline{x})J_{\alpha\alpha}(\omega)S_p(\omega).$$

Thus, the displacement power spectral density depends on the joint acceptance $J_{\alpha\alpha}(\omega)$, location $\underline{x}$ (via mode shape $\psi_\alpha(\underline{x})$), and frequency response function $H_\alpha(\omega)$. $J_{\alpha\alpha}(\omega)$ is weakly dependent on ω (see ref. 6) and can be considered to be constant in the vicinity of the resonance peak. The mode shape ψ_α is essentially a scaling factor giving maximum deflection at an antinode and zero deflection at a node. Therefore, for a single mode, the displacement power spectral density is proportional to the square of the frequency response function, or

$$S_w(\underline{x},\omega) = K|H_\alpha(\omega)|^2 S_p(\omega),$$

where K is a factor that depends on the location of the measuring probe and the joint acceptance. If the excitation pressure power spectral density is approximately constant in the frequency range of interest, the frequency response function and the damping of the system can be estimated from the displacement power spectral density function. The viscous damping ratio is given by

$$\zeta_\alpha = \frac{\Delta\omega_\alpha}{2\omega_\alpha} = \frac{\Delta f_\alpha}{2f_\alpha},$$

where Δf_α is the half-power bandwidth of the resonance peak of mode α, occurring at a frequency of f_α.

For a single-point excitation, with power spectral density $S_p(\omega)$ at location $\underline{x}_0$, the displacement power spectral density function is

$$S_w(\underline{x},\omega) = \sum_\alpha \psi_\alpha^2(\underline{x})|H_\alpha(\omega)|^2 \int_A \int_A \psi_\alpha(\underline{x}')\psi_\alpha(\underline{x}'')S_p(\omega)\delta(\underline{x}'-\underline{x}_0)\delta(\underline{x}''-\underline{x}_0)d\underline{x}'d\underline{x}''$$

$$(19)$$

$$= \sum_\alpha \psi_\alpha^2(\underline{x})\psi_\alpha^2(\underline{x}_0)|H_\alpha(\omega)|^2 S_p(\omega).$$

4.1.3 Statistical Coupling

Equation (17) for the displacement power spectral density function can be written in the form

$$S_W(\underline{x},\omega) = \sum_\alpha \psi_\alpha^2(\underline{x})|H_\alpha(\omega)|^2 I_{\alpha\alpha}(\omega) + \sum_\alpha \sum_\beta \psi_\alpha(\underline{x})\psi_\beta(\underline{x})H_\alpha^*(\omega)H_\beta(\omega)I_{\alpha\beta}(\omega). \quad (20)$$
$$(\alpha \neq \beta)$$

The cross terms, for which $\alpha \neq \beta$, are due to statistical coupling between the modes of the panel, and these terms will cause the response peaks to deviate from the $|H_\alpha(\omega)|^2 I_{\alpha\alpha}(\omega)$ shape. Thus, the statistical coupling or cross terms will influence the damping measurements.

Three factors will affect the contributions from statistical coupling between modes α and β: cross acceptances $J_{\alpha\beta}(\omega)$, frequency response functions $H_\alpha(\omega)$, $H_\beta(\omega)$, and mode shapes $\psi_\alpha(\underline{x})$, $\psi_\beta(\underline{x})$. (Strictly speaking, the real function $[H_\alpha^*(\omega)H_\beta(\omega)J_{\alpha\beta}(\omega) + H_\alpha(\omega)H_\beta^*(\omega)J_{\beta\alpha}(\omega)]$ should be considered as a whole). Thus, the effects of statistical coupling on the measured displacement spectrum will depend on the damping and natural frequencies of the modes, the excitation cross-power spectral density, and the location at which the measurements are made.

As an illustration of the effects of the cross terms, the response of a simply supported plate to turbulent boundary layer excitation has been calculated using the methods of reference 6. The plate is assumed to be aluminum with dimensions of 30.48 by 17.78 by 0.102 cm (12 by 7 by 0.04 in.) and a damping ratio that is the same for all modes. The panel is exposed to typical Mach 2.0 flow. Displacement spectra were calculated both with and without the cross terms. The contributions due to statistical coupling at the eight lowest natural frequencies of the panel are shown in figure 2. For a damping factor of 0.04, the contributions due to statistical coupling vary from about 10^{-1} to 10^{-3} times the total power spectral density (including cross terms). In all cases, the contribution due to the cross terms decreases with damping ratio.

The influence of the cross terms on the measured damping can be estimated by comparison of the calculated spectra. It is found that the error is approximately proportional to the cross-term contribution shown on the ordinate scale of figure 2. For the example under consideration and a damping factor less than 0.02, the error in the estimated damping factor will be less than 7%.

It is interesting to note that the contributions due to statistical coupling, shown in figure 2, are highest for modes (1,2), (2,2), (4,1), and (2,3). Wilby (ref. 6) has shown that, for the boundary layer model used in the above calculations,

$$J_{\alpha\beta} = 0, \quad \text{for } n + s \text{ odd}$$

$$\neq 0, \quad \text{for } n + s \text{ even}$$

where mode orders $\alpha \equiv (m,n)$ and $\beta \equiv (r,s)$. Adjacent modes that satisfy the conditions that $(n + s)$ be even will be expected to show the effects of statistical coupling most clearly. For the modes identified above, mode pairs (1,2), (2,2) and (4,1), (2,3) satisfy the condition $(n + s)$ even.

4.1.4 Background Noise and Off-Resonant Contributions

The measured displacement power spectral density function can be influenced by several undesirable effects, and the signals causing these effects can be referred to as noise. The noise may be in the form of additional excitation forces or electronic noise in the measuring equipment. Off-resonant contributions from neighboring modes also come within this definition of noise and can be treated in a similar manner.

Consider first the effects caused by a second excitation that is additional to the turbulent boundary layer pressure field. For the sake of simplicity, assume that the system is a single-degree-of-freedom dashpot and the input and output signals are related as shown in figure 1b. The two excitations are denoted by $p_1(t)$ and $p_2(t)$, where $p_2(t)$ represents the noise signal.

Then

$$S_w(\omega) = |H_\alpha(\omega)|^2 P(\omega) P^*(\omega),$$

where

$$P(\omega) = \int_{-\infty}^{\infty} [p_1(t) + p_2(t)] e^{-i\omega t} dt$$

$$= P_1(\omega) + P_2(\omega).$$

Thus,

$$S_w(\omega) = |H_\alpha(\omega)|^2 [P_1(\omega) + P_2(\omega)] [P_1(\omega) + P_2(\omega)]^*$$

If $p_1(t)$ and $p_2(t)$ are uncorrelated,

$$P_1(\omega) P_2^*(\omega) = 0 = P_1^*(\omega) P_2(\omega)$$

and

$$S_w(\omega) = |H_\alpha(\omega)|^2 \left[1 + \frac{S_{p2}(\omega)}{S_{p1}(\omega)} \right] S_{p1}(\omega) \ .$$

$$= K'(\omega) |H_\alpha(\omega)|^2 S_{p1}(\omega),$$

(21)

where $S_{p1}(\omega)$ and $S_{p2}(\omega)$ are the power spectral density functions associated with $p_1(t)$ and $p_2(t)$, respectively. If $S_{p1}(\omega)$ and $S_{p2}(\omega)$ are slowly varying functions of ω, then even in the presence of noise in the excitation, the displacement power spectral density function is approximately proportional to the squares of the frequency response function. Under these conditions, noise in the excitation introduces only negligible errors in the damping measured using the response power spectral density method.

Extending the above analysis to the case of a single mode of a rectangular panel, equation (21) becomes

$$S_w(\underline{x},\omega)_\alpha = \psi_\alpha^2(\underline{x})|H_\alpha(\omega)|^2 \int_A \int_A \psi_\alpha(\underline{x}')\psi_\alpha(\underline{x}'')[S_{p1}(\underline{x}',\underline{x}'',\omega) + S_{p2}(\underline{x}',\underline{x}'',\omega)]\,d\underline{x}'d\underline{x}'', \quad (22)$$

where $S_{p1}(\underline{x}',\underline{x}'',\omega)$ and $S_{p2}(\underline{x}',\underline{x}'',\omega)$ represent the cross-power spectral density functions of the two signals, which are again assumed to be mutually uncorrelated. Thus, if damping estimates are now made directly from $S_w(\underline{x},\omega)_\alpha$, the displacement power spectral density for mode α, it is required that both $S_{p1}(\underline{x}',\underline{x}'',\omega)$ and $S_{p2}(\underline{x}',\underline{x}'',\omega)$ be slowly varying with frequency. (In fact, the requirement applies only to the real part of each cross-power spectral density function.)

When noise is present in the response signal also, the measured response, for a single-degree-of-freedom system, has the form

$$S_w(\omega)_\alpha = \left\{|H_\alpha(\omega)|^2\left[1 + \frac{S_{p2}(\omega)}{S_{p1}(\omega)}\right] + \frac{S_n(\omega)}{S_{p1}(\omega)}\right\}S_{p1}(\omega)$$

$$= \left\{K'(\omega)|H_\alpha(\omega)|^2 + K''(\omega)\right\}S_{p1}(\omega), \quad (23)$$

where the noise signal $n(t)$ is uncorrelated with the response $w(t)$. Thus, noise in the response introduces an additional term $K''(\omega)$ in the total response power spectral density function. The displacement power spectrum can be used for an accurate estimate of the damping ratio only when $K''(\omega)$ can be neglected or when corrections can be made to the data.

The effects of contributions from the off-resonant modes will be similar to those of background noise in the response. If the effects of statistical coupling are neglected, the displacement power spectral density function for two adjacent modes, with no other noise in the system, is obtained from equation (17).

$$S_w(\underline{x},\omega) = \frac{1}{4}A^2 S_p(\omega)\left\{|H_\alpha(\omega)|^2\psi_\alpha^2(\underline{x})J_{\alpha\alpha}(\omega) + |H_\beta(\omega)|^2\psi_\beta^2(\underline{x})J_{\beta\beta}(\omega)\right\}$$

$$= \left\{K_\alpha|H_\alpha(\omega)|^2 + K_\beta|H_\beta(\omega)|^2\right\}S_p(\omega). \quad (24)$$

Comparing equations (23) and (24) the term for mode β in the two-mode system has the same effect as the noise term $K''(\omega)$ in equation (23). Therefore, these two sources of error can be investigated using the following representation for the displacement power spectral density function:

$$S_w(\underline{x},\omega) = \left[1 + \sigma\left(\frac{\omega}{\omega_\alpha}\right)^\eta\right]|H_\alpha(\omega)|^2 K(\omega)S_p(\omega), \quad (25)$$

where σ denotes the ratio of background noise power spectral density to the true response power spectral density at resonance frequency ω_α. For $\eta = 0$, the background noise has a

constant power spectral density. Other frequency dependencies for the noise can be obtained by assigning appropriate values of η. For example, in the case of two modes, the contribution of the off-resonant mode β can be approximated by assigning positive and negative values to η for $f_\beta > f_\alpha$ and $f_\beta < f_\alpha$, respectively.

The errors that the response power spectral density method can introduce into measurements of the damping ratio when background noise is present have been estimated for values of η equal to 0, ±2, and ±4 and for different levels of background noise. These errors are shown in figure 3, as a percentage of the true damping factor, with ζ_α, η, and σ as parameters. For damping factor $\zeta_\alpha < 0.04$, the error is almost independent of ζ_α and η and can be treated as a function of σ only.

Figure 3 cannot be used directly to correct measured damping factors in practice. A typical response spectrum will contain a series of peaks and valleys. In such a case, the ratio of power spectral density in the valley to the resonant power spectral density of the adjacent peak can be used to obtain the level of background noise. A typical chart that can be used to correct the measured damping factor, when ζ_M is less than 0.04, is contained in figure 4.

The above procedure will not give good estimates of the error when the two natural frequencies f_α and f_β are very close together. Under such conditions the contribution from the off-resonant mode will not be represented very accurately by a function of the form ω^η.

It is interesting to note that, in the present case, where the vibration and noise are both random, mutually uncorrelated signals, the power spectral components can be added together without phase problems. This is an advantage over the deterministic case where the phase difference between resonant and off-resonant contributions is important and changes rapidly in the neighborhood of the resonant frequency f_α.

4.1.5 Filter Bandwidth

One of the critical problems in the use of the response power spectral density method is the finite bandwidth of the filter system, whether it be analog or digital. The finite bandwidth of the filter will cause loss of resolution in the spectra with associated broadening of the measured bandwidth of the resonant peak and overestimation of the damping factor. Filter bandwidth effects have been thoroughly investigated by Forlifer (ref. 11) for viscous damping and by Wilby (ref. 6) for hysteretic damping. Therefore, detailed analysis of the subject is not required here and only relevant results are presented.

Forlifer assumes rectangular filter characteristics so that the filter transfer function $\Phi(f)$ has the form

$$\Phi(f) = 1 \qquad f_F - \frac{\Delta f_F}{2} < f < f_F + \frac{\Delta f_F}{2}$$

$$= 0 \qquad \text{elsewhere.}$$

The center frequency of the filter is f_F and the bandwidth is Δf_F. Now, if Δf_M is the measured half-power bandwidth of the resonant peak, which has an actual bandwidth Δf_A, then Forlifer (ref. 11) shows that Δf_F, Δf_M, and Δf_A are related by the equation

$$\tan^{-1}\left(\frac{\Delta f_F}{\Delta f_A}\right) = \tan^{-1}\left(\frac{\Delta f_M}{\Delta f_A} + \frac{\Delta f_F}{\Delta f_A}\right) - \tan^{-1}\left(\frac{\Delta f_M}{\Delta f_A} - \frac{\Delta f_F}{\Delta f_A}\right). \tag{26}$$

This reduces to the simpler form

$$\left(\frac{\Delta f_M}{\Delta f_A}\right)^2 - \left(\frac{\Delta f_F}{\Delta f_A}\right)^2 = 1, \tag{27}$$

if the trivial solution $\Delta f_F / \Delta f_A = 0$ is excluded.

For practical application, equation (27) can be rewritten in a more convenient form that relates the filter bandwidth to the measured bandwidth. Then

$$\left(\frac{\zeta_A}{\zeta_M}\right)^2 = \left(\frac{\Delta f_A}{\Delta f_M}\right)^2 = \left(1 - \frac{1}{(\Delta f_M/\Delta f_F)^2}\right), \tag{28}$$

where ζ_A / ζ_M is the ratio of the true damping to the measured value. The curve for equation (28) is plotted in figure 5 and can be used to correct measured damping factors. As an example from the curve, the error in the uncorrected measured damping factor will be less than 14% if the filter bandwidth is less than half of the measured resonance half-power bandwidth.

From figure 5, it is obvious that the narrower the filter bandwidth, the smaller the error in the damping factor. However, there are other constraints on the filter bandwidth, the most important of which is the statistical confidence in the data. The statistical reliability of a spectral measurement can be defined in terms of the normalized standard error $\epsilon = 1/\sqrt{\Delta f_F T}$ where T is the total sample length. Thus, for a constant value of ϵ, or statistical reliability, the total sample length must increase when the filter bandwidth is decreased. In practice, the true bandwidth of the resonant peak will not be known until measurements have been made. Thus, some form of iteration will be necessary in the selection of the filter bandwidth. The filter bandwidth will also have to be a compromise between the resolution and statistical confidence requirements.

Additional discussion of the sample length will be presented in section 7.0, along with other requirements on data analysis procedures. However, it can be noted at this stage that the finite filter bandwidth problem is analogous to the truncation errors associated with some of the other methods.

4.1.6 Drift in Natural Frequency

A vibrating thin panel will generate heat due to internal dissipation of energy and will cause temperature changes in the panel. The panel is generally surrounded by relatively thick supports that will experience much smaller temperature changes. The differential temperature will cause thermal stress in the panel, and the resonance frequencies of the panel will change accordingly. Such a drift in natural frequency was noted by Wilby (ref. 12) and was also observed in the demonstration experiments of the present investigation. An exhaustive investigation of such a phenomenon should include considerations of the thermal equilibrium and thermal stresses of the panel and their effects on the vibration characteristics of the panel. Such a complete investigation is beyond the scope of the present project and, instead, an intuitive, workable model is presented here for investigation of the effect of drift of the resonance frequency on the measurement of damping.

A linear system with constant natural frequency will have a frequency response function $H_\alpha(\omega)$ that is independent of time. Drift in the natural frequency ω_α will give a time-varying frequency response function $H_\alpha(\omega,t)$. The effect of such a drift can be easily observed experimentally using discrete frequency excitation. When the panel is excited by a constant-frequency pure tone, the drift in natural frequency will give a change in vibration amplitude at the excitation frequency. When random excitation is used, the response amplitude will have random phase that will mask the change in amplitude due to the drift in natural frequency. Thus, the presence of drift in natural frequency will not be readily detected when using random excitation. For a time-invariant system (as shown earlier), the response power spectral density function will be proportional to $|H_\alpha(\omega)|^2$, whereas, for a system with time-varying frequency response function $H_\alpha(\omega,t)$, the response power spectral density function will be proportional to the time-averaged (or mean) square of the frequency response function $\overline{|H_\alpha(\omega)|^2}$.

$$\overline{|H_\alpha(\omega)|^2} = \frac{1}{T}\int_0^T |H_\alpha(\omega,t)|^2 dt,$$

where T is the data sample length.

Let ω_α' denote the equilibrium (time-independent) resonance frequency of the system. Then the drift in natural frequency can be represented as

$$\omega_\alpha(t) = \omega_\alpha' + \omega'(t),$$

where

$$\omega'(t) \ll \omega_\alpha' \qquad \text{for all } t.$$

Substituting $\omega_\alpha(t)$ in the frequency response function and neglecting terms of the order $(\omega'(t))^2$ and higher,

$$|H_\alpha(\omega,t)|^2 \approx \frac{1}{M_\alpha^2[A + B\omega'(t)]}, \tag{29}$$

where

$$A = (\omega'_\alpha{}^2 - \omega^2)^2 + 4\zeta_\alpha{}^2\,\omega'_\alpha{}^2\omega^2$$

$$B = 4\omega'_\alpha\,[\omega^2(2\zeta_\alpha{}^2 - 1) + \omega'_\alpha{}^2].$$

As an example, $\overline{|H_\alpha(\omega,t)|^2}$ has been estimated for the following form of $\omega'(t)$

$$\omega'(t) = \omega_o'e^{-kt} \qquad \text{for} \qquad t \geqslant 0$$

$$= 0 \qquad \text{for} \qquad t < 0.$$

Assuming small damping factors,

$$\overline{|H_\alpha(\omega,t)|^2} = |H_\alpha(\omega)|^2(1 + \epsilon_1),$$

where $|H_\alpha(\omega)|^2 = 1/(M_\alpha{}^2A)$ = square of the amplitude of the equilibrium frequency response function and error $\epsilon_1 = (1/kT)\log_e\,[(A + B\omega_o e^{-kT})/(A + B\omega_o)]$.

Substituting for B and A in the expression for ϵ_1, it can be seen that the error depends on kT, nondimensional frequency drift ω'_o/ω'_α, and the damping factor ζ_α. The error ϵ_1 is such that, in general, drift in the natural frequency will produce an average frequency response function with a bandwidth that is wider than that for the corresponding time-invariant frequency response function.

In practice, the error can be reduced by minimizing frequency drift using two approaches. First, by keeping panel deflection at the smallest possible level, the heat generated in the panel and the frequency drift can be kept to a minimum. Second, the thermal time constant of the panel can be reduced by blowing low-velocity air over the panel. This is equivalent to increasing kT in the above discussion.

4.1.7 N-Point Measurements

In general, the power spectral density method of determining damping factors uses a single measuring location. The problem of off-resonant vibration in adjacent modes, and background noise, could be alleviated by the use of several measuring transducers that record the response simultaneously.

The displacement cross-power spectral density of an L-degree-of-freedom system can be written as

$$S_w{}^{ij} = \sum_{n=1}^{L}\,\sum_{m=1}^{L}\,\psi^*_{ni}\psi_{mj}\Gamma_{mn} \qquad (i,j = 1,2,\dots L), \tag{30}$$

where

$$\Gamma_{mn}(\omega) = H_n^*(\omega)H_m(\omega)I_{mn}$$ (31)

and I_{mn} is defined as in equation (18).

In equation (30) $S_w^{ij} \equiv S_w(\underline{x}^i,\underline{x}^j,w)$ and $\psi_{nj} \equiv \psi_n(\underline{x}^j)$.

Now, λ_{ij} is a unitary matrix such that

$$\sum_{j=1}^{L} \sum_{i=1}^{L} \lambda_{pi} S_w^{ij} \lambda_{jq}^* = \eta_{pp}\delta_{pq},$$ (32)

where

$$\delta_{pq} = 1 \qquad \text{for } p = q$$
$$= 0 \qquad \text{for } p \neq q.$$

Multiplying the right side of equation (30) by the appropriate unitary matrix,

$$\eta_{pp}\delta_{pq} = \sum_{n=1}^{L} \sum_{m=1}^{L} \beta_{pn} \Gamma_{nm} \beta_{mq}^*,$$ (33)

where

$$\beta_{pn} = \sum_{i=1}^{L} \lambda_{pi}\psi_{ni}^*.$$ (34)

For a single-degree-of-freedom system,

$$\Gamma_{nm} = X_a \delta_{na}\delta_{ma}$$ (35)

and equation (33) reduces to

$$\eta_{pp}\delta_{pq} = X_a\beta_{pa}\beta_{aq}^* \qquad \text{or} \qquad \eta_{pp} = X_a[\beta_{aa}\beta_{aa}^*].$$ (36)

For a general case where Γ_{mn} can be represented by sum of L modes (corresponding to L degrees of freedom),

$$\Gamma_{mn} = \sum_{i=1}^{L} X_i \delta_{ni}\delta_{mi}$$ (37)

and

$$\eta_{pp}\delta_{pq} = \sum_{i=1}^{L} X_i \beta_{pi} \beta_{iq}^*$$

If the response is now measured at only N different positions, the cross-power spectral density functions can be represented by an [N x N] matrix, i.e., the measuring system will allow only N degrees of freedom and there are only N distinct values of η_{pp}'s. Thus, from equations (35), (36), and (37), the following conclusions can be drawn:

a)   For L = 1, all the power will be concentrated in only one mode.

b)   For L $<$ N, one can separate the power in each mode.

c)   For L $>$ N, the scheme will fail to separate contributions from different modes.

It should be noted that power η_{pp} represents the sum of the response power spectral densities in a particular mode at the N measuring locations. In practice, in a given frequency range, there are only a few modes with significant contributions. Thus, the condition L $<$ N can be effectively satisfied. In practice, with the advances in digital data processing, the response power spectral density matrix can be calculated readily. The matrix diagonalization can be achieved easily with the use of a computer.

The method appears to have certain advantages for resolving close natural frequencies and damping factors in the presence of high background noise. For all other applications, the method is considered to be unduly complicated when compared with the single-point measurement of the power spectral density method.

4.1.8 Summary

The basic characteristics of the displacement power spectral density method for damping measurement have been discussed with particular reference to a panel exposed to a moving airstream. In principle, the method is straightforward, requires no excitation other than the turbulent airflow, and has no instrumentation requirements other than those normally associated with the measurement of panel response to turbulent airflow. However, there are a series of problems in practice—statistical coupling, off-resonant vibration, background noise, filter bandwidth, and drift in the natural frequency—that have to be evaluated with respect to other methods.

The influences of these problem areas on the accuracy of the damping measurements have been discussed, and methods of alleviating the problems have been proposed. Suitable positioning of the measuring transducer can emphasize the vibration in the mode of interest, and errors caused by background noise and filter bandwidth can be corrected by the use of appropriate correction charts. For optimum location of the transducer, some initial knowledge of the panel mode shapes is required. This is not difficult for laboratory structures but may pose problems for large, complicated structures of typical aerospace construction.

In general use, only the response power spectral density is measured. This is adequate if the excitation power spectral density is constant (or approximately constant) in a frequency range close to the natural frequency of interest, but measurements should be made of the pressure field to confirm the assumption.

The use of a multipoint measuring array has been proposed as a way of reducing the effects of background noise and close natural frequencies. However, the use of such arrays involves considerable analysis problems that detract from the value of the method for general application.

One problem, the drift of panel natural frequencies, is really a problem of the test specimen rather than the analysis method. The drift would introduce measurement errors in all the test methods and the only satisfactory solution lies in the correct design of the experiment.

4.2 RESPONSE AUTOCORRELATION FUNCTION

4.2.1 Introduction

The response autocorrelation method uses the decay rate of the autocorrelation function as a measure of the damping of the system. Thus, the approach is similar to the deterministic method where the damping is estimated from the reverberant decay of the vibration when the excitation is removed. For the ideal case of a single-degree-of-freedom system, the method has obvious practical value, but for multimodal systems, such as a panel, the method has several limitations. These limitations will be discussed in the analysis where it will be assumed that the vibration of the panel results from exposure to the airflow and that no secondary excitation is intentionally introduced.

4.2.2 Basic Analysis

The basic theoretical analysis for a rectangular panel exposed to random excitation, particularly that due to a turbulent boundary layer, has been discussed in detail by Rechtien (ref. 13) and Wilby (ref. 6). Consequently, the present analysis will provide only an outline of the method.

The displacement autocorrelation function for the panel has been shown in equation (14) to be

$$R_w(\underline{x},\tau) = \sum_\alpha \sum_\beta \psi_\alpha(\underline{x})\psi_\beta(\underline{x}) \int_A \int_A \psi_\alpha(\underline{x}')\psi_\beta(\underline{x}'') \int_{-\infty}^{\infty} H_\alpha^*(\omega)H_\beta(\omega)S_p(\underline{x}',\underline{x}'',\omega)e^{i\omega\tau}d\omega d\underline{x}'d\underline{x}''. \quad (38)$$

The integration with respect to ω can be performed by contour integration, provided that $S_p(\underline{x}',\underline{x}'',\omega)$ is of order less than ω^3. When $\tau > 0$,

$$\int_{-\infty}^{\infty} H_\alpha^*(\omega) H_\beta(\omega) S_p(\underline{x}',\underline{x}'',\omega) e^{i\omega\tau} d\omega = \frac{2\pi e^{-\zeta_\alpha \omega_\alpha \tau}}{M_\alpha M_\beta \omega_d |D_{\alpha\beta}|} \left\{ S_\alpha^r \sin(\omega_d \tau + \theta_{\alpha\beta}) \right.$$
$$\left. + S_\alpha^i \cos(\omega_d \tau + \theta_{\alpha\beta}) \right\}, \tag{39}$$

where

$$S_\alpha^r \equiv S_\alpha^r(\underline{x}',\underline{x}'', \omega_d + i\omega_\alpha \zeta_\alpha)$$

$$S_\alpha^i \equiv S_\alpha^i(\underline{x}',\underline{x}'', \omega_d + i\omega_\alpha \zeta_\alpha)$$

$$S_p(\underline{x}',\underline{x}'', \omega_d + i\omega_\alpha \zeta_\alpha) = S_\alpha^r - iS_\alpha^i$$

$$D_{\alpha\beta} = D_{\alpha\beta}^r + iD_{\alpha\beta}^i$$

$$= (\omega_\alpha^2 - \omega_\beta^2) - 2\omega_\alpha \zeta_\alpha(\omega_\alpha \zeta_\alpha + \omega_\beta \zeta_\beta) + 2i\omega_d(\omega_\alpha \zeta_\alpha + \omega_\beta \zeta_\beta)$$

$$\sin \theta_{\alpha\beta} = \frac{D_{\alpha\beta}^i}{|D_{\alpha\beta}|}, \qquad \cos \theta_{\alpha\beta} = \frac{-D_{\alpha\beta}^r}{|D_{\alpha\beta}|}$$

and $\omega_d = \omega_\alpha \sqrt{1 - \zeta_\alpha^2}$ is the natural frequency for damped free vibrations.

To advance further, assume that the damping is small so that $\omega_\alpha \zeta_\alpha \ll \omega_d$ and $S_p(\underline{x}',\underline{x}'', \omega_d + i\omega_\alpha \zeta_\alpha)$ can be replaced by $S_p(\underline{x}',\underline{x}'', \omega_d)$. Then S_α^r becomes $C_p(\underline{x}',\underline{x}'', \omega_d)$ and S_α^i becomes $Q_p(\underline{x}',\underline{x}'', \omega_d)$, where

$$S_p(\underline{x}',\underline{x}'',\omega) = C_p(\underline{x}',\underline{x}'',\omega) - iQ_p(\underline{x}',\underline{x}'',\omega).$$

Also, since, by definition, the autocorrelation function is symmetrical about $\tau = 0$, the solution to equation (38) can be extended to include all τ if τ is replaced by $|\tau|$ in equation (39). Thus,

$$R_w(\underline{x},\tau) = \sum_\alpha \sum_\beta \frac{2\pi e^{-\omega_\alpha \zeta_\alpha |\tau|}}{M_\alpha M_\alpha \omega_d |D_{\alpha\beta}|} \psi_\alpha(\underline{x}) \psi_\beta(\underline{x}) \int_A \int_A \psi_\alpha(\underline{x}')\psi_\beta(\underline{x}'') \left\{ C_p(\underline{x}',\underline{x}'',\omega_d) \sin(\omega_d |\tau| + \theta_{\alpha\beta}) \right.$$
$$\left. + Q_p(\underline{x}',\underline{x}'',\omega_d) \cos(\omega_d |\tau| + \theta_{\alpha\beta}) \right\} d\underline{x}' d\underline{x}''$$

for all τ.

It has been shown (ref. 6) that

$$\int_A \int_A \psi_\alpha(\underline{x}')\,\psi_\alpha(\underline{x}'')Q_p(\underline{x}',\underline{x}'',\omega)d\underline{x}'d\underline{x}'' = 0,$$

so that

$$R_w(\underline{x},\tau) = \sum_\alpha \frac{\pi e^{-\omega_\alpha \zeta_\alpha |\tau|}}{2M_\alpha^2 \omega_d \omega_\alpha^2 \zeta_\alpha}\,\psi_\alpha^2(\underline{x}) \int_A \int_A \psi_\alpha(\underline{x}')\psi_\alpha(\underline{x}'')C_p(\underline{x}',\underline{x}'',\omega_d)\sin(\omega_d|\tau| + \theta_{\alpha\alpha})d\underline{x}'d\underline{x}''$$

$$+ \sum_\alpha \sum_\beta \frac{2\pi e^{-\omega_\alpha \zeta_\alpha |\tau|}}{M_\alpha M_\beta \omega_d |D_{\alpha\beta}|}\,\psi_\alpha(\underline{x})\psi_\beta(\underline{x}) \int_A \int_A \psi_\alpha(\underline{x}')\psi_\beta(\underline{x}'') \qquad (40)$$

$$\left\{ C_p(\underline{x}',\underline{x}'',\omega_d)\sin(\omega_d|\tau| + \theta_{\alpha\beta}) + Q_p(\underline{x}',\underline{x}'',\omega_d)\cos(\omega_d|\tau| + \theta_{\alpha\beta}) \right\}d\underline{x}'d\underline{x}''$$

for all τ.

Equation (40) shows that the response autocorrelation function for the panel displacement is a sum of contributions from all normal modes plus additional cross terms associated with the statistical coupling of the modes. Some simplification has to be achieved before the method has a reasonably practical form.

From (ref. 6), when the natural frequencies are well separated and the damping is small ($\zeta_\alpha \ll 1$), the cross terms can be neglected. When the natural frequencies are close together, the conditions for small cross terms are more difficult to establish but are similar to those associated with the displacement power spectral density function.

Neglecting cross terms equation (40) becomes

$$R_w(\underline{x},\tau) \approx \sum_\alpha \frac{\pi e^{-\omega_\alpha \zeta_\alpha |\tau|}}{2M_\alpha^2 \omega_\alpha^3 \zeta_\alpha(1 - \zeta_\alpha^2)^{\frac{1}{2}}}\,\psi_\alpha^2(\underline{x})\sin(\omega_d|\tau| + \theta_{\alpha\alpha})$$

$$(41)$$

$$\int_A \int_A \psi_\alpha(\underline{x}')\psi_\alpha(\underline{x}'')C_p(\underline{x}',\underline{x}'',\omega_d)d\underline{x}'d\underline{x}''.$$

From equation (41), the autocorrelation function is a sum of the contributions from the different modes and it is difficult to estimate the damping coefficient unless the vibration due to one mode can be isolated. This can be achieved to a certain extent if the natural frequencies are widely separated and the vibration in the vicinity of one natural frequency can be effectively isolated by filtering. The integral term in equation (41) is the joint acceptance term in equation (17) for the displacement power spectral density function.

If the vibration for one mode can be isolated, then the autocorrelation function becomes an exponentially decaying sine function where the decay rate is proportional to the damping and the sine function has a nonzero phase angle. For small damping $\theta_{\alpha\alpha} \approx \pi/2$.

From equation (41), the autocorrelation function for a single-degree-of-freedom system, such as a dashpot, is

$$R_W(\tau) = \frac{\pi e^{-\omega_\alpha \zeta_\alpha |\tau|} \sin(\omega_d |\tau| + \theta_{\alpha\alpha})}{2M_\alpha^2 \omega_\alpha^3 \zeta_\alpha (1 - \zeta_\alpha^2)^{\frac{1}{2}}} S_p(\omega_d). \tag{42}$$

4.2.3 Multimodal System With Close Natural Frequencies

The autocorrelation function $R_W(\underline{x}, \tau)$ for a multimodal system has been obtained in approximate form in equation (41) where the cross terms ($\alpha \neq \beta$) have been neglected. When a single mode can be considered alone, the autocorrelation function can be used to calculate the modal damping, but when there are two or more modes with close natural frequencies, modal isolation is not possible.

Consider the case of two modes of a panel where the natural frequencies are closely spaced. Using the approximate form for the displacement autocorrelation function (equation (41)), the autocorrelation for the two modes can be written as:

$$R_W(\underline{x}, \tau) = A_\alpha \sin(\omega_{d\alpha} |\tau| + \theta_{\alpha\alpha}) + A_\beta \sin(\omega_{d\beta} |\tau| + \theta_{\beta\beta}), \tag{43}$$

where

$$A_\alpha = \frac{\psi_\alpha^2(\underline{x}) \pi e^{-\omega_\alpha \zeta_\alpha |\tau|}}{2M_\alpha^2 \omega_\alpha^3 \zeta_\alpha (1 - \zeta_\alpha^2)^{\frac{1}{2}}} \int_A \int_A \psi_\alpha(\underline{x}') \psi_\alpha(\underline{x}'') C_p(\underline{x}', \underline{x}'', \omega_{d\alpha}) d\underline{x}' d\underline{x}'',$$

and

$$\omega_{d\alpha} = \omega_\alpha (1 - \zeta_\alpha^2)^{\frac{1}{2}}.$$

Similar definitions hold for A_β and $\omega_{d\beta}$.

To illustrate the relative importance of coefficients A_α and A_β, assume that $\theta_{\alpha\alpha} = \theta_{\beta\beta} = \theta$ for closely spaced modes since it is unlikely that the damping of the two modes will differ by a large amount ($\theta_{\alpha\alpha} = \tan^{-1}[(1 - \zeta_\alpha^2)^{\frac{1}{2}}/\zeta_\alpha]$). Then, for $\tau \geq 0$, equation (43) becomes

$$R_W(\underline{x}, \tau) \approx A_\alpha \sin(\omega_{d\alpha} \tau + \theta) + A_\beta \sin(\omega_{d\beta} \tau + \theta)$$

where A_α and A_β are always positive.

Letting $\omega_{d\beta} = \omega_{d\alpha} + \omega'$, then

$$R_w(\underline{x},\tau) = (A_\alpha^2 + A_\beta^2 + 2A_\alpha A_\beta \cos\omega'\tau)^{1/2} \sin(\omega_{d\alpha}\tau + \theta + \phi(\tau)), \qquad (44)$$

where $\tan\phi(\tau) = (A_\beta \sin\omega'\tau)/(A_\alpha + A_\beta \cos\omega'\tau)$.

Thus, $\phi(\tau)$ acts as a varying phase angle and $2A_\alpha A_\beta \cos\omega'\tau$ causes beating of the amplitude of the autocorrelation function, varying from $A_\alpha + A_\beta$ to $A_\alpha - A_\beta$. The maximum error in the autocorrelation amplitude will be $\pm A_\beta$. These results are similar to those of White (ref. 14) for the impulse response function.

To demonstrate the effect of close natural frequencies on the displacement autocorrelation function, equation (43) has been evaluated for two modal pairs of a 30.48- by 17.78- by 0.102-cm (12- by 7- by 0.04-in.) simply supported panel exposed to Mach 2.0 airflow and a boundary layer displacement thickness of 0.589 cm (0.232 in.). The method of reference 6 was used to calculate the terms A_α and A_β. In one example (fig. 6), the mode pair is $\alpha = (3,1)$, $\beta = (1,2)$ and the damping is assumed to be $\zeta_\alpha = 0.007 = \zeta_\beta$. For the second example (fig. 7), $\alpha = (2,2)$, $\beta = (4,1)$, and the damping is again $\zeta_\alpha = 0.007 = \zeta_\beta$. The data in figures 6 and 7 are plotted in terms of the normalized autocorrelation function or autocorrelation coefficient, and the autocorrelation curves are compared with the corresponding curves for mode α alone.

Figure 6 clearly shows the beating between the contributions from the two modes, and experimental data of this type would indicate the presence of more than one mode. However, in figure 7, for the time-delay range shown, the beating phenomenon is not evident, and experimental data in this form could be interpreted as being associated with a single heavily damped mode. Thus, it is essential that, for proper evaluation of the data, the maximum time delay τ_m in the autocorrelation function must be sufficiently large to indicate the presence of more than one mode. To identify one period in the beat signal, τ_m must be greater than $2\pi/\omega'$. In figure 6, $2\pi/\omega' = 12.45$ milliseconds, τ_m is 17.3 milliseconds, and the beat can be identified. In figure 7, $2\pi/\omega' = 22.57$ milliseconds and τ_m is 12.6 milliseconds, so the beat cannot be identified.

In practice, the dominant factors in the coefficients A_α and A_β will probably be the mode shape functions $\psi_\alpha(\underline{x})$ and $\psi_\beta(\underline{x})$, and choice of measuring position $\underline{x}$ will have an important influence on the form of the autocorrelation function. For the examples in figures 6 and 7, a location $x_1 = 5.08$ cm (2 in.), $x_3 = 4.45$ cm (1.75 in.) was chosen.

4.2.4 Band-Limited Signal

For the multimodal system, it has been shown above that the presence of more than one natural frequency has a distorting effect on the single-mode autocorrelation function. Even in the case of two modes, the distortion can cause large errors in the damping estimates.

In practice, the effects of neighboring natural frequencies can be minimized by the use of filters, although this method has very limited application. The filters exclude vibration at frequencies away from the natural frequency of interest and should have steep cutoff

characteristics. However, since the filters cannot exclude off-resonant vibration contributions at the natural frequency under investigation, they can be used successfully only if the ratio of resonant to off-resonant vibration is large. The use of filters may introduce adverse effects on the autocorrelation function if the bandwidth is too narrow. Thus, an optimum filter band-width has to be selected.

The effect of filter bandwidth on the autocorrelation function of the mode of interest can be investigated using a single-degree-of-freedom system as the model. The narrowband vibration signal could be the result of introducing a band-pass filter in the excitation or in the response. If the narrowband autocorrelation function is denoted by $R_w(\tau; \Delta\omega)$, then

$$R_w(\tau; \Delta\omega) = \int_{-\infty}^{\infty} \Phi(\omega) |H_\alpha(\omega)|^2 S_p(\omega) e^{i\omega\tau} d\omega. \tag{45}$$

The function $\Phi(\omega)$ represents the filter, and, for a rectangular filter,

$$\Phi(\omega) = 1 \qquad \omega_1 < |\omega| < \omega_2$$
$$= 0 \qquad \text{elsewhere.} \tag{46}$$

If it is assumed that, within the filter bandwidth, the excitation pressure power spectral density function has a constant value S_p, then equation (45) reduces to

$$R_w(\tau; \Delta\omega) = S_p \int_{-\infty}^{\infty} \Phi(\omega) |H_\alpha(\omega)|^2 e^{i\omega\tau} d\omega. \tag{47}$$

Evaluation of the integral in equation (47) is discussed in appendix A.

The problem is similar to that discussed by Kandianis (ref. 15) for the excitation-response cross-power spectral density method. Using the approximations of Kandianis, the presence of the filter modifies the autocorrelation function by the addition of terms that include functions of the form $(\cos\omega_2\tau)/\tau$ and $(\sin\omega_2\tau)/\tau$, which decay rapidly as τ increases.

4.2.5 Background Noise

Background noise can occur either as an additional excitation or as electronic noise in the equipment used to measure the vibration. The effects of the noise signals on the response autocorrelation function for a single-degree-of-freedom system have been discussed by Kandianis (ref. 16) and the results can be incorporated in this discussion.

Considering first the excitation, assume that a second signal $p_2(t)$ is superimposed on the initial signal $p_1(t)$ and that the two signals are mutually uncorrelated. Then, from equation (16), the response autocorrelation signal is

$$R_w(\tau) = \int_0^{\infty}\int_0^{\infty} h(\tau_1)h(\tau_2) [R_{p1}(\tau + \tau_1 - \tau_2) + R_{p2}(\tau + \tau_1 - \tau_2)] d\tau_2 d\tau_1. \tag{48}$$

Thus, the displacement autocorrelation function for the noise-free excitation, equation (16), is modified by the addition of the noise autocorrelation function to the pressure autocorrelation

function. The change, as expected, is a parallel of the effect demonstrated in equation (21) for the displacement power spectral density.

If the signals $p_1(t)$ and $p_2(t)$ represent white noise,

$$R_{p1}(\tau) = 2\pi S_{p1}\delta(\tau),$$

$$R_{p2}(\tau) = 2\pi S_{p2}\delta(\tau),$$

and

$$R_w(\tau) = 2\pi(S_{p1} + S_{p2})\int_0^\infty\int_0^\infty h(\tau_1)h(\tau_2)\delta(\tau + \tau_1 - \tau_2)d\tau_1 d\tau_2. \qquad (49)$$

In equation (49) S_{p1} is replaced by $[S_{p1} + S_{p2}]$, which has the effect of simply magnifying the autocorrelation function.

As an alternative to equation (48), the autocorrelation function can be written in the form

$$R_w(\tau) = \int_{-\infty}^\infty |H_\alpha(\omega)|^2 \, [S_{p1}(\omega) + S_{p2}(\omega)] \, e^{i\omega\tau}d\omega, \qquad (50)$$

where there are now no restrictions on the excitation power spectral density functions, and $[S_{p1}(\omega) + S_{p2}(\omega)]$ replaces the term $S_{p1}(\omega)$ found in the noise-free equations.

Referring now to the multimodal system associated with a panel and assuming that the statistical coupling cross terms can be neglected as in equation (41), the effect of the second (noise) excitation is determined by the real part of the cross-power spectral density function. Using equation (41) as the reference, the integral

$$\int_A\int_A \psi_\alpha(\underline{x}')\psi_\alpha(\underline{x}'') \, C_p(\underline{x}', \underline{x}'',\omega)d\underline{x}'d\underline{x}'',$$

associated with the noise-free case, becomes

$$\int_A\int_A \psi_\alpha(\underline{x}')\psi_\alpha(\underline{x}'')[C_{p1}(\underline{x}', \underline{x}'', \omega) + C_{p2}(\underline{x}', \underline{x}'', \omega)] \, d\underline{x}'d\underline{x}''$$

when noise is present in the excitation. Here the effect of the noise signal depends not only on the power spectral density, but also on the spatial correlation in relation to the mode shapes of the panel. The function $C_{p2}(\underline{x}', \underline{x}'',\omega)$ represents the real part of the complex cross-power spectral density function associated with the noise signal.

When noise is present in the response system, there will be no influence on the panel vibration, and the noise will appear as an additional term in the autocorrelation function. If $R_n(\tau)$ is the autocorrelation function associated with the noise in the response system, and if the autocorrelation function for the vibration is denoted by $R_w'(\tau)$, then the measured autocorrelation function will be

$$R_w(\tau) = R_w'(\tau) + R_n(\tau). \qquad (51)$$

If the noise signal n(t) is broadband white noise with power spectral density S_n, then

$$R_n(\tau) = 2\pi S_n \delta(\tau),\tag{52}$$

where $\delta(\tau)$ is the delta function. Therefore, the measured autocorrelation function differs from the noise-free correlation only when $\tau = 0$, at which time delay the noise introduces a delta function spike.

In practice, it is more likely that the noise will resemble band-pass noise rather than wide-band noise. The autocorrelation function then becomes

$$R_n(\tau) = 2S_n\left[\frac{\sin \omega_2\tau}{\tau} - \frac{\sin \omega_1\tau}{\tau}\right],\tag{53}$$

where ω_2 and ω_1 are the upper and lower cutoff frequencies, respectively, for the band-pass filter. If noise of the type represented by equation (53) is present in the measurements, it will be difficult to make suitable corrections to the data. Thus, if $R_n(\tau)$ is a significant fraction of $R_w(\tau)$, the damping measurements will show appreciable errors.

4.2.6 Summary

The response autocorrelation method involves analysis of the vibration in the time domain, and this results in additional complications when compared with frequency domain analyses. Analyses of the basic characteristics of the method show that severe problems will occur in practice unless the natural frequencies of interest are well separated. In such cases, the vibration in the neighborhood of a given natural frequency is due essentially to only one mode. Unfortunately, these very restrictive conditions are satisfied by very few modes of a structure, even a simple panel.

In an attempt to isolate the vibration of one mode, the use of band-pass filters has been suggested. Here a compromise has to be reached so that the filters have a bandwidth wide enough not to distort the results for the mode of interest, yet narrow enough to exclude vibration from other modes. Irrespective of filter characteristics, they will not exclude off-resonant vibrations within the band-pass frequency range. Thus, the filters are of little use unless the resonant vibration is large with respect to the off-resonant vibration.

Background noise, either in the excitation or the response, can cause errors in the damping measurements. This is particularly true if the noise is in the response signal. However, if the noise in the excitation has a constant power spectral density within the frequency range of interest, the associated errors in the measured damping will be negligible.

4.3 EXCITATION-RESPONSE CROSS-POWER SPECTRAL DENSITY

4.3.1 Introduction

The excitation-response cross-power spectral density method was proposed by Clarkson and Mercer (ref. 17) and is the stochastic equivalent of the response amplitude phase method (see Kennedy-Pancu, ref. 4) for discrete frequency excitation. Phase information, which is not used in the response power spectral density or autocorrelation methods, is used in the cross-power spectral density approach. Therefore, at least in principle, the method is capable of separating contributions from off-resonant modes and background noise. However, in practice, several limitations are imposed on the method, and these limitations are discussed in this section.

When studying structural response in the presence of an airflow, a severe limitation arises because of the inability to measure the excitation and response fields simultaneously. Introduction of a microphone would disturb the flow field or require modifications to the structure. Thus, it is necessary to provide a second excitation that can be used as a reference. The pressure field due to the airflow then takes on the role of unwanted noise as far as the damping measurement technique is concerned, and the problem of signal-to-noise ratio becomes very important.

4.3.2 Basic Analysis

The basic analysis for the method will be performed under the assumption that there is only one excitation present, and this excitation will be used as the reference signal. Thus, the system is identical to that shown in figure 1a.where the excitation signal is $p(\underline{x}',t)$ and the response of the system is denoted by $w(\underline{x},t)$. It is assumed in the analysis that the excitation is applied at a single point rather than being distributed over the panel, but this assumption is not necessary in general. The cross-power spectral density function relating the excitation and response can be represented by the equation:

$$S_{w,p}(\underline{x},\underline{x}',\omega) = W(\underline{x},\omega)\, P^*(\underline{x}',\omega), \tag{54}$$

where $W(\underline{x},\omega)$ and $P(\underline{x}',\omega)$ are the complex Fourier amplitudes of $w(\underline{x},t)$ and $p(\underline{x}',t)$ respectively, and the asterisk denotes the complex conjugate. From equations (8), (9), (10), and (11),

$$W(\underline{x},\omega) = \sum_{\alpha} \psi_{\alpha}(\underline{x})\, H_{\alpha}(\omega) \int_A \psi_{\alpha}(\underline{x})\, P(\underline{x},\omega)\, d\underline{x}.$$

Substituting for $W(\underline{x},\omega)$ in equation (54),

$$\begin{aligned}
S_{w,p}(\underline{x},\underline{x}',\omega) &= \sum_{\alpha} H_{\alpha}(\omega)\, \psi_{\alpha}(\underline{x}) \int_A S_p(\omega)\, \psi_{\alpha}(\underline{x})\delta(\underline{x}'-\underline{x})\, d\underline{x} \\
&= \sum_{\alpha} H_{\alpha}(\omega)\, \psi_{\alpha}(\underline{x})\, \psi_{\alpha}(\underline{x}')S_p(\omega),
\end{aligned} \tag{55}$$

where $S_p(\omega)$ is the power spectral density of the pressure signal at $\underline{x}'$.

The right side of equation (55) indicates that the cross-power spectral density function, which is complex, depends on the frequency response function $H_\alpha(\omega)$, the mode shapes $\psi_\alpha(\underline{x})$ of the panel, and the excitation force. The two mode-shape terms will give a multiplying factor that determines the efficiency with which the vibration is being excited and measured. For example, if the point of excitation and the location of the measuring probe are at antinodes of the mode being measured, then $\psi_\alpha(\underline{x}') = \psi_\alpha(\underline{x}) = 1$ and the measured cross-power spectral density function will be a maximum for a given excitation force.

Conversely, if the exciter or measuring transducer is located at a node of a given mode, then no vibration will be recorded in that mode. These properties are valuable in practice for augmenting or suppressing the response in a particular mode.

If an excitation force with constant spectrum level is used, then $S_p(\omega)$ will be independent of ω and the excitation-response cross-power spectral density function will be directly proportional to the sum of the frequency response functions of all modes. Comparing equation (55) with equation (20), note that the cross-power spectral density function does not contain the double summation present in equation (20) for the response power spectral density function. Cross terms that arise from the statistical coupling in the power spectral density function are absent in the excitation-response cross-power spectral density. However, the frequency-dependent term $H_\alpha(\omega)$ will still impose filter bandwidth requirements if adequate resolution is to be achieved in the data reduction of the cross-power spectra.

At some stages in the subsequent analysis, it will be convenient to refer to the non-dimensional cross-power spectral density function $\Gamma_{w,p}(\underline{x}, \underline{x}', \omega)$, which is defined as

$$\Gamma_{w,p}(\underline{x}, \underline{x}', \omega) = \frac{S_{w,p}(\underline{x}, \underline{x}', \omega)}{[S_w(\underline{x}, \omega) \cdot S_p(\omega)]^{1/2}}. \tag{56}$$

The function $\Gamma_{w,p}(\underline{x}, \underline{x}', \omega)$ is a measure of the coherence between the excitation and response.

For a single-mode system, the dimensional and nondimensional cross-power spectral density functions for a single excitation and the associated response are

$$S_{w,p}(\underline{x}, \underline{x}', \omega)_\alpha = H_\alpha(\omega) \psi_\alpha(\underline{x}) \psi_\alpha(\underline{x}') S_p(\omega) \tag{57}$$

and

$$\Gamma_{w,p}(\underline{x}, \underline{x}', \omega)_\alpha = H_\alpha(\omega) \psi_\alpha(\underline{x}) \psi_\alpha(\underline{x}') \left[\frac{S_p(\omega)}{S_w(\underline{x}, \omega)_\alpha} \right]^{1/2} \tag{58}$$

Since $S_w(\underline{x}, \omega)_\alpha$, the displacement power spectral density in mode α, is proportional to $|H_\alpha(\omega)|^2$, then $\Gamma_{w,p}(\underline{x}, \underline{x}', \omega)$ is proportional to $H_\alpha(\omega)/|H_\alpha(\omega)|$.

4.3.3 Background Noise

As stated earlier, one important problem when applying the excitation-response cross-power spectral density method to a panel exposed to turbulent airflow is the difficulty in measuring the excitation. To overcome this problem, the introduction of a second excitation has been proposed (refs. 6 and 18) as the reference signal. The system then resembles that shown in figure 1b where the boundary layer pressure field $p_1(\underline{x}',t)$ is regarded as undesirable noise and the signal $p_2(\underline{x}'',t)$ becomes the reference signal.

The modified cross-power spectral density function can be determined following the approach of section 4.3.2, except that the panel total displacement now depends on two excitations, only one of which (p_2) is being measured. If $p_1(\underline{x}',t)$ and $p_2(\underline{x}'',t)$ are assumed to be statistically independent, the nondimensional cross-power spectral density function for a single mode becomes

$$\Gamma_{w,p2}(\underline{x},\underline{x}'',\omega)_\alpha = \frac{\psi_\alpha(\underline{x})\,\psi_\alpha(\underline{x}'')\,[S_{p2}(\omega)]^{1/2}\,H_\alpha(\omega)}{\left[A^2 S_{p1}(\omega)J_{\alpha\alpha}(\omega)/4 + \psi_\alpha^2(\underline{x}'')\,S_{p2}(\omega)\right]^{1/2}\,\psi_\alpha(\underline{x})|H_\alpha(\omega)|}. \quad (59)$$

When $[A^2 S_{p1}(\omega)J_{\alpha\alpha}(\omega)/4]$ is much smaller than $[\psi_\alpha^2(\underline{x}'')S_{p2}(\omega)]$, which means physically that the panel vibration is due mainly to the introduced excitation $p_2(\underline{x}'',t)$, then $\Gamma_{w,p2}(\underline{x},\underline{x}'',\omega)$ in equation (59) tends to the noise-free form in equation (58).

If noise $n(t)$ is introduced into the response, as indicated in figure 1c, and $n(t)$ is assumed to be uncorrelated with the vibration $w(\underline{x},t)$ and the excitation $p_2(\underline{x}'',t)$, then the measured nondimensional cross-power spectral density function for mode α will be given by the expression

$$\Gamma_{w,p2}(\underline{x},\underline{x}'',\omega)_\alpha = \frac{\psi_\alpha(\underline{x})\,\psi_\alpha(\underline{x}'')\,[S_{p2}(\omega)]^{1/2}\,H_\alpha(\omega)}{\left\{|H_\alpha(\omega)|^2\,\psi_\alpha^2(\underline{x})\,[A^2 S_{p1}(\omega)J_{\alpha\alpha}(\omega)/4 + \psi_\alpha^2(\underline{x}'')S_{p2}(\omega)] + S_n(\omega)\right\}^{1/2}}. \quad (60)$$

Equations (58), (59), and (60) all have the same numerator which, apart from the omission of a factor $[S_{p2}(\omega)]^{1/2}$, is the dimensional cross-power spectral density function relating excitation $p_2(\underline{x}'',t)$ and panel displacement. The differences between the three equations occur in the denominator which, in the form shown, is the square root of the response power spectral density. Since the addition of noise in the excitation or response increases the measured response power spectral density, the nondimensional cross-power spectral density decreases as the noise increases.

The decrease of $\Gamma_{w,p2}(\underline{x},\underline{x}'',\omega)_\alpha$ as the noise increases identifies an important problem area for the case of a panel excited by a moving airstream, namely, the accurate measurement of small correlation coefficients or functions obtained from large signals. To perform the data analysis with sufficient accuracy, it is necessary that the data reduction system should have high amplitude resolution and large dynamic range. For a given instrument system, the dynamic range will be constant and the maximum signal will be determined by the vibration-plus-noise signal. Only a small fraction of this signal will be correlated with the excitation reference, thereby creating a signal processing problem.

4.3.4 Multimodal System

The excitation-response cross-power spectral density function for a noise-free, multimodal system is given in equation (55) as

$$S_{w,p}(\underline{x},\underline{x}\,',\omega) = \sum_{\alpha} \psi_{\alpha}(\underline{x})\psi_{\alpha}(\underline{x})\, H_{\alpha}(\omega)S_p(\omega). \tag{61}$$

Comparing this equation with the corresponding equation for the displacement power spectral density function (equation (20)), the main advantage of the cross-power spectral density can be identified.

In equations (20) and (61), the value of the function at a given frequency is determined by a summation over all modes. For the power spectra, each modal contribution is proportional to the real function $|H_{\alpha}(\omega)|^2$ and is added algebraically to the other contributions. In contrast, the modal contributions to the cross-power spectral density are proportional to the complex function $H_{\alpha}(\omega)$ and are summed vectorially. The vectorial addition is the direct equivalent of the Kennedy and Pancu method (ref. 4), and permits separation of the resonant vibration from the off-resonant/noise components. This identifies the advantage of the cross-power spectral density method.

From equation (61), if $S_p(\omega)$ is essentially constant, the locus of the measured cross-power spectral density function will be a constant multiple of the frequency response function obtained from the Kennedy and Pancu method with discrete frequencies. Properties of the frequency response functions discussed in section 3.3 will be equally applicable to the cross-power spectra, and resonance circles can be drawn as an aid to the measurement of modal damping. This technique corrects for the presence of off-resonant and noise contributions.

The nondimensional cross-power spectral density function for the multimodal system can be obtained by following the procedure outlined in section 4.3.3 and using equation (61). The nondimensionalizing factor $[S_p(\omega)\, S_w(\underline{x},\omega)]^{1/2}$ in equation (58) will be replaced by $[S_p(\omega) \cdot \sum_{\alpha} S_w(\underline{x},\omega)_{\alpha}]^{1/2}$, thereby reducing the value of the nondimensional cross-power spectral density function.

4.3.5 Filter Bandwidth

The fundamental quantity being measured in the cross-power spectral density method is the frequency response function $H_{\alpha}(\omega)$. Thus, one of the problems in the data reduction will be the loss of resolution due to the finite bandwidths of the analyzing filters. Essentially, the problem is similar to that encountered in the power spectral density method. In practice, the cross-power spectral density function can be determined in two ways that will be referred to as the direct and indirect methods. If digital techniques of data analysis are used, the direct method indicates that the Fourier transforms (or complex Fourier amplitudes) of the time series are computed and multiplied together to give the cross-power spectral density function. The indirect method first computes the excitation-response cross-correlation function and then Fourier transforms the correlation function to obtain the cross-power spectral density function. Again, referring to digital techniques for data analysis, the filter bandwidth is related to the data sample length for the direct method or maximum delay time for the indirect method.

Considering first the direct method, the filter bandwidth requirements can be established using the discussion in section 4.1.5 as a guideline. For a filter with rectangular characteristics, the error in the damping measurements obtained from the power spectrum is shown in figure 5 as a function of filter bandwidth and measured half-power bandwidth. In practice, the filter characteristics in the direct method will be determined by the presence, or absence, of data smoothing but will differ from the ideal rectangular shape. Filter bandwidth is discussed further in section 7.0.

The filter bandwidth problem for the indirect method has been discussed by Clarkson and Mercer (ref. 17) and Soovere and Clarkson (ref. 19) in terms of truncation, which is the equivalent time domain problem. As will be seen in section 4.4, truncation problems occur also in the single-sided Fourier transform method.

In the indirect method, the theoretical excitation-displacement cross-power spectral density function $S_{w,p}(\underline{x}, \underline{x}', \omega)$ is obtained as the Fourier transform of the cross-correlation function $R_{w,p}(\underline{x}, \underline{x}', \tau)$, where

$$S_{w,p}(\underline{x}, \underline{x}', \omega) = \frac{1}{2\pi} \int_{-\infty}^{\infty} R_{w,p}(\underline{x}, \underline{x}', \tau) e^{-i\omega\tau} d\tau. \tag{62}$$

However, in practice, it is not possible to measure $R_{w,p}(\underline{x}, \underline{x}', \tau)$ for an infinitely long time delay, and the function must be measured for a finite range, say $-\tau_m \leqslant \tau \leqslant \tau_m$. The computed cross-power spectral density function is then

$$S_{w,p}(\underline{x}, \underline{x}', \omega; \tau_m) = \frac{1}{2\pi} \int_{-\infty}^{\infty} D(\tau) R_{w,p}(\underline{x}, \underline{x}', \tau) e^{-i\omega\tau} d\tau, \tag{63}$$

where $D(\tau)$ is a weighting function, or lag window, such that $D(\tau) = 0$ for $|\tau| > \tau_m$.

Alternatively,

$$S_{w,p}(\underline{x}, \underline{x}', \omega; \tau_m) = \int_{-\infty}^{\infty} \Phi(\omega - \omega') S_{w,p}(\underline{x}, \underline{x}', \omega') d\omega', \tag{64}$$

where

$$\Phi(\omega - \omega') = \frac{1}{2\pi} \int_{-\infty}^{\infty} D(\tau) e^{-i(\omega - \omega')\tau} d\tau$$

and is called the spectral window. $\Phi(\omega - \omega')$ represents the filter characteristics referred to above.

For the case of single-point excitation, as considered in section 4.3.2, and assuming constant excitation spectral density, equation (64) can be written in the form

$$S_{w,p}(\underline{x}, \underline{x}', \omega; \tau_m) = \sum_{\alpha} K_{\alpha}(\underline{x}, \underline{x}') \int_{-\infty}^{\infty} \Phi(\omega - \omega') H_{\alpha}(\omega') d\omega'. \tag{65}$$

The form of the lag window $D(\tau)$ can be selected from several standard representations. Clarkson and Mercer (ref. 17) selected the rectangular lag window

$$\begin{aligned} D(\tau) &= 1 & |\tau| &\leqslant \tau_m \\ &= 0 & \text{elsewhere.} \end{aligned} \left.\vphantom{\begin{aligned} D(\tau) &= 1 \\ &= 0 \end{aligned}}\right\} \tag{66}$$

As a modification, Soovere and Clarkson (ref. 19) use the Bartlett triangular window,

$$D(\tau) = 1 - \frac{|\tau|}{\tau_m} \qquad |\tau| \leqslant \tau_m$$
$$= 0 \qquad \text{elsewhere} \qquad \Big\} (67)$$

since this is more reliable, statistically, than is the rectangular window. In both cases, the effect of truncation is determined with respect to the parameter $(1/\rho)(ds/df)$ where ρ is the radius of curvature of the cross-power spectral density curve at resonance and ds/df is the rate of change of arc length with frequency at resonance. Assuming small damping, $\zeta_\alpha^2 \ll 1$, Clarkson and Mercer (ref. 17) show that

$$\frac{1}{\rho}\frac{ds}{df} \approx \frac{4\pi}{\omega_\alpha \zeta_\alpha} \left[\frac{1 - e^{-\omega_\alpha \zeta_\alpha \tau_m} [1 + \omega_\alpha \zeta_\alpha \tau_m + \omega_\alpha^2 \zeta_\alpha^2 \tau_m^2/2]}{1 - e^{-\omega_\alpha \zeta_\alpha \tau_m} (1 + \omega_\alpha \zeta_\alpha \tau_m)} \right], \qquad (68)$$

and a similar equation is derived by Soovere and Clarkson for the triangular lag window. Curves of $(1/\rho)(ds/df)$ as a function of $\omega_\alpha \zeta_\alpha$ and τ_m can be used as a means of correcting for truncation (or filter bandwidth) errors. Examples of such curves for the rectangular and triangular lag windows are contained in figure 8. The curves show that, for a given maximum time delay τ_m, the error created by the rectangular lag window is less than that due to the triangular window. This is expected since the equivalent bandwidth of the triangular lag window is larger than that of the rectangular window, for a given value of τ_m. The advantage of the triangular window lies in the improved statistical reliability.

Some simplification of the curves is possible if it assumed that the filter bandwidth Δf_F is a fraction of the resonance bandwidth Δf_α, i.e.,

$$\Delta f_F = \frac{1}{n} \Delta f_\alpha.$$

From reference 20, the effective filter bandwidth for the rectangular lag window can be taken as

$$\Delta f_F = \frac{1}{2\tau_m}.$$

Then

$$\omega_\alpha \zeta_\alpha \tau_m = n\pi/2$$

and

$$\frac{1}{\rho}\frac{ds}{df} \approx \frac{4\pi}{\omega_\alpha \zeta_\alpha} \Psi(n)$$

where

$$\Psi(n) = \left[\frac{1 - e^{-n\pi/2} (1 + n\pi/2 + n^2 \pi^2/8)}{1 - e^{-n\pi/2} (1 + n\pi/2)} \right]. \qquad (69)$$

The curve for $\Psi(n)$ is shown in figure 9. At low values of $\Delta f_\alpha / \Delta f_F$ (less than 3), the curve for $\Psi(n)$ indicates larger errors in the damping measurement than are predicted by figure 5 for the rectangular filter.

The above discussion on truncation errors has assumed that the instrument is ideal in that there are no dynamic range or noise problems. In practice, there will be a dynamic range problem when the time delay exceeds a certain value that will depend on the equipment. Any correlation information obtained for time delays in excess of the critical value will be spurious, and the critical time delay will determine the maximum useful time delay.

4.3.6 Summary

In concept, the excitation-response cross-power spectral density method has several highly desirable features that result from the inclusion of phase information. Using the excitation force as a reference, the response vector diagram can be drawn and the effects of background noise and off-resonant vibration minimized. Additional benefits arise if the point of application of the excitation can be varied, thereby suppressing vibration in certain modes.

When the method is applied to the case of structural response to a moving airstream, measurement of the excitation force becomes a significant problem. If the aerodynamic pressure field is used as a reference, a measuring transducer has to be located in the airstream or in the surface of the structure. In either case, the experimental environment would be changed. As an alternative solution, a second excitation can be introduced to act as the reference, and the boundary layer excitation then takes on the characteristics of unwanted noise. However, under these circumstances the problem of signal-to-noise ratio becomes important. The vibration induced by the second excitation has to be significantly greater in amplitude than that induced by the aerodynamic pressures if reasonable accuracy is to be achieved in the damping measurements. To satisfy this requirement, the second excitation force must be large, with resultant dynamic range problems in the instrumentation. If the test panel is enclosed by a pressure equalizing chamber, difficulties may arise in locating the exciter within the chamber.

4.4 RESPONSE SINGLE-SIDED FOURIER TRANSFORM METHOD

4.4.1 Introduction

The important characteristic of the single-sided Fourier transform method is that it uses phase information that is hidden in the power spectral density and autocorrelation function. The method was introduced by Kandianis (ref. 16) as a means of reducing the effects of noise interference in the analysis of transient signals. However, the theoretical background applies strictly to stationary signals and, for simplification, the characteristics of the signals are usually assumed to be those of white noise.

In operation, the method computes the response autocorrelation function, either directly, or indirectly via the power spectral density function, and then performs Fourier transformation on half of the autocorrelation function (e.g., for $\tau > 0$). The resulting single-sided Fourier

transform is a complex function of the frequency response function $H(\omega)$, and the damping can be estimated from the complex plane diagram in a manner similar to that developed by Kennedy and Pancu (ref. 4) and used in the excitation-response cross-power spectral density method (sec. 4.3).

Discussion in this section will be concerned with vibration induced by random excitation such as the turbulent boundary layer. Application of the method to transient excitation techniques where a second excitation is introduced will be discussed later in section 5.0.

4.4.2 Basic Analysis

The basic properties of the method can be demonstrated most easily by a single-degree-of-freedom system. The displacement autocorrelation function for such a system has the form, from equation (42),

$$R_w(\tau) = \frac{\pi e^{-\omega_\alpha \zeta_\alpha |\tau|}}{2M_\alpha^2 \omega_\alpha^3 \zeta_\alpha (1 - \zeta_\alpha^2)^{\frac{1}{2}}} \sin(\omega_d |\tau| + \theta_{\alpha\alpha}) S_p(\omega_d). \tag{70}$$

Then the single-sided Fourier transform is defined as

$$F_w(\omega) = \frac{1}{2\pi} \int_0^\infty R_w(\tau) e^{-i\omega\tau} d\tau. \tag{71}$$

Substituting equation (70) in equation (71), $F_w(\omega)$ can be evaluated using standard integrals, and

$$F_w(\omega) = \frac{S_p(\omega_d)}{4\zeta_\alpha \omega_\alpha^2 M_\alpha} \left[2\zeta_\alpha + i\frac{\omega}{\omega_\alpha} \right] H_\alpha(\omega) \tag{72}$$

$$= \frac{1}{2} S_p(\omega_d) |H_\alpha(\omega)|^2 \left[1 + \frac{i}{2\zeta_\alpha} \left(\frac{\omega}{\omega_\alpha}\right)\left(1 - \left(\frac{\omega}{\omega_\alpha}\right)^2 - 4\zeta_\alpha^2\right) \right]. \tag{73}$$

As expected from general principles, the real part of $F_w(\omega)$ is half of the displacement power spectral density function and is proportional to $|H_\alpha(\omega)|^2$. Thus, the real part can provide estimates of the damping in precisely the same way as in the power spectral density method. However, the advantage of the method lies in the combined use of the real and imaginary parts in the form indicated by equation (72).

The locus of $H_\alpha(\omega)$ in the complex Argand plane has been discussed in section 3.3 where it was stated that $H_\alpha(\omega)$ was a circle only for the case of hysteretic damping. For viscous damping, the frequency response function is approximately a circle in the neighborhood of the natural frequency when the damping is small. Similar restrictions apply to the function $F_w(\omega)$ of equation (72).

Using the Kennedy and Pancu method (ref. 4), estimates of the damping coefficient are obtained from the locations of the half-power points of $H_\alpha(\omega)$. This is an approximation that is valid for light damping and it is again valid for the function $F(\omega)$. To demonstrate the validity of the approximation, consider a parameter χ defined by

$$\left| H_\alpha\left(\omega_\alpha + \frac{\omega_\alpha \zeta_\alpha}{2}\right) \right|^2 = \frac{1}{\chi}|H_\alpha(\omega_\alpha)|^2.$$

Then χ can be assumed to be equal to 2 (which gives the half-power law) within an accuracy of about $\zeta_\alpha/2$ for hysteretic damping and $3\zeta_\alpha/2$ for viscous damping. In the case of the single-sided Fourier transform $F(\omega)$, the error in χ is approximately $2\zeta_\alpha$. Thus, for the single-degree-of-freedom system, the single-sided Fourier transform and the excitation-response cross-power spectral density methods are closely allied.

The single-sided Fourier transform method can be extended to include the multimodal case typical of panel vibration by the use of equation (40). Substituting equation (40) in equation (71),

$$F_w(\omega) = \sum_\alpha \frac{\left(2\zeta_\alpha + i\left(\frac{\omega}{\omega_\alpha}\right)\right)\psi_\alpha^2(\underline{x})H_\alpha(\omega)}{4\zeta_\alpha \omega_\alpha^2 M_\alpha} \cdot \int_A \int_A \psi_\alpha(\underline{x}')\psi_\alpha(\underline{x}'')C_p(\underline{x}',\underline{x}'',\omega_d)d\underline{x}'d\underline{x}''$$

$$+ \sum_\alpha \sum_\beta \frac{\psi_\alpha(\underline{x})\psi_\beta(\underline{x})H_\alpha(\omega)}{M_\beta|D_{\alpha\beta}|} \left\{ \left(\cos\theta_{\alpha\beta} + \frac{\zeta_\alpha \omega_\alpha + i\omega}{\omega_\alpha(1-\zeta_\alpha^2)^{1/2}}\sin\theta_{\alpha\beta} \right) \right.$$

(74)

$$\int_A \int_A \psi_\alpha(\underline{x}')\psi_\beta(\underline{x}'')C_p(\underline{x}',\underline{x}'',\omega_d)d\underline{x}'d\underline{x}'' + \left(\frac{\zeta_\alpha \omega_\alpha + i\omega}{\omega_\alpha(1-\zeta_\alpha^2)^{1/2}}\cos\theta_{\alpha\beta} - \sin\theta_{\alpha\beta} \right)$$

$$\left. \int_A \int_A \psi_\alpha(\underline{x}')\psi_\beta(\underline{x}'')Q_p(\underline{x}',\underline{x}'',\omega_d)d\underline{x}'d\underline{x}'' \right\}$$

where ω_d, $D_{\alpha\beta}$, $\sin\theta_{\alpha\beta}$, and $\cos\theta_{\alpha\beta}$ are defined in section 4.2.2 for equation (39).

Immediately obvious in equation (74) are the cross terms ($\alpha \neq \beta$), which are absent in the excitation-response cross-power spectral density function but do occur in the power spectral density function. The joint terms ($\alpha = \beta$) pose no problem since they represent a sum of terms of the type $K_\alpha(2\zeta_\alpha + i\omega/\omega_\alpha)H_\alpha(\omega)$ where the parameter K_α is a function of mode shape and measuring location and is independent of frequency ω. Thus, for small damping, the locus of the joint terms can be analyzed in a straightforward manner using the complex Argand diagram and constructing resonance circles at the natural frequencies. The practical application of the method to a panel excited by turbulent airflow depends on the magnitude of the interference from the cross terms.

When the natural frequencies are well separated, the function $(\cos\theta_{\alpha\beta}/)|D_{\alpha\beta}|$ is of order ω_α^{-2} and $(\sin\theta_{\alpha\beta}/)|D_{\alpha\beta}|$ is of order $\zeta_\alpha \omega^{-2}$. Thus, if $\zeta_\alpha \ll 1$, these functions can be

considered small relative to the joint term of order $\zeta_\alpha^{-1}\omega^{-2}$. However, when the natural frequencies are close together, $\theta_{\alpha\beta}$ and $D_{\alpha\beta}$ approach the corresponding joint term values $\theta_{\alpha\alpha}$ and $D_{\alpha\alpha}$, and the influence of the cross terms will depend on the measuring location $\underline{x}$ (through $\psi_\alpha(\underline{x})$, $\psi_\beta(\underline{x})$), and the integral terms.

4.4.3 Background Noise

The effects of noise on the damping estimates obtained from the single-sided Fourier transform method have been discussed by Kandianis (ref. 16) for a single-degree-of-freedom system. From equation (50), noise in the excitation, if it is uncorrelated with the excitation, is additive in terms of the power spectral density functions. Noise in the response, if it is uncorrelated with the response, is additive in terms of the autocorrelation function—equation (51). Translating these effects into the single-sided Fourier transform function of equation (72), then

$$F_w(\omega) = \frac{H(\omega)}{4\zeta_\alpha\omega_\alpha^2 M_\alpha}(S_{p1}(\omega_d) + S_{p2}(\omega_d))\left(2\zeta_\alpha + \frac{i\omega}{\omega_\alpha}\right) + S_n(\omega). \tag{75}$$

The presence of the noise $p_2(t)$ in the excitation increases the coefficient of $H(\omega)(2\zeta_\alpha + i\omega/\omega_\alpha)$ but has no influence on the damping estimates. Noise $n(t)$ in the response signal shifts the plot of $F_w(\omega)$ along the real axis. In principle, if $S_n(\omega)$ is constant, the accuracy of the damping measurements is again unaltered, but, in practice, if $n(t)$ is large so that the dynamic range constraints of the instrumentation become important, accuracy may be impaired. Further, if $S_n(\omega)$ varies in the neighborhood of a natural frequency, additional errors will appear in the damping estimates.

4.4.4 Truncation Errors

Truncation errors, encountered when the excitation-response cross correlation function is transformed into the cross power spectral density function, are discussed in section 4.3.5 as an equivalent of the resolution losses associated with finite bandwidth filters. The single-sided Fourier transform method is also susceptible to truncation errors associated with the transformation of the autocorrelation function.

The truncation errors arise because it is not practical to compute the displacement auto-correlation function for infinitely long time delays. Thus, equation (71) for a single-degree-of-freedom system becomes, in practice,

$$F_w(\omega;\tau_m) = \frac{1}{2\pi}\int_0^\infty D(\tau)R_w(\tau)e^{-i\omega\tau}d\tau, \tag{76}$$

where $D(\tau) = 0$ for $\tau > \tau_m$.

Equation (76) is the direct equivalent of equation (63) for the cross-power spectral density case. Since the correlation functions in equations (63) and (76) show some differences, equation (76) will be evaluated for the case of a rectangular lag window

$$
\begin{aligned}
D(\tau) &= 1 \qquad 0 \leqslant \tau \leqslant \tau_m \\[1em]
&= 0 \qquad \text{elsewhere.}
\end{aligned} \right\} \tag{77}
$$

Assuming that the excitation has a constant power spectral density S_p, and that the system lightly damped such that $\zeta_\alpha^2 \ll 1$, then, from appendix B,

$$
\frac{1}{\rho}\frac{ds}{df} \approx \frac{-4\pi}{\omega_\alpha \zeta_\alpha}\left\{ \frac{1 - e^{-\omega_\alpha \zeta_\alpha \tau_m}\left[1 + \omega_\alpha \zeta_\alpha \tau_m(1 - \zeta_\alpha \sin\omega_\alpha \tau_m \cos\omega_\alpha \tau_m) + \frac{1}{2}\omega_\alpha^2 \zeta_\alpha^2 \tau_m^2\right]}{1 - e^{-\omega_\alpha \zeta_\alpha \tau_m}\left[1 + \omega_\alpha \zeta_\alpha \tau_m(1 - \zeta_\alpha \sin\omega_\alpha \tau_m \cos\omega_\alpha \tau_m)\right]}\right\}. \tag{78}
$$

Comparing with equation (68), it is seen that equation (78) contains an extra term $\zeta_\alpha \sin\omega_\alpha \tau_m \cos\omega_\alpha \tau_m$ in the numerator and denominator. If it can be assumed that the damping system is so small that

$$
\zeta_\alpha \sin\omega_\alpha \tau_m \cos\omega_\alpha \tau_m \ll 1,
$$

then equation (78) reduces to

$$
\frac{1}{\rho}\frac{ds}{df} \approx \frac{-4\pi}{\omega_\alpha \zeta_\alpha}\left\{ \frac{1 - e^{-\omega_\alpha \zeta_\alpha \tau_m}\left[1 + \omega_\alpha \zeta_\alpha \tau_m + \frac{1}{2}\omega_\alpha^2 \zeta_\alpha^2 \tau_m^2\right]}{1 - e^{-\omega_\alpha \zeta_\alpha \tau_m}\left[1 + \omega_\alpha \zeta_\alpha \tau_m\right]}\right\}, \tag{79}
$$

which is identical to equation (68). Thus, curves of the type shown in figures 8 and 9 can be used to estimate the truncation errors in the single-sided Fourier transform method, although it should be remembered that the condition on the damping is now, effectively, $\zeta_\alpha \ll 1$ rather than $\zeta_\alpha^2 \ll 1$.

In a similar manner, the truncation errors in the single-sided Fourier transformation with a triangular lag window will be approximately equal to those predicted by Soovere and Clarkson (ref. 19) for the cross-power spectral density function (see fig. 8).

4.4.5 Summary

The single-sided Fourier transformation method operates on the response autocorrelation function in such a manner that hidden phase angle information is exposed. For the application considered in the preceding sections, the panel response is that due solely to the aerodynamic pressure fluctuations; the introduction of a second excitation will be discussed in section 5.0.

The ability to use phase information places the single-sided Fourier transform in a similar category to the cross-power spectral density method, without the need to measure the excitation and response simultaneously. Both methods can make allowances for background noise and off-resonant vibration more easily than when only amplitude data are measured. In practice, errors arising in the single-sided Fourier transform due to noise, off-resonant vibration, and truncation effects will be similar to those encountered in the cross-power spectral density method. Correction procedures developed for the latter method can be used for the single-sided Fourier transform although now the restrictions on small damping will be slightly more severe.

5.0 NON-STEADY-STATE METHODS

5.1 INTRODUCTION

The category of non-steady-state methods includes quasi-steady-state and transient methods. Quasi-steady-state methods are usually associated with sinusoidal excitations, which are slowly swept through the frequency range of interest. Narrowband random excitation sweeps have been proposed for structural testing (refs. 21 and 22), but their application is mainly that of determining response amplitude rather than the measurement of damping. Recently, transient methods (refs. 23 and 24) have been proposed as replacements for the slow sweep rates when there is a need for a significant reduction in testing time. An example of such a test environment is the flutter testing of an airplane, where it is difficult to achieve stable flight conditions in some parts of the flight envelope. Development of the transient method has been carried out by White (refs. 14, 25, 26, and 27) and Kandianis (refs. 16 and 28), the latter having utilized random analysis methods to reduce the errors from noise interference.

With regard to the current problem of damping measurement of panels exposed to a moving airflow, the use of any non-steady-state method implies the introduction of a second excitation at a given point of application. This has the advantage of allowing selection of a suitable location for the excitation and alleviates to some extent the effect of the cross terms of the type shown in equation (20) when $\alpha \neq \beta$. The non-steady-state methods have a second common characteristic because, with the exception of the narrowband random noise sweep, which is not applicable to the present problem, the excitation in all the above methods is deterministic in form.

5.2 QUASI-STEADY-STATE EXCITATION

The use of sinusoidal excitation in the experimental determination of the natural vibration characteristics of a system has been a standard technique for many years. The technique involves a frequency sweep to determine the approximate locations of the natural frequencies, followed by a detailed frequency analysis in the neighborhood of each resonance. During the detailed analysis stage, the system is allowed to achieve steady-state vibration at each frequency before recording the response and moving to the next excitation frequency. Unfortunately, the method is very time consuming. The slow frequency sweep method was therefore introduced in an attempt to speed up the process.

In the slow frequency sweep approach the excitation frequency is slowly scanned through the range of interest, and it is assumed that the vibration attains quasi-steady-state conditions. Choice of the scanning rate depends on the natural frequencies and damping ratios of the system under investigation, and the assumption of quasi-steady-state conditions may not be valid in many cases. Several errors arise in practice. The response at resonance will be less than the steady-state maximum, and the frequency at which the maximum occurs is shifted in the direction in which the excitation frequency is changing. Additional errors are introduced by the averaging time of the function analyzer used to derive the vector diagrams. Background noise errors, similar to those encountered in the steady-state sinusoidal method, will also be present. Thus, the method has very limited application in practice.

5.3 TRANSIENT EXCITATION

5.3.1 Single Pulse

The frequency response function $H(\omega)$, which is the basis for all the damping measurements, is the Fourier transform of the impulse response function. Thus, if the system under investigation is exposed to a unit impulse, the measured response will provide a direct measurement of $H(\omega)$ and hence of the damping. In practice the unit impulse is not attainable because sufficient energy cannot be supplied to the system in an infinitesimal time period. However, an acceptable approximation can be achieved by the use of a single pulse of short duration. The use of such pulses has been discussed by White (ref. 25).

To illustrate the single-pulse method, consider a single-degree-of-freedom system, with steady-state frequency response function $H(\omega)$. If the excitation is $p(t)$ and the response is $w(t)$, then

$$H(\omega) = \frac{W(\omega)}{P(\omega)} \tag{80}$$

where $P(\omega)$ and $W(\omega)$ are the Fourier transforms of the transient excitation $p(t)$ and response $w(t)$, respectively, i.e.,

$$P(\omega) = \frac{1}{2\pi} \int_{-\infty}^{\infty} p(t)e^{-i\omega t}\, dt;$$

$$W(\omega) = \frac{1}{2\pi} \int_{-\infty}^{\infty} w(t)e^{-i\omega t}\, dt.$$

White (ref. 25) discusses several impulse shapes—rectangular, triangular, and trapezoidal—but, for current demonstration purposes, only the rectangular pulse need be considered. Then

$$p(t) = A \qquad 0 \leqslant t \leqslant T$$
$$= 0 \qquad \text{elsewhere,}$$

where T is the duration of the pulse, and

$$P(\omega) = AT \frac{\sin(\omega T/2)}{(\omega T/2)} e^{-i\omega T/2}.$$

In certain cases, when the duration of the pulse is short with respect to the shortest period present in the vibration of the system (ref. 25), only the response of the system need be analyzed without creating large errors in the measured values of the natural frequencies and damping ratios. However, it is difficult to determine the magnitude of the errors in advance, and in practice usually both the excitation and the response have to be measured. A plot of $W(\omega)/P(\omega)$ will represent the frequency response function (equation (80)), and estimates of the natural frequency and damping factor can be obtained using the Kennedy and Pancu method (ref. 4).

Although simple in concept, the single-pulse method suffers from several disadvantages which limit its usefulness in practice. If the pulse is short, to simulate an ideal impulse and

excite a wide-frequency range, the energy of excitation and vibration at a particular frequency will be low, and accurate measurements will be difficult. Secondly, it is difficult to control the frequency content of the excitation, with the result that many modes which are outside the range of interest may be excited while modes of interest may not be excited because of zeros in the excitation spectrum (see the above example). Thirdly, difficulties may arise in maintaining the pulse shape, thereby requiring measurement of the excitation signal as well as the response. Finally, noise problems will severely interfere with the accuracy of the results.

5.3.2 Pulse Train

As a modification of the single-pulse method, Reed et al. (ref. 23) have investigated the use of a series of rectangular and triangular pulses having a continuously decreasing time period. Reed et al. claim that the rectangular pulse train has a practical advantage over the triangular pulse train and the swept sine wave in that the rectangular pulses are simpler to generate. However, the rectangular pulse train suffers from the disadvantage that the energy is spread over a large frequency range. Also, pulse trains in general present many of the problems associated with the single pulse.

5.3.3 Rapid Frequency Sweep

To overcome the difficulties of frequency control, energy input, and pulse shape associated with pulse excitation, an alternative form of transient excitation, the rapid frequency sweep, has been introduced by Reed et al. (ref. 23) and Skingle (ref. 24), with further developments by White (ref. 14, 25, 26, and 27) and Kandianis (refs. 16 and 28). The rapid frequency sweep is achieved by scanning a sine wave signal from frequency ω_1 to ω_2 in a very short time period T. In contrast to the slow sweep, quasi-steady-state conditions are not assumed, the response being considered as transient in nature. Obviously there are an infinite number of ways by which the frequency can change from ω_1 to ω_2, but, for simplicity, a linear variation is considered here. Thus, the frequency of excitation can be represented by the equation

$$
\begin{aligned}
\omega &= \alpha t + \omega_1 \qquad 0 \leqslant t \leqslant T \\
&= 0 \qquad\qquad \text{elsewhere.}
\end{aligned}
\tag{81}
$$

The excitation signal is then

$$
\begin{aligned}
p(t) &= p_0 \sin \int_o^t (\alpha t + \omega_1)\, dt \\
&= p_0 \sin\left(\frac{\alpha}{2} t^2 + \omega_1 t\right) \qquad 0 \leqslant t \leqslant T \\
&= 0 \qquad\qquad\qquad\qquad \text{elsewhere.}
\end{aligned}
\tag{82}
$$

As is the case for the pulse methods, the excitation and response signals are deterministic, and the steady-state frequency response function can be obtained by means of equation (80).

The Fourier transform $P(\omega)$ of $p(t)$ is a complicated function, and the characteristics of the spectral amplitudes have been summarized by White (ref. 27). The spectrum amplitude is not constant within the frequency range ω_1 to ω_2 but has two peaks, one at a frequency of $\omega_1 + 1.2 \sqrt{\alpha/2}$ and the other at a frequency of $\omega_2 - 1.2 \sqrt{\alpha/2}$. The mean amplitude of the spectrum is $\pi/2\alpha$ and the height of each peak is 1.4 times the mean amplitude. Between the two peaks, the spectrum is oscillatory about the mean value, the amplitude of the oscillation being proportional to $1/\sqrt{T}$. For given values of ω_1 and ω_2, a long duration time T can be selected so that the spectrum amplitude is large enough to avoid problems of signal-to-noise ratio and to reduce the spectral ripple to an acceptable value. The cutoff rate of the spectrum at ω_1 and ω_2 is high.

Instrumentation to produce the rapid frequency sweep has been developed by White (ref. 27), and the modulus of the Fourier spectrum for the excitation shows characteristics similar to those described above. The phase spectrum is very irregular.

In practical applications, the transient method involves problems similar to those encountered in the steady-state methods. This is not surprising, since the problems are all related to Fourier transformation of the impulse and frequency response functions $h(\tau)$ and $H(\omega)$ and to the presence of noise in the excitation and response signals.

The resolution of close natural frequencies is one example of a common problem. In practice this has been interpreted as a requirement on frequency resolution in the power spectral density analysis, and as a specification of the maximum time delay for the autocorrelation function. For the latter case it was shown (equation (44)) that the displacement autocorrelation function for two signals $A_\alpha \sin [\omega_d \tau + \theta]$ and $A_\beta \sin [(\omega_d + \omega')\tau + \theta]$ was

$$R_w(\underline{x}, \tau) = (A_\alpha^2 + A_\beta^2 + 2A_\alpha A_\beta \cos \omega' \tau)^{1/2} \sin (\omega_d \tau + \theta + \phi(\tau)) \qquad (83)$$

for $\tau > 0$, and

$$\tan \phi(\tau) = \frac{A_\beta \sin \omega' \tau}{A_\alpha + A_\beta \cos \omega' \tau}.$$

White (ref. 26) has shown that for the corresponding impulse case, where the total impulse function is

$$h(t) = h_1(t) \pm h_2(t)$$

and

$$h_1(t) = a_1 \sin \omega_1 t$$

$$h_2(t) = a_2 \sin (\omega_1 + \omega')t,$$

then

$$h(t) = (a_1^2 + a_2^2 + 2a_1 a_2 \cos \omega' t)^{1/2} \sin (\omega_1 t \pm \phi_1(t)), \qquad (84)$$

where

$$\tan \phi_1(t) = \frac{a_2 \sin \omega't}{a_1 \pm a_2 \cos \omega't} .$$

The similarity between equations (83) and (84) is immediately apparent. Positive and negative signs in equation (84) are required to take into account the initial phase difference (0 or π) between $h_1(t)$ and $h_2(t)$, but this is not necessary in the random excitation case.

For equations (83) and (84) the maximum time delay has to be sufficiently long to identify the frequency ω'. This was demonstrated in figures 6 and 7 for the autocorrelation function. Under ideal conditions the choice of maximum time delay τ_m is solely a matter of convenience, but in practice it may be dictated by the dynamic range of the analysis equipment (ref. 26) or by computer storage problems. When severe truncation occurs, the errors involved in the estimation of the damping from the measured locus of $W(\omega)/P(\omega)$ are similar to those in the cross-power spectral density (sec. 4.3.5) and single-sided Fourier transform (sec. 4.4.4) methods. Correction curves derived from equation (68), examples of which are contained in figure 8, can be used to improve the accuracy of the damping estimates from the single-sided Fourier transform.

One important problem, which is difficult to solve by means of the deterministic approach to the transient excitation method, is that of noise interference in the excitation and response signals. Examples of the distortion in the frequency response function, obtained by means of equation (80) when noise is present, are shown in reference 16. Since the noise is usually random in nature, Kandianis (ref. 16) has applied random analysis methods to the system which, with the exception of the noise, is deterministic in nature. Kandianis discusses two possible approaches. The first one computes the power spectral density of the response, including the effects of the noise signals. Instead of equation (80) for the Fourier components, the power spectral density for the displacement is given by an equation similar to that obtained by combining equations (22) and (23). Thus, the displacement power spectral density function for mode α of the panel is

$$S_w(\underline{x},\omega)_\alpha = \psi_\alpha^2(\underline{x}) \, |H_\alpha(\omega)|^2 \left\{ \psi_\alpha^2(\underline{x}'') \, S_{p2}(\omega) + \frac{1}{4} A^2 S_{p1}(\omega) \, J_{\alpha\alpha}(\omega) \right\} + S_n(\omega), \qquad (85)$$

where $S_{p2}(\omega)$ is the power spectral density for the transient excitation applied at $\underline{x}''$, $S_{p1}(\omega)$ is the power spectral density for the noise in the excitation (in the present context this is the turbulent boundary layer pressure field), and $S_n(\omega)$ is the noise in the response signal. It is assumed that $p_1(\underline{x}'', t)$, $p_2(\underline{x}'',t)$, and $n(t)$ are statistically independent.

One word of caution is appropriate at this stage. The analysis of Kandianis assumes that the excitation signal is stationary and, at a later stage in the single-sided Fourier transformation analysis, that the excitation is white noise. This assumption is valid only with certain restrictions. Skingle (ref. 24) shows that, under certain assumptions, the autocorrelation function for the rapid frequency sweep signal can be written in the approximate form

$$R_{p2}(\tau) \approx \frac{\sin(\omega_2 \tau)}{(\omega_2 \tau)}, \qquad (86)$$

where ω_2 is the upper cutoff frequency and the lower frequency ω_1 is assumed to be zero. Equation (86) can be interpreted as implying that there is constant power spectral density in the excitation. Referring to the notation of equation (81), the assumptions associated with equation (86) are that

$$\alpha \tau^2 \ll 1 \qquad \text{and} \qquad \alpha T^2 \ll 1,$$

which in turn imply that $T^2 \gg \tau^2$. Thus, the assumption that the transient signal represents white noise is valid only if the maximum time delay in the autocorrelation function is small with respect to the duration of the frequency sweep.

The second approach used by Kandianis (ref. 16) is the single-sided Fourier transform of the autocorrelation function. The response autocorrelation function obtained from the transient excitation in the presence of noise is similar to that encountered in the analysis of the autocorrelation function associated with boundary-layer-induced vibration (sec. 4.2.5) and suffers from the same experimental problems. Thus, Kandianis proposed the single-sided Fourier transform method. The analysis of the method has been discussed in section 4.4 with reference to the response to the turbulent boundary layer, and there is no need to repeat the analysis in this section. The main difference between the two approaches is that in section 4.4 the turbulent boundary layer represented the excitation of interest and all other signals were noise, whereas in the present case the rapid frequency sweep represents the signal of interest and the turbulent boundary layer is classified as noise.

Combining the results of equations (74) and (75), the single-sided Fourier transform of the displacement autocorrelation function will be:

$$
\begin{aligned}
F_w(\omega) = \sum_\alpha & \frac{(2\zeta_\alpha + i(\omega/\omega_\alpha))\psi_\alpha^2(\underline{x})\, H_\alpha(\omega)}{4\zeta_\alpha \omega_\alpha^2 M_\alpha} \Bigg\{ \psi_\alpha(\underline{x}'')\, S_{p2}(\omega_d) \\
& + \int_A \int_A \psi_\alpha(\underline{y}')\, \psi_\beta(\underline{y}'')\, C_{p1}(\underline{y}',\underline{y}'',\omega_d)\, d\underline{y}'d\underline{y}'' \Bigg\} \\
& + \sum_\alpha \sum_\beta \frac{\psi_\alpha(x)\psi_\beta(x)\, H_\alpha(\omega)}{M_\beta\, |D_{\alpha\beta}|} \Bigg\{ \left(\cos\theta_{\alpha\beta} + \frac{\zeta_\alpha \omega_\alpha + i\omega}{\omega_d}\sin\theta_{\alpha\beta}\right) \\
& \int_A \int_A \psi_\alpha(\underline{y}')\, \psi_\beta(\underline{y}'')\, C_{p1}(\underline{y}',\underline{y}'',\omega_d)\, d\underline{y}'d\underline{y}'' + \left(\frac{\zeta_\alpha \omega_\alpha + i\omega}{\omega_d}\cos\theta_{\alpha\beta} - \sin\theta_{\alpha\beta}\right) \\
& \int_A \int_A \psi_\alpha(\underline{y}')\, \psi_\beta(\underline{y}'')\, Q_{p1}(\underline{y}',\underline{y}'',\omega_d)\, d\underline{y}'d\underline{y}'' \Bigg\} + S_n(\omega).
\end{aligned}
\tag{87}
$$

The function $F_w(\omega)$ still contains cross terms ($\alpha \neq \beta$) associated with the boundary layer spatially distributed excitation. However, the single-point transient excitation does not introduce additional cross terms, with the consequence that the relative importance of the cross terms in equation (87) is less than in equation (74), where only boundary layer excitation is present.

Truncation effects associated with the single-sided Fourier transform, and discussed in section 4.4.4, will be applicable to the transient excitation case also.

5.4 SUMMARY

The non-steady-state methods discussed in section 5.0 cover a wide range of excitation signals. However, the practical value of several of these signals is very limited because of interference effects from noise in the excitation or response. All the methods are associated with deterministic excitation signals, and there are difficulties in coping with random noise interference unless random data analysis methods are adopted.

For the methods discussed, the rapid frequency sweep method provides the best frequency control without having to assume quasi-steady-state conditions. In addition, the rapid sweep method can be incorporated with random analysis techniques, provided that the maximum time delay in the correlation functions is small relative to the time period of the sweep. Two steady-state random methods—power spectral density and single-sided Fourier transform of the autocorrelation function—have been considered, and the practical problems are very similar to those discussed in section 4.0 for steady-state excitation. Within the same constraints on time delay, the excitation-response cross-power spectral density method provides a third approach for transient excitation, and the problems encountered in practice would again be similar to those for the corresponding steady-state excitation method.

6.0 COMPARATIVE EVALUATION OF METHODS OF DAMPING MEASUREMENT

In sections 4.0 and 5.0, several methods of measuring the damping of a system have been analyzed on an individual basis. Each method is found to have a number of associated problems that, in practice, limit the useful range of test conditions. As a consequence, no method is applicable to all test conditions. Thus, for a particular experiment, the applicability of each method has to be evaluated and the most suitable method(s) selected. An evaluation of this sort will be carried out in this section, with specific reference to the test conditions associated with the vibration of panels exposed to a moving airstream.

First it is appropriate to restate the experimental conditions under which the selected method of damping measurement will be applied. Damping measurements are to be made on rectangular panels that will be mounted in the wall of a wind tunnel. One face of the panel will be exposed to turbulent boundary layer pressure fluctuations in the wind tunnel, and the other face will be enclosed in a chamber whose volume can be adjusted within a certain range. The tunnel will be operated under stable flow conditions. Panel dimensions, at least in the initial phases of the experimental program, will not exceed 30.48 cm (12 in.) in length or breadth.

In this section, the damping measurement methods will be compared and evaluated on the basis of the theoretical analyses in sections 4.0 and 5.0, with constraints imposed by the above experimental conditions. Experimental support for the selected methods will be presented in section 7.0, although the test setup in that section will not attempt to reproduce the conditions described above.

Several requirements that the selected methods must satisfy can be identified immediately. These requirements are:

a) The method must be able to exclude, or correct for, background noise in the excitation and response signals.

b) The method must be able to exclude, or correct for, off-resonant vibration in neighboring modes.

c) The method must not require simultaneous measurement of the boundary layer excitation and the associated panel vibration, although independent measurements may be necessary.

d) The required instrumentation must be compatible with the space restrictions imposed by the test chamber.

Referring to the analyses in sections 4.0 and 5.0, requirement a) disqualifies the non-steady-state methods, with the exception of the rapid frequency sweep method, which uses the power spectral density function or the single-sided Fourier transformation of the auto-correlation function. The response autocorrelation function for boundary layer excitation is eliminated by requirements a) and b), and the excitation-response cross-power spectral density method, using turbulent boundary layer excitation, is eliminated by requirement c). A

combination of requirements a) and d) causes the rejection of the cross-power spectral density method when a second excitation is introduced.

The methods still retained are the power spectral density and single-sided Fourier transform methods associated with either boundary layer or transient excitation. Retention of the power spectral density method may appear surprising at first, since many of the other methods have been introduced in the past as improvements over the power spectral density approach. Thus, some explanation of the decision is necessary.

The two main criticisms of the power spectral density method concern the difficulties of separating resonant vibration from off-resonant vibration and background noise. Difficulties that may have been encountered in the past because of too wide a filter bandwidth can be adequately overcome with the narrow bandwidths now available through digital analysis and the use of correction terms. The use of these same narrow filter bandwidths enables the separation of close natural frequencies, but there still exists the problem of off-resonant vibration and background noise at a natural frequency. Methods can be devised to correct for the errors imposed by these interference signals, and one such method has been discussed in section 4.0. Although rather crude in form, the correction procedure appears fairly satisfactory, particularly if used in conjunction with the optimum positioning of the measuring transducer. The more sophisticated methods, which have been proposed as improvements over the power spectral density approach, are correspondingly more sensitive to experimental scatter.

The comparison has now reduced to one of steady-state random excitation versus rapid frequency sweep. Historically, transient excitation methods were introduced for use in experimental conditions that are stable for only short periods of time. Since the present test conditions are stable over relatively long periods, the basic property of the transient excitation cannot be classified as an advantage. Further, the method involves the introduction of a second excitation, with accompanying instrumentation problems, and a severe signal-to-noise ratio problem because the boundary layer induced vibration is now regarded as noise. The transient excitation has to be transmitted to the test panel and, unless a suitable choice of panel material has been made, some mass loading of the panel may be necessary.

However, the transient method possesses advantages associated with single-point excitation. Mode isolation can be controlled to a certain extent by choice of excitation location, although the benefits of the technique are limited by the presence of the boundary layer induced vibration. Also, single-point excitation does not introduce cross-term contributions in the response spectra, so the adverse effects of the cross terms ($\alpha \neq \beta$), induced by the spatially distributed boundary layer excitation, are reduced. In addition, the rapid frequency sweep method uses deterministic excitation, thereby tending to reduce the experimental scatter in the measurements. The sinusoidal nature of the excitation allows concentration of the excitation energy at selected frequencies and improves the signal-to-noise ratio.

Basically, the steady-state and rapid frequency sweep methods appear to offer similar degrees of accuracy in the damping measurements. Thus, the instrumentation requirements will play a major role in determining the most suitable method. Using this as the criterion, the power spectral density and single-sided Fourier transform methods associated with turbulent boundary layer excitation were selected for subsequent experimental demonstra-

tion. The instrumentation requirements are no different from those normally associated with the measurement of structural response to turbulent boundary layer excitation, and the panel displacement power spectrum due to boundary layer excitation is an immediate byproduct of the damping measurements. The theoretical analysis does not indicate the superiority of either the power spectral density method or the autocorrelation single-sided Fourier transform method, with the consequence that both methods are selected for experimental testing.

7.0 DATA REDUCTION REQUIREMENTS

7.1 INTRODUCTION

Many of the methods of damping measurement discussed in sections 4.0 and 5.0, including both of the methods selected in section 6.0, require random process techniques for data analysis. It is possible that analog or digital techniques could be used, but, for damping measurements, digital methods are recommended because of the greater flexibility in choice of filter bandwidth and other characteristics and because the digital methods are usually more economical. For some of the Fourier transformation calculations, digital techniques of data reduction are almost essential.

The use of digital data reduction methods introduces a number of requirements on data sample length, digitization rate, filter bandwidth, etc., and some comments on the requirements are necessary to show their influence on the measured damping. For this reason, the present section will provide a general discussion on the requirements. Comprehensive discussions of digital data reduction techniques, as applied to random time series, can be found in references 20, 29, 30, and 31.

The data reduction scheme followed in the demonstration experiment, which can be considered as a typical procedure, is shown in the flow chart in figure 10. The data reduction is carried out in four stages that are strongly interdependent, the output of one stage being the input of the next. Thus, even the last step in the data reduction cycle can impose restrictions on the data acquisition. As an example, the required statistical reliability of the estimated response power spectral density will determine the initial length of the data recording. Although some of the data reduction requirements may be peculiar to the current data analysis technique, most requirements will be common to all similar damping measurement experiments.

7.2 DISCRETE FOURIER TRANSFORMS

A function $p(t)$, continuous in time t, can be represented by a series of discrete samples $p(n,t)$ in time. Generally, the discrete points p_n are sampled at equal time intervals $\Delta\tau$, and the sampling rate s is defined as $s = 1/\Delta\tau$. If N discrete points $p_n = p(n,\Delta\tau)$ are given for $n = 1,2,...N$, then the time series is known in a finite time interval ΔT where $\Delta T = N \cdot \Delta\tau$, and ΔT can be referred to as a "subinterval." An infinite discrete time series can be obtained by letting $N \to \infty$. The complex Fourier amplitude of a continuous function $p(t)$ is given by equation (10) as

$$P(\omega) = \frac{1}{2\pi} \int_{-\infty}^{\infty} p(t)e^{-i\omega t} dt$$

or

$$P(f) = \int_{-\infty}^{\infty} p(t)e^{-i2\pi ft} dt \tag{88}$$

The equivalent of equation (88) in a finite discrete time series is

$$P_k = P(k, \Delta f_F) = \frac{1}{N} \sum_{n=-N/2}^{\frac{N}{2}-1} p_n \, e^{-i2\pi kn/N} \tag{89}$$

where N is an even integer and the fundamental frequency interval

$$\Delta f_F = \frac{1}{\Delta T} = \frac{1}{N \cdot \Delta \tau} \tag{90}$$

For $k = 0$, P_0 gives the mean of p_n. It can be shown that $-N/2 \leqslant k \leqslant N/2$, i.e., the number of distinct Fourier amplitudes P_k is equal to the number N of discrete samples in time p_n. Thus, ΔT determines the frequency resolution and $s = 1/\Delta \tau$ determines the maximum frequency $f_{max} = N \cdot \Delta f_F/2$. The Fourier amplitude P_k will have a frequency window of the form $(\sin \Delta f_F)/\Delta f_F$.

If the direct method of calculating power spectral density is used, as indicated by equation (12), then the power spectral density of p_n is given by

$$S_k = S_k(k, \Delta f_F) = P_k P_k^* \tag{91}$$

where the asterisk denotes the complex conjugate. The Fourier amplitude and the complex conjugate will each have a frequency window of the form $(\sin \Delta f_F)/\Delta f_F$. Thus, the spectral window of the estimate of the power spectral density S_k will be of the form $[(\sin \Delta f_F)/\Delta f_F]^2$, and has an associated triangular, or Bartlett, lag window.

When the power spectral density $S_k(k, \Delta f_F)$ is obtained by means of the direct method of equation (91), the autocorrelation function $R_n = R_n(n, \Delta \tau)$ is computed by transforming $S_k(k, \Delta f_F)$. The autocorrelation function will be given in the time interval $-N/2 \cdot \Delta \tau \leqslant t \leqslant N \cdot \Delta \tau/2$, at discrete time lags $\Delta \tau$, and the transformation process will incorporate the above triangular lag window.

The single-sided Fourier transform of the discrete autocorrelation coefficients can be represented by equation (89). Therefore, the calculated single-sided Fourier transform will have a spectral window of the form $(\sin \Delta f_F)/\Delta f_F$ and the description that follows equation (89) will also be applicable. Computer programs that use the fast Fourier transform algorithm to calculate power spectral density, autocorrelation, and single-sided Fourier transform functions will introduce the above characteristics into the computed functions.

7.3 DATA REDUCTION REQUIREMENTS

There are several data reduction requirements. Some are peculiar to digital analysis, while others are common to all random data analysis techniques—digital or analog. These requirements are discussed below.

7.3.1 Filter Bandwidth

Errors introduced by finite bandwidths of the analyzing filters are discussed in section 4.0, where it is shown that, for rectangular filters, a bandwidth that is half of the measured resonance bandwidth, will introduce an error of about 14% in the estimated damping factor. Theoretically, corrections can be applied to measured damping factors obtained by means of any filter bandwidth, but in practice the correction procedure has acceptable accuracy only if the errors are relatively small. Thus, for power spectral density measurements, a filter bandwidth requirement can be specified as $\Delta f_F \leq \Delta f_M/2$. Obviously, some prior knowledge of the damping in the system is required, or an iteration method has to be applied in the selection of Δf_F.

For a given set of digitized data, the effective filter bandwidth will be a function of the time length of the data sample and the digital analysis process used in the computation. The frequency-dependent function will be obtained from a time series that can be either the original data or a correlation function. Fourier transformation from time to frequency domains will be performed with some time or lag window because of the finite limits on the time series. This lag window will, in turn, determine the characteristics of the spectral window or filter in the frequency domain, as indicated in reference 20. For example, a rectangular lag window of width ΔT has a spectral window of equivalent width equal to $1/\Delta T$. Lag windows, such as triangular, Hanning, Hamming, and Parzen windows, have the effect of improving the statistical reliability of the data but increase the effective bandwidth of the filters for a given value of ΔT. The advantage of these nonrectangular lag windows lies in the reduced amplitude of the filter side lobes.

7.3.2 Total Sample Length

The length of the data samples used in the random analyses will influence the statistical reliability of the reduced data; the shorter the sample length the lower will be the reliability. However, long samples require long processing time, and a compromise has to be reached between long sample length and practical limitations on cost and computer core storage requirements.

The reliability of the power spectral density estimate is characterized by the normalized standard error ϵ where

$$\epsilon = \frac{1}{\sqrt{\Delta f_F \cdot T}} \tag{92}$$

If the total sample length T consists of V subintervals, each of length ΔT, then $T = V \cdot \Delta T$ and, using equation (90),

$$\epsilon = \frac{1}{\sqrt{V}}$$

Thus, in practice, statistical scatter can be reduced by increasing the number of subintervals, or subspectra, used to obtain an ensemble average. The effect is illustrated in figure 11, where the four power spectra are calculated using four different values of V, i.e., V = 9, 25, 50 and 100 (ϵ = 0.33, 0.2, 0.14, and 0.1). For V = 9 (fig. 11a), resonance peaks in the vicinity of

1000 Hz are completely obscured by the statistical scatter. As V increases, the statistical scatter is reduced and the peaks are better defined. The statistical scatter in the power spectral density will introduce equivalent scatter in the autocorrelation and the single-sided Fourier transform functions. Thus, when filter bandwidth requirements are specified, based on considerations stated in earlier sections, the total sample length requirements can be estimated so that a desired degree of statistical reliability can be achieved.

When the vibration spectrum is obtained by an ensemble average of a series of sub-spectra, the vibration autocorrelation function is calculated from the average spectrum by means of the inverse Fourier transformation. This method reduces the statistical scatter in the autocorrelation function, with a minimum of computer operating time.

7.3.3 Digitization Rate

Analog-to-digital conversion of a signal requires the selection of a digitization or sampling rate s that is determined by the upper frequency of interest in the spectral analysis. Too low a sampling rate will introduce aliasing errors in the spectrum, but too high a sampling rate will lead to problems in data handling and economics. Thus, a compromise is again required. For Fourier analysis of a time series using the fast Fourier transform algorithm, the relation between the upper frequency of interest f_{max} and the lowest acceptable sampling rate is given as $s = 2f_{max}$, but, in practice, a higher sampling rate is necessary. Aliasing errors will depend on the spectral content of the signal to be analyzed, but, in general, for stationary time series analysis, a sampling rate of $s = 2.5f_{max}$ is adequate.

7.3.4 Number of Data Points

The filter bandwidth and sampling rate together determine the number of data points to be used in the calculations. Thus, the number of data points N is given as $N = \Delta T/\Delta \tau = s/\Delta f_F$ when $\Delta f_F = 1/\Delta T$. The fast Fourier transform algorithm requires that the number, L, of data points used in the transform be an integer power of 2, i.e., $L = 2^j$ where j is a positive integer. If $N < L$, then $(N - L)$ zeros are added to the data points and the calculation carried through with L points. The addition of zeros to the time series will not change the filter band-width since this is still a function of the original sample length ΔT. However, the presence of the zeros will change the frequency interval $\Delta f'$ at which the Fourier transform is calculated since $\Delta f' = 1/\Delta T'$ where $\Delta T'$ is the sample length after the addition of the zeros. Obviously, selection of the number of zeros is again a compromise, with computer storage and cost providing a constraint.

The addition of zeros to reduce the frequency interval has been used in the single-sided Fourier transform method (ref. 26) for the analysis of ship vibration.

8.0 DEMONSTRATION EXPERIMENTS

8.1 TEST OBJECTIVES

Two methods—the response power spectral density method and the response autocorrelation single-sided Fourier transform method—have been selected in section 6.0 as being the most suitable for the measurement of damping in panels exposed to a moving airflow. These two methods have been used to calculate damping factors of a rectangular panel from data obtained in laboratory demonstration experiments. The primary objective of the experiments is the demonstration of the validity of the two selected methods under laboratory conditions, with a secondary objective being the illustration of the various errors and limitations discussed in the analytical investigation. Both objectives are essentially met by the demonstration experiments described in the following sections.

8.2 DESCRIPTION OF DEMONSTRATION EXPERIMENTS

8.2.1 Introduction and Planning

Typical work elements of the demonstration experiments are shown in the flow diagram in figure 12. The experiments can be divided into three parts:

a)   Fundamental vibration characteristics of the test panel. (Analytical and experimental determination of natural frequencies and mode shapes.)

b)   Measurement of panel damping using discrete frequency excitation. (These values of the damping are used as standards in the evaluation of the random excitation methods.)

c)   Measurement of panel damping using random excitation.

The test specimen chosen for the experiments was a 30.48- by 17.78- by 0.127-cm (12- by 7- by 0.05-in.) rectangular aluminum panel with clamped boundaries. The 20 lowest natural frequencies of the panel were calculated using Warburton's method (ref. 32), and these are listed in table I. It can be seen that the test panel possesses some modes whose natural frequencies are fairly well isolated, e.g., modes (1,1), (2,1), and (3,1), and other modes with close natural frequencies, e.g., modes (4,2), (5,1), and (1,3) and modes (5,2), (3,3), and (6,1). Thus, the two methods of damping measurement can be evaluated for single modes and for closely spaced groups of modes.

As is anticipated from section 3.1, the damping of the test specimen is very low. Since this low damping is not necessarily typical of all environments likely to be encountered in the wind tunnel, it was considered that the damping measurement methods should be evaluated also under conditions of relatively high damping. To this end, the demonstration was carried out first on the bare panel and then repeated with a single layer of damping tape (table II) applied to one surface of the panel. The damping tape increased the panel damping by an

order of magnitude and permitted evaluation of the measurement techniques over a wide range of values for the damping factor. In the present discussion, therefore, the high and low damping cases will refer to the test panel with and without damping tape, respectively. The application of the damping has only a small effect on the panel natural frequencies. Based on the change in total surface density, the calculated natural frequencies will change by a factor of 0.943.

To make a consistent evaluation of the selected methods, it is essential that there be no change in damping of the test panel when the excitation changes from discrete frequency to random. This can be achieved with certainty only if the same means of excitation is used for both test conditions, and it is for this reason that turbulent airflow was not used as the source of the random excitation. There was no guarantee that the acoustic radiation damping would not change in the presence of the airflow.

Two possible excitation methods, single point or distributed loading, were available for the experiment. Single-point excitation has the advantage that selected modes can be excited or suppressed. However, since the panel material was aluminum, noncontacting magnetic excitation could not be used and single-point excitation would have involved mass loading of the panel. Acoustic excitation does not have the modal selectivity of single-point loading but is more typical of the loading distribution imposed by a moving airstream. Furthermore, the two selected measurement methods do not specifically require point excitation. Thus acoustic plane wave excitation was chosen for the demonstration experiments.

Knowledge of the panel mode shapes is highly desirable, even essential, if reasonable accuracy is to be achieved in the damping estimates. Identification of the nodal and antinodal lines allows selection of the measuring transducer locations so that vibration in a particular mode can be given preference. Qualitative information, such as that obtained from Chladni or nodal patterns, is sufficient for the selection of the measurement positions.

8.2.2 Experimental Setup and Instrumentation

A block diagram of the experimental setup and instrumentation is shown in figure 13. The aluminum test panel was mounted on a heavy pedestal such that it could be excited by acoustic waves with angles of incidence varying from grazing to normal by changing the orientation of the acoustic horn and panel. The test panel could be mounted in the vertical or horizontal plane, the horizontal plane being used only when obtaining the Chladni figures. The excitation was either single-frequency (pure-tone) or band-limited white-noise acoustic waves, and the intensity of the excitation was controlled by means of the voltage across the acoustic horn.

The panel response was measured in terms of displacement, using a noncontacting Photocon proximity transducer, Model PT5, which was mounted on a traverse bar. It was possible to locate the probe at any position over the plate, with the gap between the probe and the test panel adjusted to any desired value. The gap between the probe and the test panel at rest was chosen as 0.076 cm (0.03 in.) to provide the required sensitivity for the displacement measurements. The Photocon proximity probe was calibrated, and the ac voltage output of the probe provided a measure of the displacement of the panel.

The excitation signal could be measured either in terms of the voltage input to the driver unit of the acoustic horn or in terms of the acoustic output of the horn. To measure the sound field, a 1/4-inch-diameter Bruel and Kjaer microphone was located near the horn exit. When a band-limited white-noise signal was applied to the driver unit the acoustic pressure field in the neighborhood of the test panel had a power spectral density that was flat to within ±5 dB in the frequency range of 200 to 2000 Hz and ±2 dB in any octave band in this frequency range. The horn response did not contain sharp spikes but varied slowly with frequency. In the vicinity of any panel natural frequency, the horn response could be considered to be flat.

During the discrete frequency tests, the phase angle between the voltage input to the horn and the voltage output of the proximity or displacement probe was measured in addition to the amplitudes of the two signals. The data were analyzed on line. For the random excitation methods, the voltage input to the driver, the acoustic output of the horn, and the panel response were recorded on magnetic tape to provide an analog source tape. The analog signals were subsequently passed through an analog-to-digital converter to produce a digital data tape. A CDC 6600 digital computer was used to process the digitized data.

The experiments were conducted in an acoustical test room where the acoustic environment could be controlled.

8.3 EXPERIMENTAL PROCEDURE

8.3.1 Preliminary Experiments

The preliminary experiments included experimental determination of the natural frequencies, qualitative estimates of mode shapes by means of Chladni figures, determination of suitable angles of incidence of the acoustic waves for exciting desired modes, and coarse estimates of the half-power bandwidths of a few modes. Using acoustic waves of grazing incidence, it was possible to excite all mode orders in the direction of propagation of the acoustic waves. Therefore, waves of grazing incidence propagating along the length of the panel were used in most of the investigation. Only when obtaining the Chladni figures for modes with even order along the width of the panel was the excitation changed such that waves of grazing incidence would propagate along the width.

To obtain the nodal line patterns (Chladni figures) for the test structure, the panel was mounted horizontally and white, dry sand or fine aluminum filings were spread thinly on the panel surface. The panel was excited at each natural frequency in turn, and the nodal pattern was photographed when the excitation was turned off.

Figure 14 shows Chladni figures for the bare panel. Chladni figures for the panel with damping tape are almost the same as the corresponding figures for the panel without tape. Thus, the patterns shown in figure 14 can be considered as representative of the low and high damping conditions. The irregular nodal patterns that occur at some natural frequencies are most likely due to inhomogeneities in the thickness and flatness of the panel and to initial stresses. However, for the present demonstration, these details are irrelevant.

One peculiarity observed during the preliminary experimental stage is worthy of comment. In the process of obtaining a quick estimate of the half-power bandwidth of the (2,1) mode for the low damping case, the response amplitude varied significantly even when the amplitude and frequency of the excitation were held constant. A systematic investigation of the phenomenon ruled out the possibility of drift in the measuring instruments, and it was deduced that the variation in the amplitude was inherent to the panel response and was due to drift in natural frequency. The frequency drift (measured via variation of response amplitude as indicated above) showed a strong dependence on the peak response amplitude. When the panel displacement was slowly increased, the first noticeable occurrence of the drift was observed at a peak amplitude of about 0.0102 mm (0.0004 in.). The drift increased significantly when the peak displacement exceeded 0.025 mm (0.001 in). but no drift was observed below 0.0076 mm (0.0003 in.) peak displacement. Therefore, the excitation was adjusted to give a peak displacement of less than 0.0076 mm (0.0003 in.). A similar, but less pronounced, frequency drift was observed for mode (1.1). No frequency drift was observed for the high damping case.

8.3.2 Discrete Frequency Excitation

For this phase of the experiment, similar procedures were used for the high and low damping cases. The panel was excited by a pure tone at the natural frequency of a mode under investigation. The measuring displacement probe was located at an antinode of the mode, the location being selected by means of the previously obtained Chladni figures. The excitation was then adjusted such that the peak deflection at resonance was less than 0.0076 mm (0.0003 in.). For the higher order modes and for the high damping case, the maximum allowable input voltage to the driver was often the limiting factor; under these conditions, the peak deflection was substantially less than 0.0076 mm (0.0003 in.). The response amplitude and the phase with respect to the excitation were measured at a series of frequencies in the vicinity of the resonance. For a few selected modes, the excitation frequency was varied in both ascending and descending directions to ensure repeatability.

In the case of a mode with a natural frequency close to other natural frequencies, the contributions from other modes were minimized by locating the measuring probe on or near nodes of the undesired modes. In such a case, the probe may be located off the antinode of the mode under investigation. For example, when investigating mode (6,1), the measuring probe was located at $x_1 = 8.89$ cm (3.5 in.), $x_3 = 11.43$ cm (4.5 in.) so that the contribution of the (3,3) mode was eliminated, the probe being located on a node line of the (3,3) mode (see fig. 14), and the contribution of the (5,2) mode was minimized. Similarly, when investigating the (5,2) mode, the contribution of the (3,3) mode was eliminated by locating the probe at $x_1 = 12.07$ cm (4.75 in.), $x_3 = 13.34$ cm (5.25 in.). Measurement locations used during the discrete frequency test are given in table III.

The effects of background noise and off-resonant contributions have been discussed in section 4.0. To obtain estimates of the magnitude of these contributions in the displacement spectra, the response spectra were investigated on either side of each natural frequency, and the spectral minima adjacent to each natural frequency were identified. The spectral densities and frequencies associated with these minima were recorded.

8.3.3 Random Excitation

A procedure similar to that described above for discrete frequency excitation was used for the random excitation, except for the following two differences: (1) band-limited white noise was substituted for the pure tone and (2) the excitation, the response, and the input voltage to the driver of the acoustic horn were recorded on a magnetic tape to produce an analog source tape. Measurement locations and excitation bandwidths are given in table IV.

Reduction of the random data for the demonstration experiment was carried out in four steps: data acquisition and recording to produce the analog tape, analog-to-digital conversion, use of a computer program to calculate the displacement power spectral density and autocorrelation functions, and, finally, calculation of the single-sided Fourier transform of the autocorrelation function. The procedure is the same as that outlined in figure 10.

The voltage signals representing the panel displacement, acoustic excitation, and current supplied to the driver unit of the acoustic horn were recorded on magnetic tape at a tape speed of 152 cm/sec (60 in./sec), to produce the analog source tape. The analog tape was then replayed into digitizing equipment to produce a digital tape. Since the maximum frequency of interest was specified as 2000 Hz, a digitization rate of 8000 samples per second was used. This satisfied the condition $s > 4f_{max}$, required by the single-sided Fourier transform computations (see below), for all run conditions. Digitizing rates less than 8000 samples per second could be used if $f_{max} < 2000$ Hz, and these lower sampling rates were obtained from the original digitized data by means of a decimation process. However, the condition $s < 4f_{max}$ was always satisfied. A total of 60 sec of data was recorded for each test run and, from this, a total of 54 sec was digitized.

For the high damping case, all data runs were averaged over 50 subspectra. Thus, the normalized standard error ϵ of the power spectral density estimates was about 0.15 for the high damping case. When the low damping data reduction was carried out, the maximum available sample time length of 54 sec became a critical factor, and in only three runs (7A, 7B, and 8B) could the spectra be computed by averaging 50 subspectra. A smaller number of subspectra was used in all other low damping runs.

Filter bandwidth requirements are extremely critical at low frequencies in the low damping case. For example, in modes (2,1) and (3,1), filter bandwidths of 0.35 and 0.9 Hz are desirable. However, the limited data sample length of 54 sec was not sufficient to provide acceptable statistical scatter ($\epsilon < 0.15$) for such narrow filter bandwidths, so a larger bandwidth of about 1.0 Hz was used. Filter bandwidth did not pose a problem for the high damping results, the condition $\Delta f_F < \Delta f_M/2$ being satisfied in all cases.

The computer program used to calculate the single-sided Fourier transform imposed additional constraints on the data. The program was checked with respect to known analytical functions and it was found that, for a transformation error of less than 1%, Δf_F should be less than $\Delta f_M/4$ and digitizing rate s should be greater than $4f_{max}$. For an error of less than 15%, $\Delta f_F < \Delta f_M/2$ and $s > 4f_{max}$. In the computation of the single-sided Fourier transform, zero terms were added to the autocorrelation function so that an adequate number of data points was available for the plotting of the response function. Addition of zero terms increased the maximum time delay by a factor of four for the low damping case, and by a factor of at least seven for the high damping case.

8.4 DISCUSSION OF RESULTS: DISCRETE FREQUENCY EXCITATION

Three possible ways of calculating damping factors using the discrete frequency excitation are presented in figures 15a, b, and c. For a single mode, such as the (2,1) mode, which has a natural frequency well separated from the adjacent natural frequencies, all three methods would yield damping estimates of similar accuracy. Because of the low damping in the case of the bare test panel, most of the modes can be considered to satisfy, approximately, the conditions for a single mode. Thus, for the low damping case, the response amplitude method and the Kennedy-Pancu vector diagram (amplitude phase plot) give damping factors that are within an acceptable experimental scatter, e.g., the damping factors calculated using the two methods are within ±2.5% of each other for all modes except three. Two of the three exceptions have experimental scatter of ±5%, whereas, for the remaining mode (5,2), the Kennedy-Pancu method gives a damping factor that is 67% of the one calculated from the response amplitude method. The higher estimate from the response amplitude method is attributed to the off-resonant contribution from the (6,1) mode.

When damping tape is applied to the test panel, only a few lower order modes, e.g. (2,1), (3,1), and (4.1), satisfy the conditions for a single mode. Due to contributions from the off-resonant modes, damping factors calculated from the response amplitude method are generally higher (by an average of 15%) than those calculated by the Kennedy-Pancu method. No background noise corrections are applied to the discrete frequency response amplitude data because of problems in determining the correct phase-angle relationships.

The effect of background noise and contributions from the off-resonant modes can be readily seen from the Kennedy-Pancu diagram. For a single-degree-of-freedom system, when the off-resonant contribution is zero, the center of the resonance circle will be located at half the peak amplitude, i.e., at 0.5 when the normalized amplitude is used. Thus, a deviation from 0.5 is a measure of the off-resonant contributions. As an example, figures 16 and 17 show the Kennedy-Pancu diagrams from the low and high damping cases, respectively, of mode (2,3). The centers of the resonance circles for the low and high damping cases are located at 0.44 and 0.26, respectively.

As a contrast, consider mode (2,1), which is well separated from other modes. The Kennedy-Pancu diagram for the (2,1) mode, even for the high damping case (fig. 18), shows that the center of the resonance circle is at 0.46.

When the natural frequencies of the two modes are so close that the two resonance circles cannot be clearly defined in the frequency range of the half-power bandwidth of the response peak, the damping factors can be calculated from the phase-angle plot (fig. 15b). The damping factors for the (5,1), (4,2), and (1,3) modes for the high damping case were obtained using this technique. All other damping factors shown in table III were obtained using Kennedy-Pancu diagrams. The damping factors shown in table III are used as the datum damping factors for the test panel with and without damping tape.

8.5 DISCUSSION OF RESULTS: RANDOM EXCITATION

The stochastic equivalents of the three schemes of calculating damping factors are shown in figures 15d, e, and f. Once again, in principle, all three methods can yield estimates of similar accuracy for a single mode that is free from background noise and contributions from off-resonant modes. The practical application of these methods to a multimodal system is described here. The primary objective is to assess the response power spectral density and single-sided Fourier transform of the response autocorrelation methods. Therefore, no attempt is made to calculate the damping factors of each and every mode. Since the panel was excited by acoustic waves propagating along the length of the panel, most of the modes with mode order higher than one in the width will not be excited very efficiently. Those modes are usually excluded from the discussion, but this exclusion does not cause any loss of generality in the conclusions.

8.5.1 Response Power Spectral Density Method

The high damping case, which will be affected by the background noise and contributions from off-resonant modes more than the low damping case, is considered first. The response spectra calculated from runs 2B, 4B, and 9B (see table IV) are shown in figures 19, 20, and 21, respectively. Spectra drawn in figures 19 and 20 indicate that the peak response in the (2,1) and (4,1) modes is higher than the nearest valley in the spectrum by a factor of more than 10. Thus, these two modes are considered to represent a single-mode case. For both the modes, $\Delta f_M / \Delta f_F > 5$; therefore, errors due to filter bandwidth are less than 2%. The calculated damping factors for the (2,1) and (4,1) modes are 1.08 and 1.12 times the datum damping factors (see table V).

Now consider mode (3,1) shown in figure 20. Due to the measurement location for run 4B (see table IV and Chladni figures in fig. 14a) the (3,1) mode is suppressed and the response peak shows some contribution from the background noise. The damping factor for mode (3,1), before applying background noise correction, is 1.28 times the datum damping factor. When the background noise correction is applied (fig. 4), the corrected damping factor in table V for the (3,1) mode is 1.11 times the datum value.

A relatively large excitation bandwidth, 200-2000 Hz, was used for run 9B. Thus, the response spectrum shown in figure 21 will be similar to that obtained by exciting a panel by broadband turbulent boundary layer pressure fluctuations. The measurement location was such that the probe would measure all modes with mode order less than six in the length direction and less than four in width direction. As expected, the spectrum shows a series of peaks with different relative levels, and the (3,2) mode can be taken as an example of very high contributions from background noise. For this mode, the damping factors calculated with and without background noise correction are, respectively, 1.06 and 1.33 times the datum damping factor.

Measured damping factors, estimated by means of the power spectral density method, are shown in table V for several modes in the high damping case. Where necessary, the measurements have been corrected for background noise using figure 4. The data are separated into two categories that are determined by the magnitude of the background noise. For

table Va, the displacement power spectral density ratio of resonant peak to adjacent valley is greater than 10 dB, whereas, in table Vb, the ratio is less than 10 dB. In all cases, the filter bandwidth is less than a quarter of the measured resonance bandwidth so that the resolution error, predicted by figure 5, is less than 3%. For the high damping case, when the background noise is low, table Va shows that the error in the measured damping factor varies from -11% to +25% of the corresponding datum value, with a root mean square (rms) error of 12%. When the background noise is high (table Vb), the error increases and, for the data shown, lies in the range of +6% to +89% with an rms error of 44%.

The problems encountered in the measurement of low damping factors are rather different from the high damping case. The off resonant/background noise contributions do not now pose problems. However, due to the narrowness of the resonance peaks, the filter bandwidth becomes a critical factor for the lower order modes. Also, as discussed in section 7.0, long sample lengths are required for good statistical reliability with narrow filter bandwidths. The response spectra calculated from low damping runs 4B, 9B, and 8B are shown in figures 22, 23, and 24, respectively, the total sample length being the same for all three cases. Filter bandwidth Δf_F, is 0.5 Hz in figures 22 and 23 and 1.0 Hz in figure 24. The two cases with the smaller filter bandwidth show higher statistical scatter, which makes it difficult to calculate accurately the half-power bandwidths of the peaks.

A comparison of the spectra in figures 23 and 24 indicates another important problem area. The excitation bandwidths for runs 8B and 9B are 800-1600 and 200-2000 Hz, respectively. Due to the wider excitation bandwidth for run 9B, the lower order modes, which can be excited relatively efficiently, dominate the spectrum in figure 23. In run 8B, the excitation has an 18-dB per octave rolloff below 800 Hz, thus, the lower order modes are de-emphasized in figure 24, and the peak response amplitudes are of similar magnitude for many of the modes shown. When the panel is excited by the broadband noise due to turbulent airflow, an effect similar to that in figure 24 can be obtained by filtering the response signal from the displacement probe before recording the data.

Measured damping factors for the low damping case are shown in table Vc for the power spectral density method. In all cases except one, the power spectral density peak-to-valley ratio is greater than 10 dB, and the damping factor lies within a range of -18% to +32% of the datum values. The rms error is 15%. Except where indicated, the damping factors in table Vc were obtained using filter bandwidths less than half of the measured peak bandwidth.

8.5.2 Single-Sided Fourier Transform Method

The single-sided Fourier transform $F_w(\omega)$ of the displacement autocorrelation function was computed using the fast Fourier transform algorithm on a digital computer. Data reduction requirements associated with the computer program have been discussed in section 8.3.3. These requirements were satisfied for all modes investigated at the higher damping condition but not for all modes with the lower damping.

Consider first the high damping case because these results show the accuracy of the method when used under satisfactory conditions. As an example, the function $F_w(\omega)$ for the (2,1) and (2,3) modes is shown in figures 25 and 26, respectively. In both cases, the locus of

F_w (ω) is approximately circular with some distortion because of truncation errors introduced by the finite maximum time delay. The curves can be compared with the corresponding figures for discrete frequency excitation shown in figures 18 and 17, respectively. Vector curves for modes (5,1), (4,2), and (1,3), which have close natural frequencies, are shown in figure 27. The figure clearly shows the effect of contributions from off-resonant vibration.

In common with the function H (ω), the natural frequency of a mode is located where the rate of change of arc length with frequency is a maximum for the function F_w (ω). In many cases, such as figures 25 and 26, the natural frequency can be located by visual inspection of the vector diagram. The resonance diameter is drawn and the damping factor calculated as illustrated in figure 15f. When there are close natural frequencies, it may be difficult to locate each resonance by visual inspection of the vector diagram, and a curve of arc length as a function of frequency is plotted as shown in the example of figure 28. If the resonance circle is not clearly defined over the half-power bandwidth, the damping can be calculated from the phase-angle plot in the neighborhood of the natural frequency.

Measured damping factors for several modes, estimated using the single-sided Fourier transform of the displacement autocorrelation function, are shown in table VI. Data for the high damping case have been separated into low and high background noise categories, as in table V for the power spectral density method. For modes with small background noise and off-resonant contributions, the estimated damping factors in table VIa are within -18% to +23% of the datum values, with an rms deviation of 13%. For high-noise conditions, defined as a power spectral density peak-to-valley ratio less than 10 dB, the estimated damping factors show deviations within the range -11% to 77% of the datum values with an rms error of 47%.

One of the requirements of the computer program for calculating the single-sided Fourier transform is that the frequency resolution of the transform would be less than a quarter of the half-power bandwidth of the resonance peak (sec. 8.3.3). Within the limits of the data reduction system used in the demonstration experiments, the above requirement could not be satisfied for all lightly damped modes, such as modes (2,1) and (3,1) in table VIc. The damping factors in table VIc, which refer to the lightly damped conditions, have been corrected for truncation errors based on figure 9 but still show a wider experimental scatter than for the higher damping. For the data in table VIc, the estimated damping factors differ from the datum values by amounts ranging from -4% to +70%, with an rms deviation of 43%.

8.5.3 Comparison of Random Analysis Methods

Damping factors for several normal modes of a rectangular panel have been estimated, from measurements made under random excitation conditions, using displacement power spectral density and single-sided Fourier transform methods. A comparison of the results identifies two important parameters, one of which is the presence of background noise and the other is the frequency resolution requirement of the single-sided Fourier transform method.

Under the best test conditions, with low background noise such that the displacement power spectral density peak-to-valley ratio exceeded 10 dB, and with good frequency resolution defined as being a filter bandwidth less than a quarter of the resonant peak bandwidth, the measured damping factors were close to the datum values. The rms errors were about 13%

for both of the methods tested. When the background noise or off-resonant vibration increased but the high-frequency resolution was maintained, the measured damping factors were less reliable, but both methods were of the same accuracy (an rms error of about 45%).

Differences between the two methods were observed when the resolution criterion was not satisfied, even though an adequate signal-to-noise ratio was achieved. This is shown in the damping estimates for the low damping data. The power spectral density method shows an rms error of about 15%, which is close to the 13% error in the high damping data, but the single-sided Fourier transform method has an rms error of about 43%. It is apparent that the frequency resolution requirements imposed by the single-sided Fourier transform computation are more stringent than those for the power spectral density method. In certain test cases, with high damping and close natural frequencies, no damping estimate could be obtained from the power spectral density function, but an estimate could be obtained using the single-sided Fourier transform. However, this estimate could be highly inaccurate.

9.0 CONCLUSIONS AND RECOMMENDATIONS

Several methods of measuring the damping of panels have been evaluated with particular emphasis being placed on the practical problems associated with the use of the methods. In particular, the techniques were evaluated for application to the measurement of the damping of panels exposed to turbulent airflow.

Based on analytical analyses, several methods were judged to be unsuitable for the proposed application. Non-steady-state methods, which do not incorporate random data analysis techniques, were rejected because of noise problems, and the response autocorrelation method was rejected because of problems of noise and off-resonant vibration interference. The excitation-response cross-power spectral density function, using either boundary layer or a second excitation, was eliminated either because it required simultaneous measurement of the boundary layer pressure field and the vibration, or because of potential low signal-to-noise ratios and problems of instrumentation location in the pressure equalization cavity.

Two basic methods were retained: the response power spectral density and the single-sided Fourier transform of the response autocorrelation function. For these methods, two alternative excitations, the turbulent boundary layer or a rapid frequency sweep, were considered. However, the latter excitation was rejected because of additional instrumentation requirements and because there was no need for transient techniques.

The power spectral density and single-sided Fourier transform methods were demonstrated experimentally under conditions of spatially distributed, random excitation. Under many test conditions, the two methods estimated damping factors with similar experimental accuracy. However, the single-sided Fourier transform method imposes more stringent requirements on frequency resolution than does the spectral density method. This becomes apparent when the damping is very low and computer restrictions do not permit the resolution requirement to be satisfied. On the other hand, the single-sided Fourier transform method has advantages when the damping is high and natural frequencies are close together. Under such conditions, the power spectral density method has little value.

From this evaluation, it is recommended that, in general, the response power spectral density method be used to measure the damping of panels exposed to turbulent airflow. Provided appropriate correction terms are introduced, the reliability and accuracy of the method appears to be as good as that associated with other methods, and the data acquisition and reduction requirements are no more than those normally demanded for structural response measurements. However, if the particular conditions of high damping and close natural frequencies are important, then the single-sided Fourier transform of the response autocorrelation function should be used for improved accuracy.

Commercial Airplane Group
The Boeing Company
Seattle, Washington, August 1971

70

APPENDIX A

Finite Bandwidth Effects in the Autocorrelation Method

The autocorrelation function for a band-limited response signal can be studied by means of the function

$$R_W(\tau; \Delta\omega) = \int_{-\infty}^{\infty} \Phi(\omega) |H_\alpha(\omega)|^2 e^{i\omega\tau} d\omega, \tag{A1}$$

where

$$\left. \begin{array}{ll} \Phi(\omega) = 1 & \omega_1 < |\omega| < \omega_2 \\[6pt] = 0 & \text{elsewhere} \end{array} \right\} \tag{A2}$$

Using convolution relationships, equation (A1) can be written in the form

$$R_W(\tau; \Delta\omega) = \frac{1}{2\pi} \int_{-\infty}^{\infty} H'(t)\phi(\tau - t) dt \tag{A3}$$

where

$$H'(t) = \int_{-\infty}^{\infty} |H_\alpha(\omega)|^2 e^{i\omega t} d\omega \tag{A4}$$

and

$$\phi(t) = \int_{-\infty}^{\infty} \Phi(\omega) e^{i\omega t} d\omega. \tag{A5}$$

From equations (A2) and (A5),

$$\phi(t) = \frac{2}{t}(\sin\omega_2 t - \sin\omega_1 t), \tag{A6}$$

and from equation (A4) and definition of $H_\alpha(\omega)$,

$$\begin{aligned} H'(t) &= \int_{-\infty}^{\infty} \frac{e^{i\omega t} d\omega}{M_\alpha^2 [(\omega_\alpha^2 - \omega^2)^2 + 4\zeta_\alpha^2 \omega_\alpha^2 \omega^2]} \\[12pt] &= \frac{\pi e^{-\omega_\alpha \zeta_\alpha |t|}}{2M_\alpha^2 \omega_\alpha^3 \zeta_\alpha} \left[\cos\omega_d |t| + \frac{\zeta_\alpha}{(1 - \zeta_\alpha^2)^{\frac{1}{2}}} \sin\omega_d |t| \right]. \end{aligned} \tag{A7}$$

The parameter ω_d is the frequency of free damped vibration, $\omega_\alpha(1 - \zeta_\alpha^2)^{1/2}$. Substituting equations (A6) and (A7) in (A3),

$$R_w(\tau;\Delta\omega) = R_w(\tau;\Delta\omega)_{\omega_2} - R_w(\tau;\Delta\omega)_{\omega_1}$$

where

$$R_w(\tau;\Delta\omega)_{\omega_2} = \frac{1}{2M_\alpha^2 \omega_\alpha^3 \zeta_\alpha} \int_0^\infty e^{-\omega_\alpha\zeta_\alpha t}\left(\cos\omega_d t + \frac{\zeta_\alpha}{(1 - \zeta_\alpha^2)^{1/2}}\sin\omega_d t\right)$$

$$\left(\frac{\sin\omega_2(\tau - t)}{(\tau - t)} + \frac{\sin\omega_2(\tau + t)}{(\tau + t)}\right)dt$$

(A8)

Two approaches are possible to solve equation (A8). In one approach, it can be shown that

$$I_1 = \int_0^\infty e^{-at}\cos bt\left[\frac{\sin c(\tau + t)}{(\tau + t)} + \frac{\sin c(\tau - t)}{(\tau - t)}\right]dt$$

$$= a\int_{-c}^c \frac{\cos z\tau}{a^2 + (b + z)^2}\, dz$$

(A9)

and

$$I_2 = \int_0^\infty e^{-at}\sin bt\left[\frac{\sin c(\tau + t)}{(\tau + t)} + \frac{\sin c(\tau - t)}{(\tau - t)}\right]dt$$

$$= \frac{b}{a}I_1 + \int_{-c}^c \frac{z\cos z\tau}{a^2 + (b + z)^2}\, dz$$

(A10)

The integrals in equations (A9) and (A10) can be related to tabulated exponential integrals for numerical evaluation. However, a better insight may be possible using the approach of Kandianis (ref. 15). Equation (A8) contains integrals of the form

$$\int_0^\infty e^{-\omega_\alpha\zeta_\alpha t}\cos\omega_d t\frac{\sin\omega_2(\tau \pm t)}{(\tau \pm t)}dt$$

and

$$\int_0^\infty e^{-\omega_\alpha\zeta_\alpha t}\sin\omega_d t\frac{\sin\omega_2(\tau \pm t)}{(\tau \pm t)}dt$$

As an example, select

$$I_3 = \int_0^\infty e^{-\omega_\alpha \zeta_\alpha t} \cos\omega_d t \frac{\sin\omega_2(\tau + t)}{(\tau + t)} dt$$

$$= e^{\omega_\alpha \zeta_\alpha \tau}\left[\int_0^\infty e^{-\omega_\alpha \zeta_\alpha t} \cos\omega_d(t - \tau)\frac{\sin\omega_2 t}{t} dt - \int_0^\tau e^{-\omega_\alpha \zeta_\alpha t} \cos\omega_d(t - \tau)\frac{\sin\omega_2 t}{t} dt\right] \quad (A11)$$

The infinite integral on the right side of equation (A11) can be evaluated using the results of Kandianis (ref. 15),

$$\int_0^\infty e^{-\omega_\alpha \zeta_\alpha t} \cos\omega_d t \frac{\sin\omega_2 t}{t} dt = \frac{1}{2}\tan^{-1}\left[\frac{2\zeta_\alpha \omega_\alpha \omega_2}{\omega_\alpha^2 - \omega^2}\right] \quad \text{if } (\omega_\alpha^2 - \omega_2^2) > 0$$

$$= \frac{1}{2}\tan^{-1}\left[\frac{2\zeta_\alpha \omega_\alpha \omega_2}{\omega_\alpha^2 - \omega^2}\right] + \pi \quad \text{if } (\omega_\alpha^2 - \omega_2^2) < 0$$

and

$$\int_0^\infty e^{-\omega_\alpha \zeta_\alpha t} \sin\omega_d t \frac{\sin\omega_2 t}{t} dt = \frac{1}{4}\log_e\left[\frac{(\zeta_\alpha \omega_\alpha)^2 + (\omega_\alpha + \omega_2)^2}{(\zeta_\alpha \omega_\alpha)^2 + (\omega_\alpha - \omega_2)^2}\right]$$

Terms of this type provide constant factors of the exponential $e^{-\omega_\alpha \zeta_\alpha |\tau|}$ and so do not influence the damping estimate.

To evaluate the finite integral on the right hand side of equation (A11), Kandianis (ref. 15) makes use of the reduction formula

$$\int x^p e^{ax}\sin bx\,dx = \frac{x^p e^{ax}}{a^2 + b^2}(a\sin bx + b\cos bx) - \frac{p}{a^2 + b^2}\int x^{p-1} e^{ax}(a\sin bx - b\cos bx)dx \quad (A12)$$

Taking the first term on the right side of equation (A12) as being an approximation for the integral on the left side, Kandianis shows that the autocorrelation function for a band-limited signal contains terms of the form $(\cos \omega_2 \tau)/\tau$ and $(\sin \omega_2 \tau)/\tau$, with similar terms in ω_1. These terms, since they are functions of τ, will distort the autocorrelation function and introduce errors in the damping estimates. Thus, the filter bandwidths have to be chosen to minimize these errors.

APPENDIX B

Truncation Effects in the Single-Sided Fourier Transform Method

In practice, truncation errors arise in the computation of the single-sided Fourier transform function, and it is necessary to correct the measured damping factor. The magnitude of the correction can be estimated by means of the integral

$$F_w(\omega;\tau_m) = \frac{1}{2\pi} \int_0^\infty D(\tau)R_w(\tau)e^{-i\omega\tau}d\tau, \tag{B1}$$

where

$$\left. \begin{array}{ll} D(\tau) = 1 & 0 \leqslant \tau \leqslant \tau_m \\[2mm] \quad\;\; = 0 & \tau > \tau_m \end{array} \right\} \tag{B2}$$

Using the faltung relationship, equation (B1) can be written in the form

$$F_w(\omega;\tau_m) = \int_{-\infty}^\infty Q(\omega - \omega_1)S_w(\omega_1)d\omega_1 \tag{B3}$$

where

$$Q(\omega) = \frac{1}{2\pi} \int_{-\infty}^\infty D(\tau)e^{-i\omega\tau}d\tau \tag{B4}$$

and

$$S_w(\omega) = \frac{1}{2\pi} \int_{-\infty}^\infty R_w(\tau)e^{-i\omega\tau}d\tau$$

$$\tag{B5}$$

$$= S_p(\omega)|H_\alpha(\omega)|^2$$

for a single-degree-of-freedom system with frequency response function $H_\alpha(\omega)$. Substituting (B4) and (B5) in (B3) gives

$$F_w(\omega;\tau_m) = \frac{iS_p}{2\pi} \int_{-\infty}^\infty \frac{\left(e^{-i(\omega-\omega_1)\tau_m} - 1\right)}{(\omega - \omega_1)}|H_\alpha(\omega)|^2 d\omega_1, \tag{B6}$$

where it is assumed that the excitation is white noise so that $S_p(\omega) = S_p$. Substituting

$$|H_\alpha(\omega)|^2 = \frac{1}{M_\alpha^2\left[(\omega_\alpha^2 - \omega^2)^2 + 4\zeta_\alpha^2\omega_\alpha^2\omega^2\right]}$$

74

in equation (B6), and using contour integration in the upper half plane, equation (B6) becomes

$$F_w(\omega;\tau_m) = \frac{S_p}{4M_\alpha^2\omega_\alpha^4\zeta_\alpha(1-\zeta_\alpha^2)^{\frac{1}{2}}}[x(\omega)+iy(\omega)] \qquad (B7)$$

where

$$x(\omega) = M_\alpha^2|H_\alpha(\omega)|^2\left\{2\omega_\alpha^3\omega_d\zeta_\alpha - [b(\omega_\alpha^2-\omega^2)+2a\zeta_\alpha\omega_\alpha\omega]e^{-\omega_\alpha\zeta_\alpha\tau_m}\right\}$$

$$y(\omega) = M_\alpha^2|H_\alpha(\omega)|^2\left\{\omega\omega_d(\omega_\alpha^2-\omega^2)-4\omega\omega_\alpha^2\omega_d\zeta_\alpha^2\right.$$

$$\left. - \left[a(\omega_\alpha^2-\omega^2)-2b\omega\omega_\alpha\zeta_\alpha\right]e^{-\omega_\alpha\zeta_\alpha\tau_m}\right\}$$

$$a = a(\omega) = \omega\omega_d\cos\omega\tau_m\cos\omega_d\tau_m +(\omega_d^2-\omega_\alpha^2\zeta_\alpha^2)\sin\omega\tau_m\sin\omega_d\tau_m$$

$$- 2\omega_\alpha\omega_d\zeta_\alpha\sin\omega\tau_m\cos\omega_d\tau_m + \omega\omega_\alpha\zeta_\alpha\cos\omega\tau_m\sin\omega_d\tau_m$$

$$b = b(\omega) = \omega\omega_d\sin\omega\tau_m\cos\omega_d\tau_m - (\omega_d^2-\omega_\alpha^2\zeta_\alpha^2)\cos\omega\tau_m\sin\omega_d\tau_m$$

$$+ 2\omega_\alpha\omega_d\zeta_\alpha\cos\omega\tau_m\cos\omega_d\tau_m + \omega\omega_\alpha\zeta_\alpha\sin\omega\tau_m\sin\omega_d\tau_m$$

$$\omega_d = \omega_\alpha(1-\zeta_\alpha^2)^{\frac{1}{2}}$$

If $(1/\rho)(ds/d\omega)$ is taken as a convenient measure of the characteristics of the locus of $F_w(\omega;\tau_m)$, as suggested by Clarkson and Mercer (ref. 17), then

$$\frac{1}{\rho}\frac{ds}{d\omega} = \frac{\left(y\frac{dx}{d\omega}-x\frac{dy}{d\omega}\right)}{(x^2+y^2)^{\frac{1}{2}}}\cdot\frac{\left[\frac{dx}{d\omega}\frac{d^2y}{d\omega^2}-\frac{d^2x}{d\omega^2}\frac{dy}{d\omega}\right]}{\left[\left(\frac{dx}{d\omega}\right)^2+\left(\frac{dy}{d\omega}\right)^2\right]^{3/2}}$$

Evaluating $(1/\rho)(ds/d\omega)$ at the frequency of maximum value of $|H_\alpha(\omega)|^2$, i.e., at

$$\omega_r^2 = (1-2\zeta_\alpha^2)\omega_\alpha^2,$$

and assuming that the damping is small so that $\zeta_\alpha^2 \ll 1$, equation (B8) reduces to

$$\frac{1}{\rho}\frac{ds}{d\omega} \approx -\frac{\frac{d^2x}{d\omega^2}}{\frac{dy}{d\omega}}$$

or, after substituting for $d^2x/d\omega^2$ and $dy/d\omega$,

$$\frac{1}{\rho}\frac{ds}{df} = -\frac{4\pi}{\omega_\alpha \zeta_\alpha}\left\{\frac{1-e^{-\omega_\alpha \zeta_\alpha \tau_m}\left[1+\omega_\alpha \zeta_\alpha \tau_m(1-\zeta_\alpha\sin\omega_\alpha\tau_m\cos\omega_\alpha\tau_m)+\frac{1}{2}\omega_\alpha^2\zeta_\alpha^2\tau_m^2\right]}{1-e^{-\omega_\alpha\zeta_\alpha\tau_m}[1+\omega_\alpha\zeta_\alpha\tau_m(1-\zeta_\alpha\sin\omega_\alpha\tau_m\cos\omega_\alpha\tau_m)]}\right\} \quad \text{(B9)}$$

REFERENCES

1. Bishop, R. E. D. and Gladwell, G. M. L.: An Investigation Into the Theory of Resonance Testing. Phil. Trans. Royal Soc. London, series A, no. 1055, vol. 255, 1963, pp. 241-280.

2. Mead, D. J.: The Internal Damping due to Structural Joints and Techniques for General Damping Measurement. Aeronautical Research Council (U.K.), Current Paper CP 452, 1959.

3. Mead, D. J.: The Practical Problems of Assessing Damping Treatments. J. Sound Vib., vol. 1, no. 3, 1964, pp. 270-291.

4. Kennedy, C. C. and Pancu, C. D. P.: Use of Vectors in Vibration Measurement and Analysis. J. Aero. Sci., vol. 14, no. 11, 1947, pp. 603-625.

5. Maestrello, L.: Test Results From the Boundary Layer Facility—Noise Radiated by the Panel. D6-9944, vol. I, The Boeing Company, 1964.

6. Wilby, J. F.: The Response of Simple Panels to Turbulent Boundary Layer Excitation. AFFDL-TR-67-70, 1967.

7. Mead, D. J.: The Damping of Stiffened Plate Structures. Ch. 26 of Acoustical Fatigue in Aerospace Structures. W. J. Trapp and D. M. Forney, eds., Syracuse University Press, 1965.

8. Mead, D. J. and Richards, E. J., eds.: Noise and Acoustic Fatigue in Aeronautics. John Wiley & Sons, Inc., 1968.

9. Clarkson, B. L. and Ford, R. D.: The Response of a Typical Aircraft Structure to Jet Noise. J. Roy. Aero. Soc., vol. 66, 1962, pp. 31-40.

10. Pendered, J. W.: Theoretical Investigation Into the Effects of Close Natural Frequencies in Resonance Testing. J. Mech. Eng. Sci., vol. 7, no. 4, 1965, pp. 372-379.

11. Forlifer, W. R.: The Effects of Filter Bandwidth in Spectrum Analysis of Random Vibration. Shock, Vibration, and Associated Environments Bulletin, no. 33, pt.2, 1964, pp. 273-278.

12. Bull, M. K., Wilby, J. F., and Blackman, D. R.: Wall Pressure Fluctuations in Boundary Layer Flow and Response of Simple Structures to Random Pressure Fields. Report AASU 243, University of Southampton, England, 1963.

13. Rechtien, R. D.: The Autocorrelation Function of Structural Response Measurements. NASA TN D-2578, 1965.

14. White, R. G.: The Resolution of Close Natural Frequencies in the Impulse Response and Severe Truncation Effects. ISVR technical report 17, University of Southampton, England, 1969.

15. Kandianis, F.: Linear System Analysis by Cross Correlation and Its Transform Techniques. ISVR technical report 33, University of Southampton, England, 1970.

16. Kandianis, F.: Frequency Response of Structures and the Effects of Noise on its Estimates From the Transient Response. J. Sound Vib., vol. 15, no. 2, 1971, pp. 203-215.

17. Clarkson, B. L. and Mercer, C. A.: Use of Cross Correlation in Studying the Response of Lightly Damped Structures to Random Forces. AIAA Journal, vol. 3, no. 12, 1965, pp. 2287-2291.

18. Blackman, D. R., Clark, D. M., McNulty, G. J., and Wilby, J. F.: Boundary Layer Pressure Fluctuations and Structural Response. AFFDL-TR-67-97, 1967.

19. Soovere, J. and Clarkson, B. L.: Frequency Response Functions from Cross Correlation: Bartlett Weighting Function. AIAA Journal, vol. 5, no. 3., 1967, pp. 601-603.

20. Blackman, R. B. and Tukey, J. W.: The Measurement of Power Spectra. Dover Publications, 1958.

21. Oleson, M. W.: A Narrow Band Random Vibration Test. Shock and Vibration Bulletin, pt. 1, 1959.

22. Broch, J. T.: A Note on Vibration Test Procedures. Technical review no. 2, Bruel and Kjaer, 1966.

23. Reed, W. H. III, Hall, A. W., and Barker, L. E., Jr.: Analog Techniques for Measuring the Frequency Response of Linear Physical Systems Excited by Frequency-Sweep Inputs. NASA TN D-508, 1960.

24. Skingle, C. S.: A Method for Analyzing the Response of a Resonant System to a Rapid Frequency Sweep Input. Technical report 66379, RAE, England, 1966.

25. White, R. G.: Use of Transient Excitation in the Dynamic Analysis of Structures. Aeronautical Journal, vol. 73, no. 708, 1969, pp. 1047-1050.

26. White, R. G.: Evaluation of the Dynamic Characteristics of Structures by Transient Testing. J. Sound Vib., vol. 15, no. 2, 1971, pp. 147-161.

27. White, R. G.: Measurement of Structural Frequency Response by Transient Excitation. ISVR technical report 12, University of Southampton, England, 1969.

28. Kandianis, F.: The Effects of Extraneous Noise on the Measurement of the Frequency Response of Structures Under Transient Excitation. ISVR technical report 20, University of Southampton, England, 1969.

29. Bendat, J. S. and Piersol, A. G.: Measurement and Analysis of Random Data. John Wiley & Sons, Inc., 1966.

30. Enochson, L. D. and Otnes, R. K.: Programming and Analysis for Digital Time Series Data. Shock and Vibration Monograph, SVM-3, U.S. Dept. of Defense, 1968.

31. Applications and Methods of Random Data Analysis. University of Southampton/AGARD lecture series, Southampton, England, 1969.

32. Warburton, G. B.: The Vibration of Rectangular Plates, Proc. Inst. Mech. Eng., vol. 168, 1954, pp. 371-384.

TABLE I.—CALCULATED[a] NATURAL FREQUENCIES OF ALUMINUM PANEL[b] WITH CLAMPED EDGES

n^c \ m^c	1	2	3	4
	Frequency,[d] Hz			
1	253	642	1226	2004
2	359	742	1327	2106
3	541	913	1492	---
4	798	1157	1728	---
5	1124	1473	2035	---
6	1519	1861	---	---
7	1980	---	---	---
8	---	---	---	---

[a]Warburton method (ref. 32)

[b]30.48 x 17.78 x 0.127 cm (12 x 7 x 0.05 in.)

[c]Mode order (m,n) defined by number of half wavelengths along length and breadth of panel.

[d]Dashes indicate natural frequencies higher than 2150 Hz.

TABLE II.—DETAILS OF DAMPING TAPE

Type	Scotch brand 428A
Thickness of aluminum foil	14.0×10^{-3} cm (5.5×10^{-3} in.)
Thickness of adhesive	6.4×10^{-3} cm (2.5×10^{-3} in.)
Thickness of foil plus adhesive	20.3×10^{-3} cm $\pm 10\%$ (8×10^{-3} in. $\pm 10\%$)
Weight	4.40 N/m^2 (0.09 ib/sq ft)
$\dfrac{\text{Weight of bare panel}}{\text{Weight of panel and tape}}$	0.89

TABLE III.—PANEL NATURAL FREQUENCIES AND DAMPING FACTORS MEASURED WITH DISCRETE FREQUENCY EXCITATION

Mode order, m,n	Location of Proximity Probe				High damping		Low damping	
	x_1		x_3					
	cm	in.	cm	in.	$f_{m,n}$, Hz	$\zeta_{m,n}$	$f_{m,n}$, Hz	$\zeta_{m,n}$
2,1	7.62	3.0	8.89	3.5	359	0.0153	362	0.00102
3,1	15.24	6.0	8.89	3.5	538	0.0115	545	0.00170
1,2	15.24	6.0	13.34	5.25	599	0.0048	612	0.00202
2,2	7.62	3.0	13.34	5.25	700	0.0089	717	0.00163
4,1	11.43	4.5	8.89	3.5	773	0.0175	778	0.00190
3,2	15.24	6.0	13.34	5.25	867	0.0113	888	0.00127
5,1	15.24	6.0	8.89	3.5	973	0.0200	1095	0.00127
4,2	15.24	6.0	8.89	3.5	1057	0.0163	——	——
1,3	15.24	6.0	8.89	3.5	1098	0.0127	1124	0.00188
2,3	7.62	3.0	8.89	3.5	1184	0.0127	1221	0.00313
3,3	15.24	6.0	8.89	3.5	1351	0.0097	1405	0.00194
6,1	8.89	3.5	11.43	4.5	1351	0.0138	1404	0.00164
5,2	12.07	4.75	13.34	5.25	1355	0.0137	1405	0.00231

TABLE IV.—MEASUREMENT LOCATIONS AND EXCITATION BANDWIDTHS FOR RANDOM EXCITATION

Run	Location of proximity probe				Frequency range,[a] Hz
	x_1		x_3		
	cm	in.	cm	in.	
2B	7.62	3.0	8.89	3.5	200-400
3A	15.24	6.0	8.89	3.5	400-800
3B	7.62	3.0	13.34	5.25	400-800
4A	5.08	2.0	13.34	5.25	200-800
4B	19.05	7.5	13.34	5.25	650-850
5B	5.08	2.0	13.34	5.25	600-1200
6B	15.24	6.0	8.89	3.5	1000-1200
7A	15.24	6.0	8.89	3.5	800-1600
7B	7.62	3.0	8.89	3.5	800-1600
8A	2.54	1.0	14.61	5.75	1250-1500
8B	2.54	1.0	14.61	5.75	800-1600
9B	5.08	2.0	13.34	5.25	200-2000

[a]Excitation signal decreases at a rate of 18 dB per octave outside indicated frequency range.

TABLE V.—SUMMARY OF MEASURED DAMPING FACTORS USING POWER SPECTRAL DENSITY METHOD

Run	Mode order, m,n	Frequency, $f_{m,n}$, Hz	Damping, $\zeta_{m,n}$	B_ζ [a]
(a) High damping (spectral peak-to-valley ratio > 10 dB)				
2B	2,1	356	0.0165	1.08
9B	2,1	359	0.0141	0.92
3A	3,1	535	0.0129	1.12
4B	3,1	538	0.0128	1.11
9B	3,1	536	0.0126	1.10
3B	3,1	539	0.0144	1.25
5B	4,1	772	0.0155	0.89
4B	4,1	772	0.0196	1.12
7B	2,3	1176	0.0133	1.05
7A	3,3	1346	0.0107	1.11
9B	3,3	1348	0.0105	1.09
(b) High damping (spectral peak-to-valley ratio < 10 dB)				
3B	4,1	780	0.0216	1.23
5B	3,2	869	0.0214	1.89
9B	3,2	865	0.0120	1.06
7A	2,3	1185	0.0155	1.22
7B	3,3	1340	0.0126	1.30
(c) Low damping				
8B	2,1	364	0.00098	0.96 [b]
4B	3,1	546	0.00188	1.10
8B	3,1	546	0.00193	1.13
8B	1,2	605	0.00273	1.35 [c]
4B	4,1	789	0.00174	0.92
8B	4,1	790	0.00246	1.29
4B	3,2	889	0.00121	0.95
8B	3,2	890	0.00104	0.82
7A	5,1	1090	0.00168	1.32
7B	5,1	1091	0.00149	1.17
7A	1,3	1120	0.00171	0.91
8B	1,3	1120	0.00198	1.06
7A	2,3	1210	0.00308	0.98
8B	2,3	1232	0.00264	0.84
7A	3,3	1400	0.00214	1.10
8B	3,3	1400	0.00189	0.98

[a] Ratio of measured damping factor to datum damping factor.

[b] Filter bandwith greater than one half of the resonance peak bandwidth.

[c] Spectral peak-to-valley ratio < 10 dB.

TABLE VI.—SUMMARY OF MEASURED DAMPING FACTORS USING SINGLE-SIDED FOURIER TRANSFORM METHOD

Run	Mode order, m,n	Frequency, $f_{m,n}$, Hz	Damping, $\zeta_{m,n}$	B_ζ[a]
(a) High damping (spectral peak-to-valley ratio, $>$ 10 dB)				
2B	2,1	357	0.0156	1.02
9B	2,1	358	0.0126	0.82
3B	3,1	537	0.0139	1.21
4B	3,1	534	0.0120	1.04
8B	3,1	536	0.0123	1.07
9B	3,1	537	0.0100	0.87
4B	4,1	775	0.0188	1.07
4B	4,1	775	0.0171	0.98
4B	4,1	770	0.0152	0.87
8B	4,1	776	0.0164	0.94
9B	4,1	773	0.0150	0.86
7B	2,3	1179	0.0126	0.99
8B	2,3	1194	0.0148	1.17
7A	3,3	1347	0.0105	1.08
8B	3,3	1354	0.0080	0.82
(b) High damping (spectral peak-to-valley ratio $<$ 10 dB)				
8B	3,2	862	0.0183	1.62
7A	5,1	970	0.0354	1.77
8B	5,1	970	0.0178	0.89
7A	4,2	1056	0.0205	1.26
7A	1,3	1091	0.0214	1.69
8B	1,3	1085	0.0120	0.94
7B	3,3	1340	0.0088	0.91
(c) Low damping				
8B	2,1	364	0.00174	1.70[b]
8B	3,1	546	0.00227	1.34[b]
8B	4,1	790	0.00216	1.14
8B	3,2	890	0.00134	1.05
8B	5,1	1099	0.00213	1.68
8B	1,3	1117	0.00279	1.48
8B	3,3	1398	0.00185	0.96

[a] Ratio of measured damping factor to datum damping factor.

[b] Filter bandwidth too wide $(\Delta f_F > 1/4 \, \Delta f_M)$

Excitation
$p(\underline{x}', t)$

Linear system
defined by
$H(\omega), h(T), \psi(\underline{x})$

Response
$w(\underline{x}, t)$

(a) Noise-Free System

Excitation
$p_1(\underline{x}', t)$

$H(\omega), h(T), \psi(\underline{x})$

Measured response
$w(\underline{x}, t)$

Noise $p_2(\underline{x}'', t)$

(b) Noise in Excitation

Excitation
$p_1(\underline{x}', t)$

$H(\omega), h(T), \psi(\underline{x})$

Vibration
$w'(\underline{x}, t)$

Measured
signal
$w(\underline{x}, t)$

Noise $p_2(\underline{x}'', t)$

Noise $n(t)$
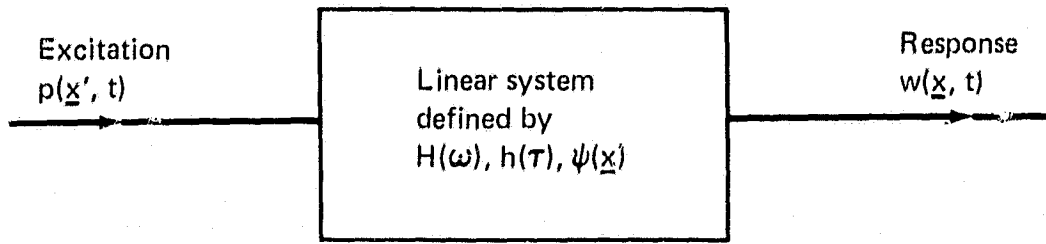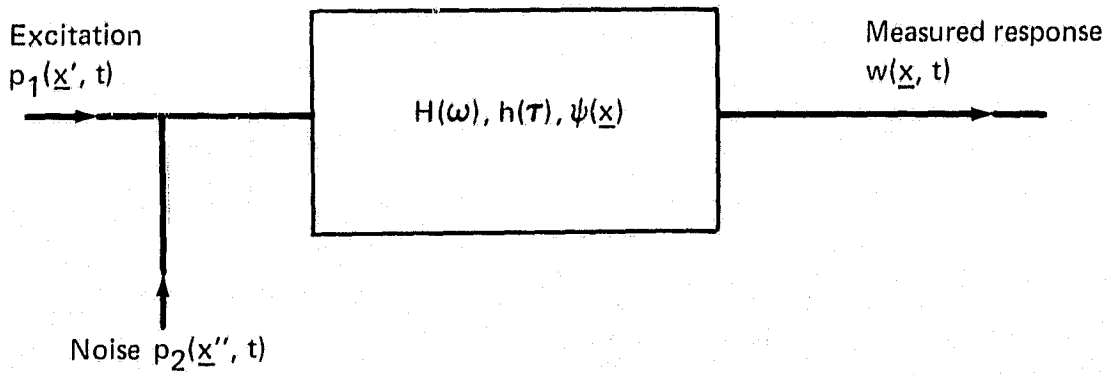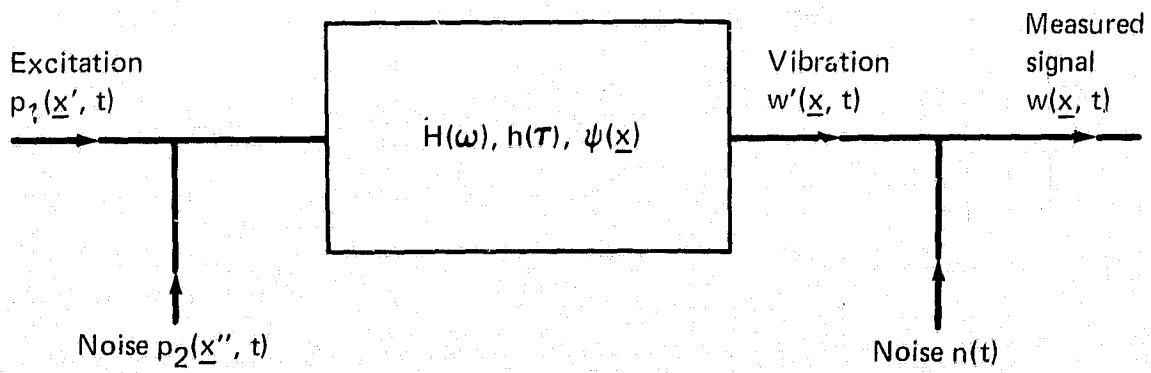
(c) Noise in Excitation and Response

Figure 1.—Schematic of Linear System Under Investigation

85
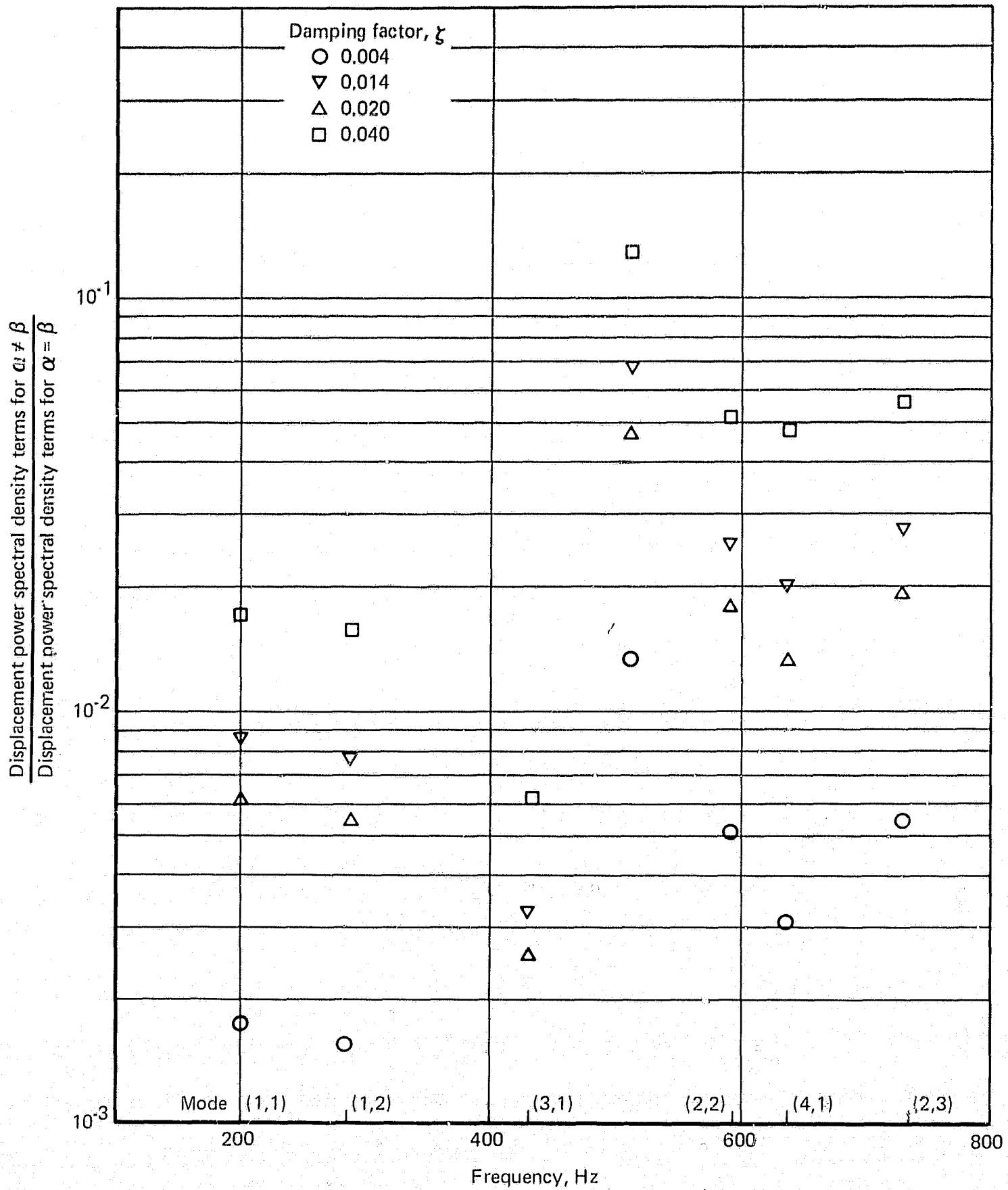
Figure 2.—Effect of Statistical Coupling
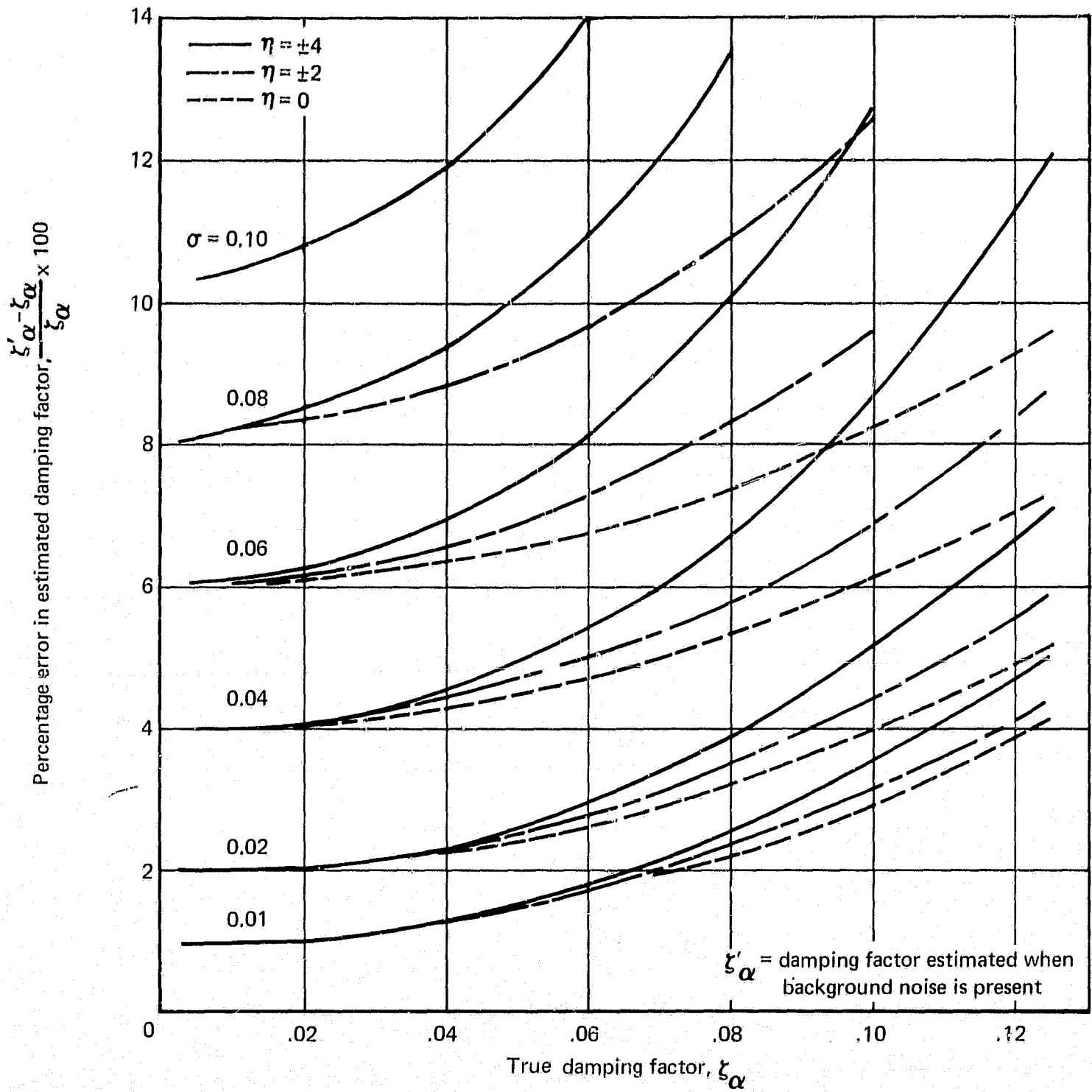
Figure 3.—Effect of Off-Resonant Contribution on Measurement of Damping Factor
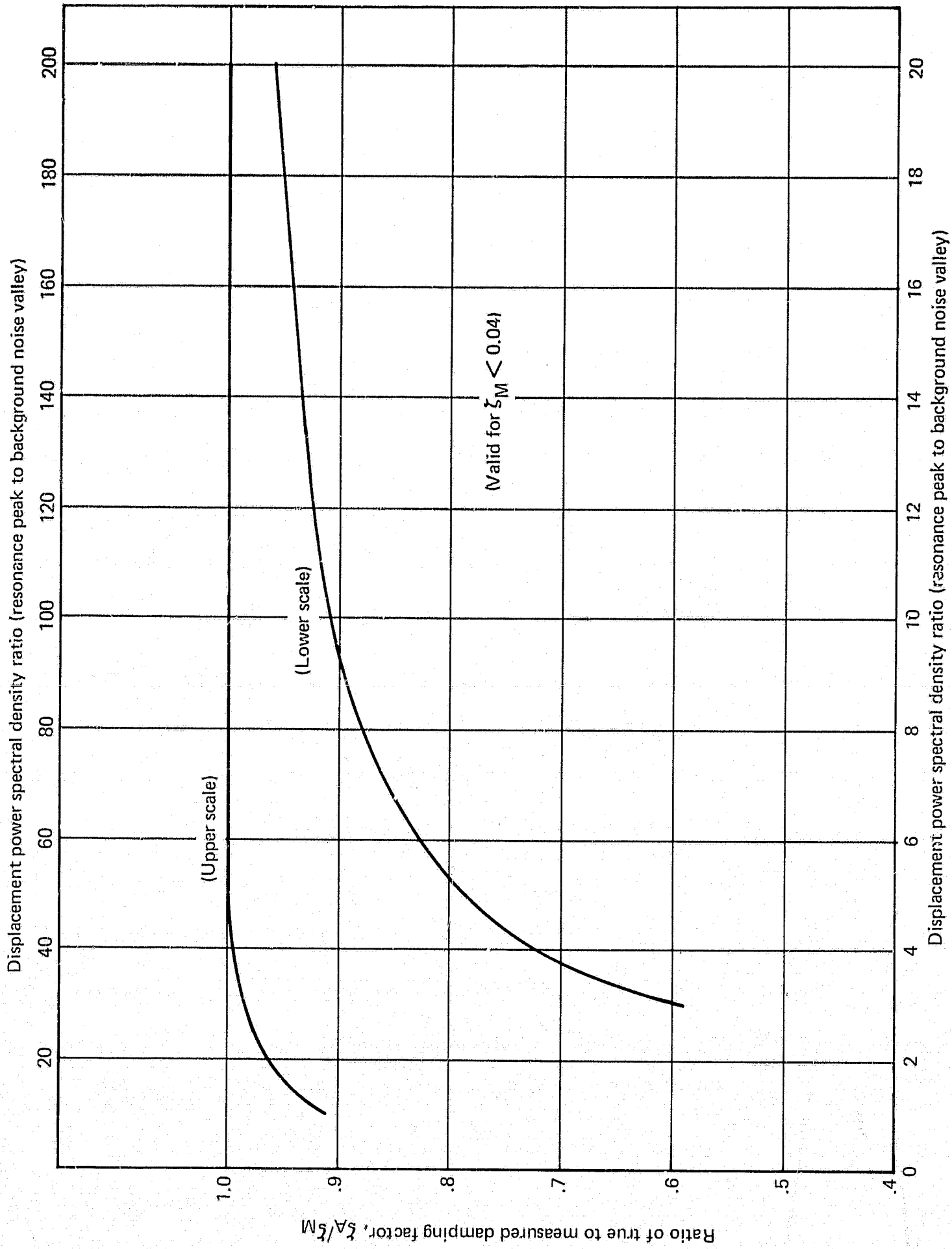
Figure 4.—Correction to Damping Factor (Background Noise Effect)
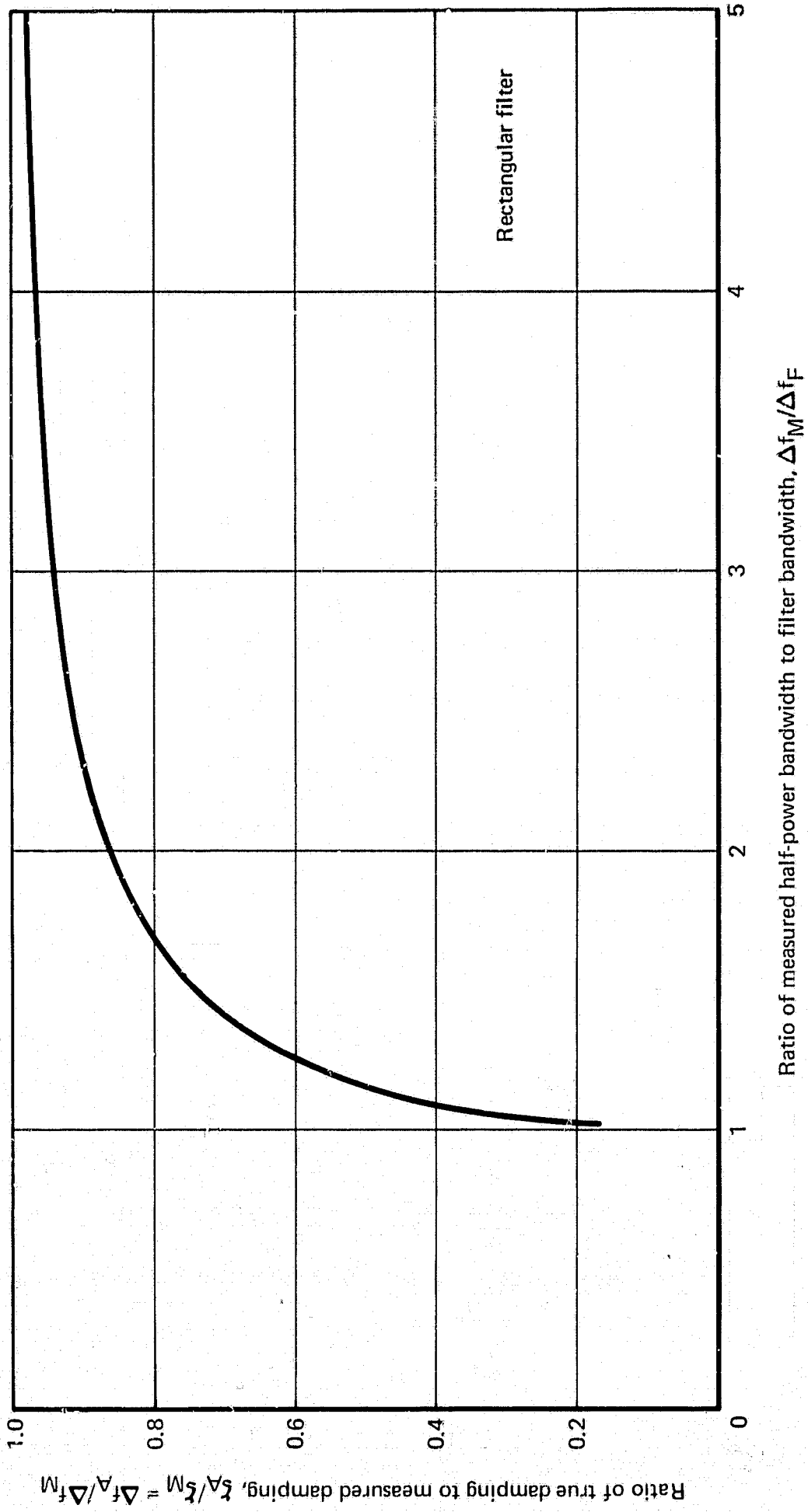
Figure 5.—Effect of Filter Bandwidth on Damping Measurements
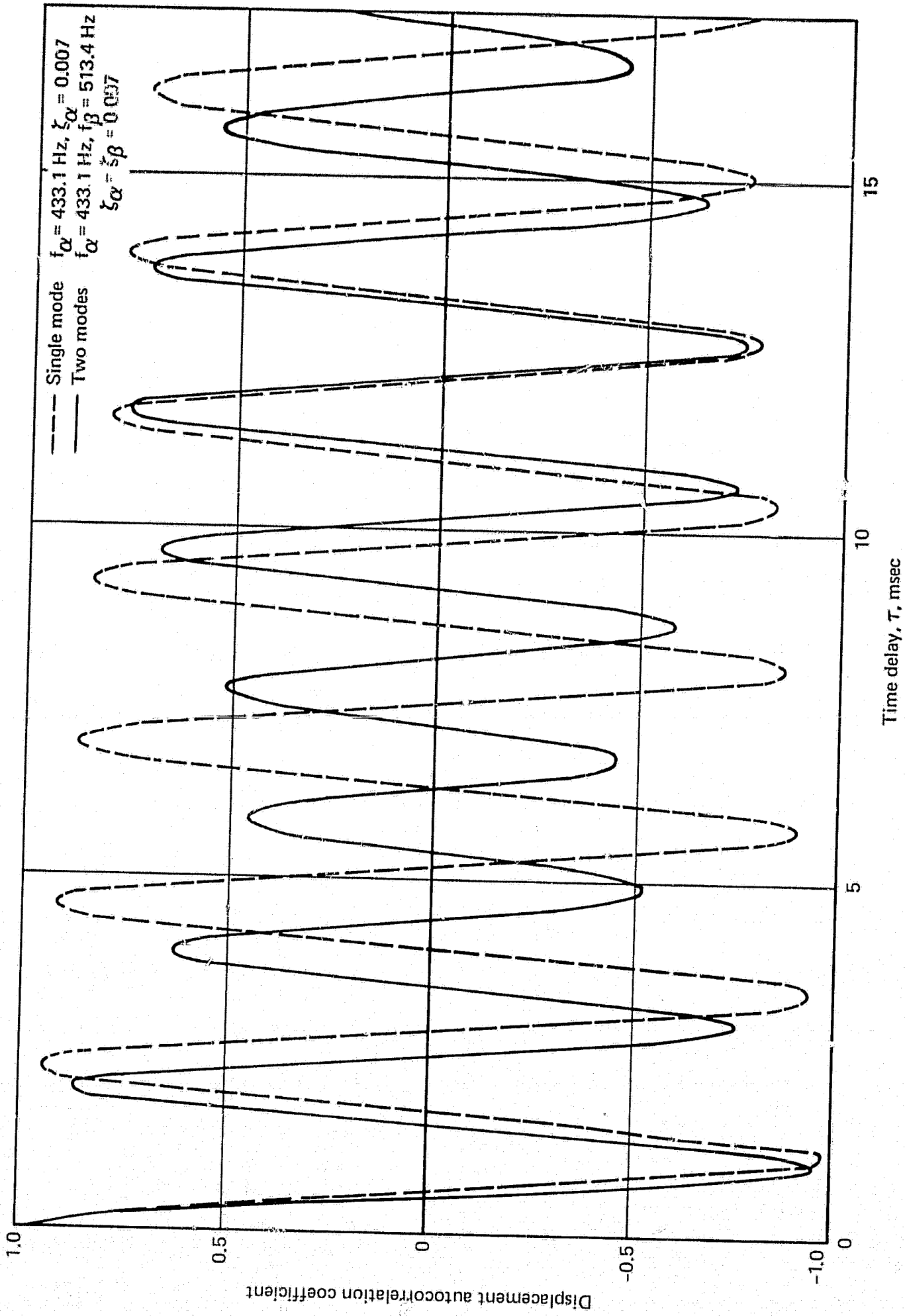
Figure 6.—*Displacement Autocorrelation Coefficient Showing Beating Effect for Two Modes With Close Natural Frequencies*

Legend (within figure):
- Single mode $f_\alpha = 433.1$ Hz, $\zeta_\alpha = 0.007$
- Two modes $f_\alpha = 433.1$ Hz, $f_\beta = 513.4$ Hz
  $\zeta_\alpha = \zeta_\beta = 0.007$

Axis labels:
- Displacement autocorrelation coefficient
- Time delay, τ, msec
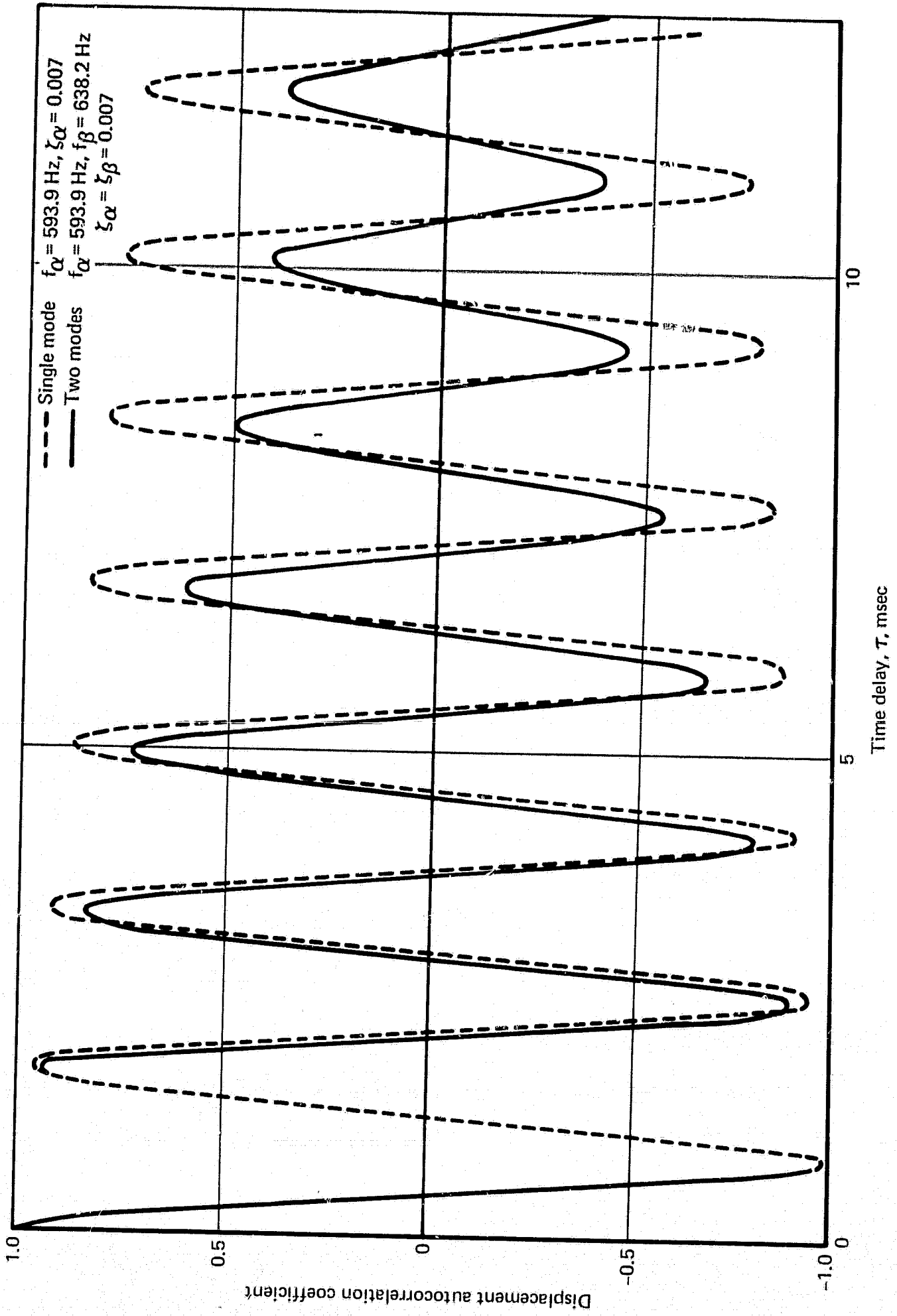
Figure 7.—Displacement Autocorrelation Coefficient, Where Beating Effect is Obscured by Finite Time Delay, for Two Modes With Very Close Natural Frequencies

Legend (as shown in figure):
- - - - Single mode $f_\alpha = 593.9$ Hz, $\zeta_\alpha = 0.007$
—— Two modes $f_\alpha = 593.9$ Hz, $f_\beta = 638.2$ Hz $\zeta_\alpha = \zeta_\beta = 0.007$

Y-axis: Displacement autocorrelation coefficient (1.0, 0.5, 0, -0.5, -1.0)

X-axis: Time delay, τ, msec (0, 5, 10)
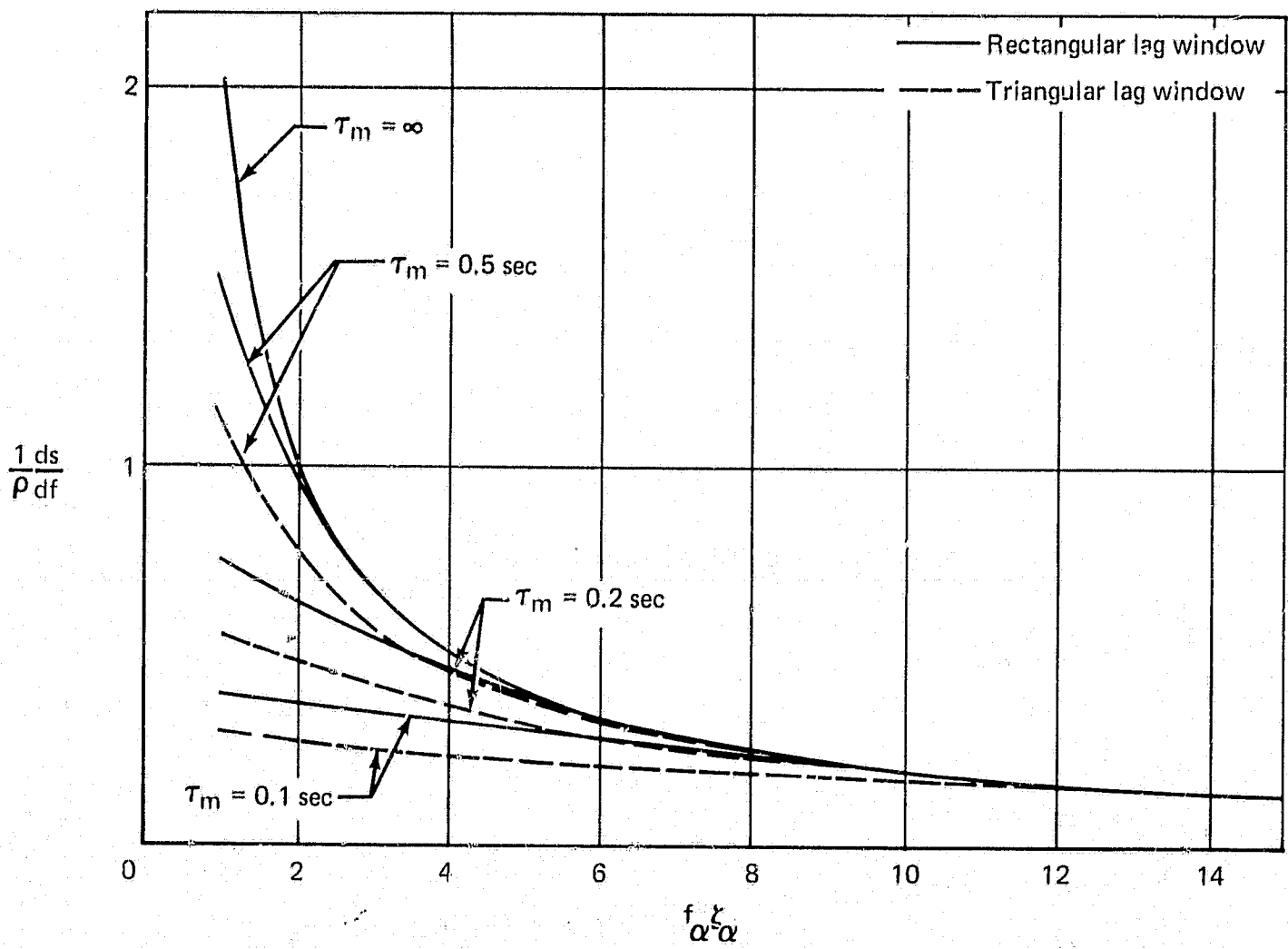
Figure 8.—Effect of Lag Window on Parameter $\frac{1}{\rho}\frac{ds}{df}$

$$\Psi(n) = \frac{1 - e^{-n\pi/2}\left(1 + n\pi/2 + \frac{1}{2}(n\pi/2)^2\right)}{1 - e^{-n\pi/2}(1 + n\pi/2)}$$

$$n = \Delta f_\alpha / \Delta f_F$$
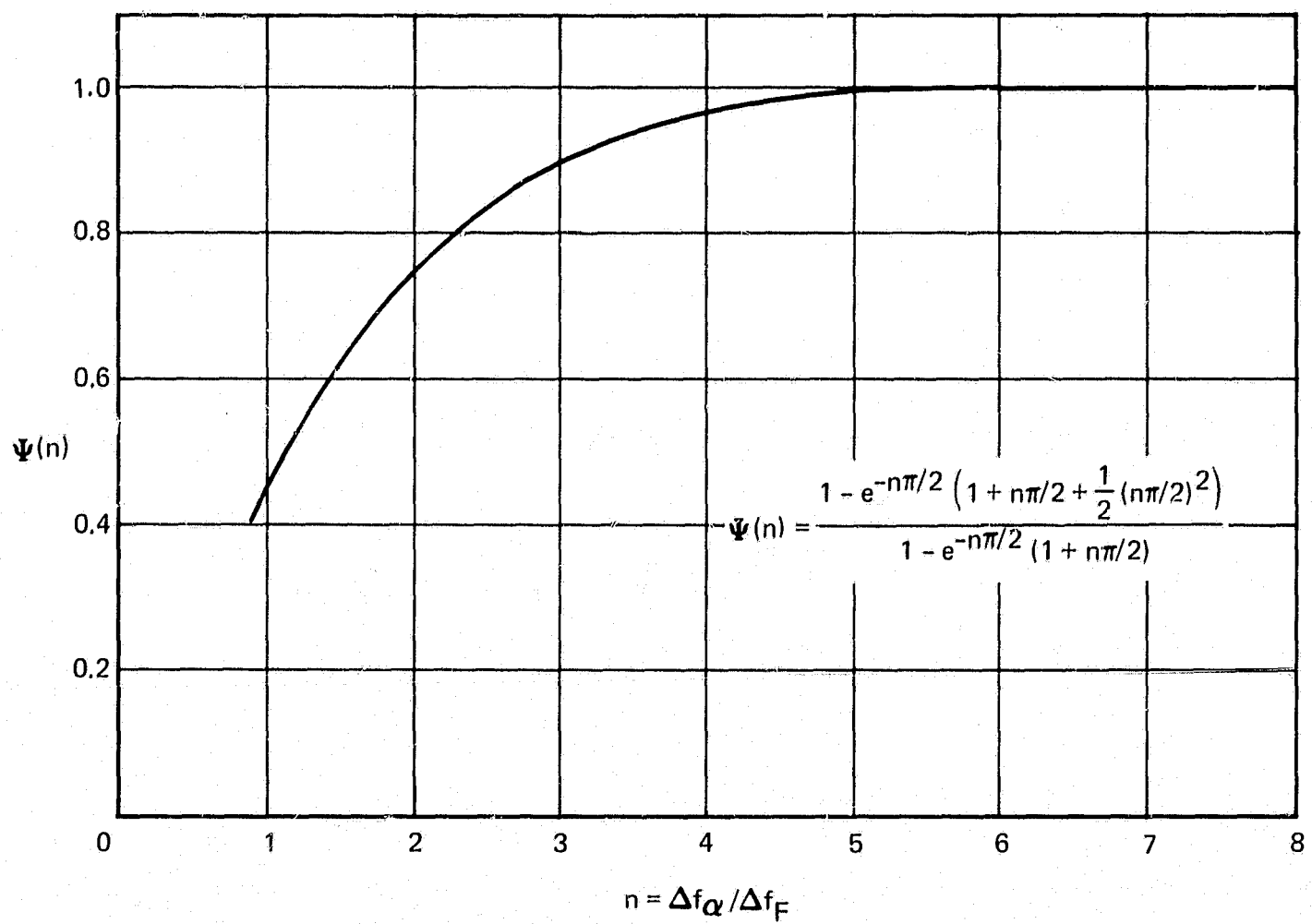
Figure 9.—Variation of $\Psi(n)$ With n

Displacement/
excitation/
driver voltage
signal

Recording system

Analog source tape

Step 1

Analog tape replay

A/D converter

Digital data tape

Step 2

Digital data tape

Data reduction
comments to SPECTRA

Computer software
SPECTRA

Digital computer
(CDC 6600)

Reduced data plots

Step 3

Reduced data (PSD, correlation, etc.) tape

Reduced data tape

Computer software
for SSFT

Digital computer
(CDC 6600)

SSFT plots

Step 4

Figure 10.—Flow Chart of Digital Data Reduction

94
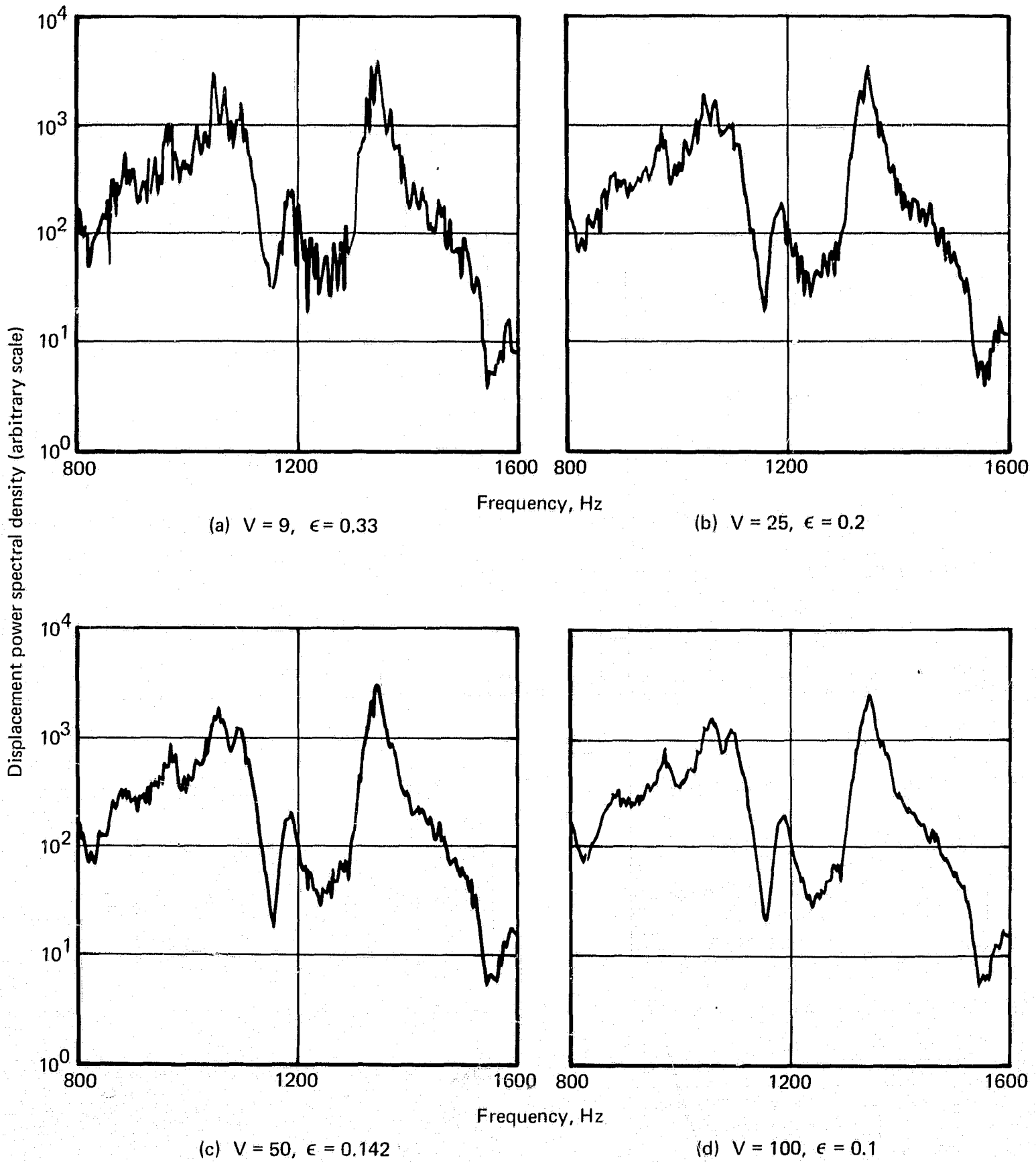
FIGURE 11.—EFFECT OF NUMBER OF SUBSPECTRA ON STATISTICAL SCATTER
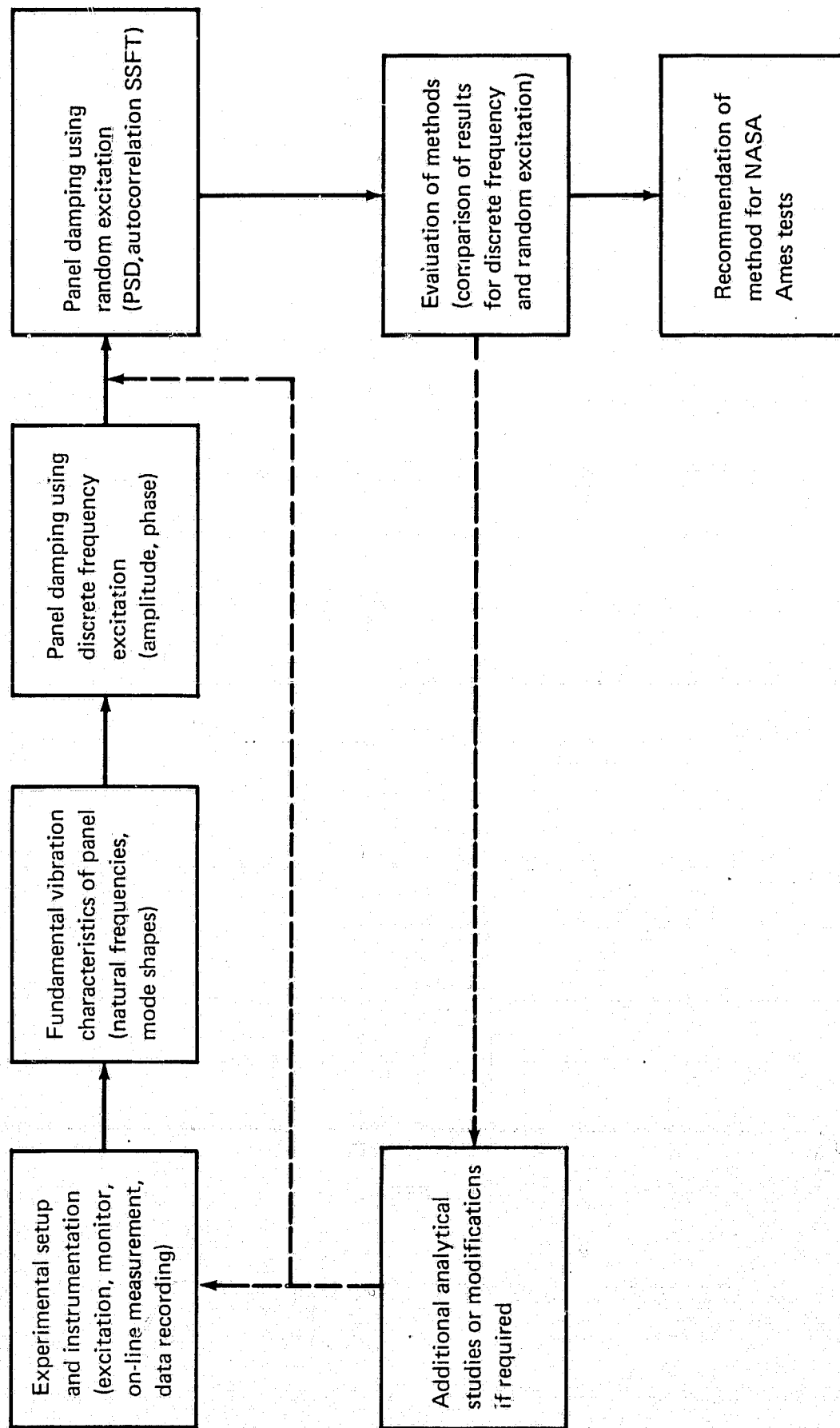
FIGURE 12.—WORK ELEMENTS AND FLOW CHART FOR DEMONSTRATION EXPERIMENTS
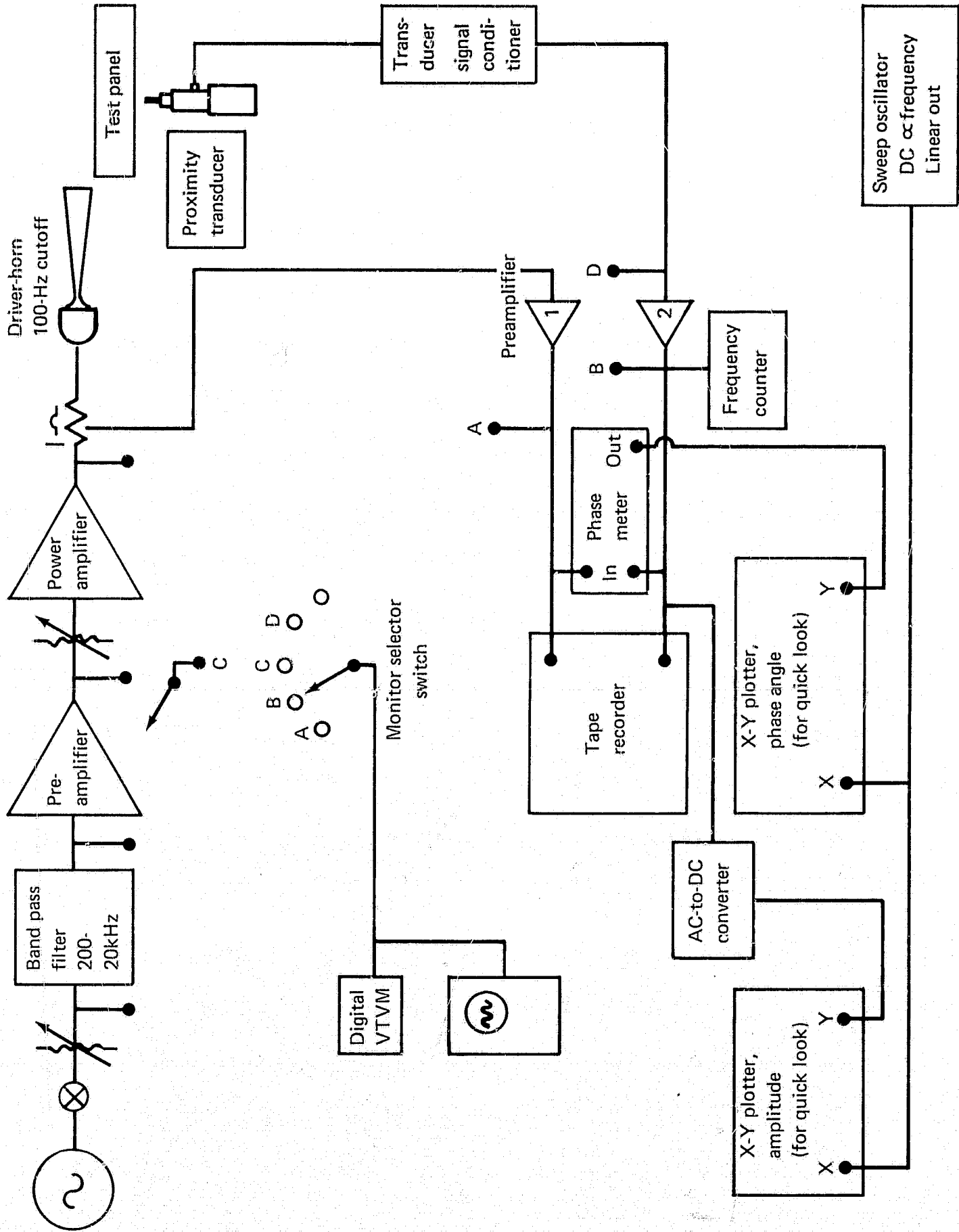
FIGURE 13.—SCHEMATIC OF EXPERIMENTAL SETUP AND INSTRUMENTATION
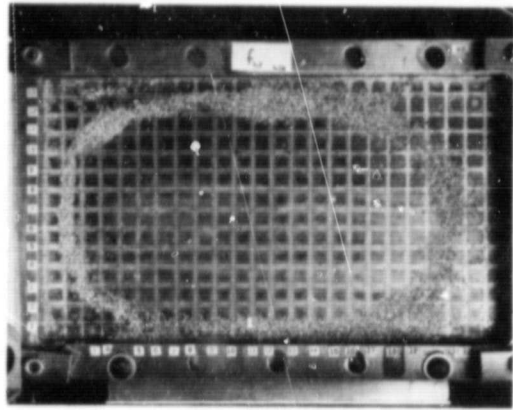
Mode (1,1)
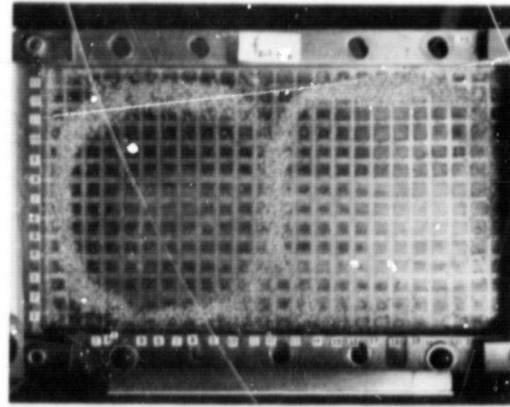
Mode (2,1)
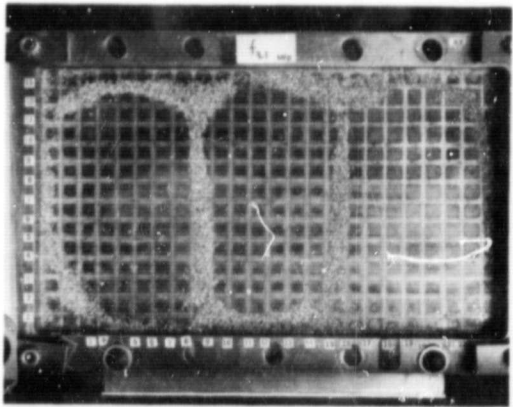
Mode (3,1)
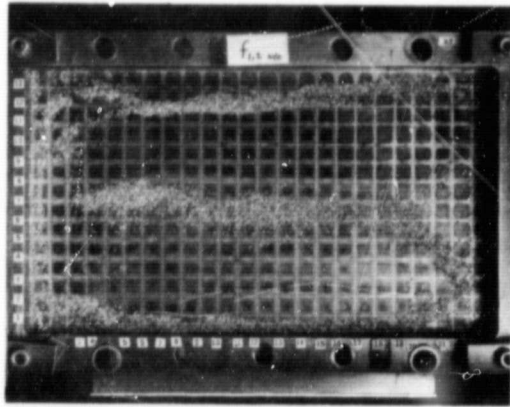
Mode (1,2)
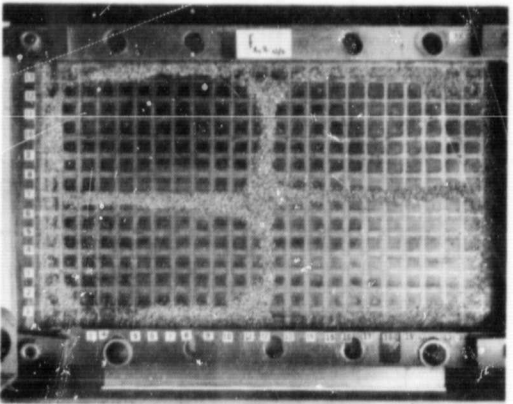
Mode (2,2)
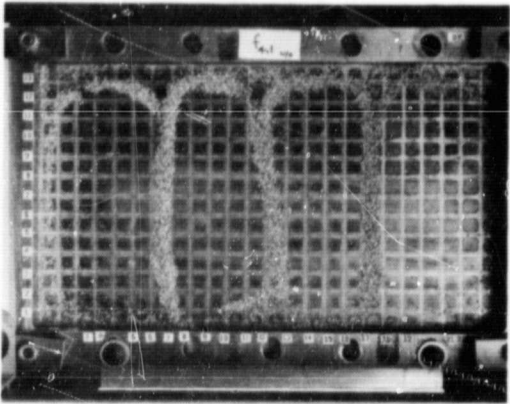
Mode (4,1)
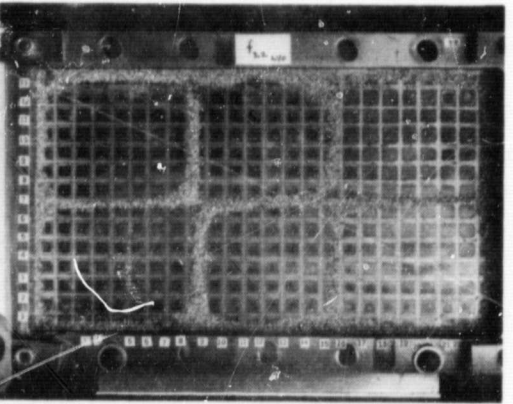
Mode (3,2)
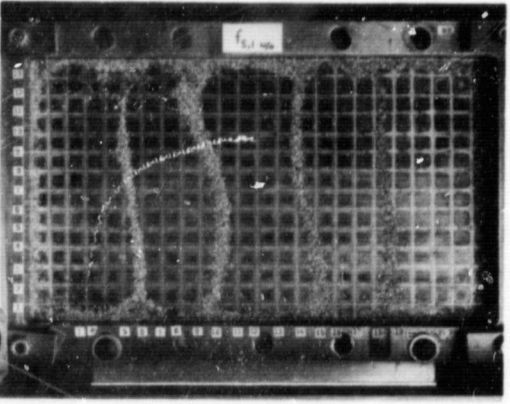
Mode (5,1)

FIGURE 14.—NODAL LINE PATTERNS FOR TEST PANEL
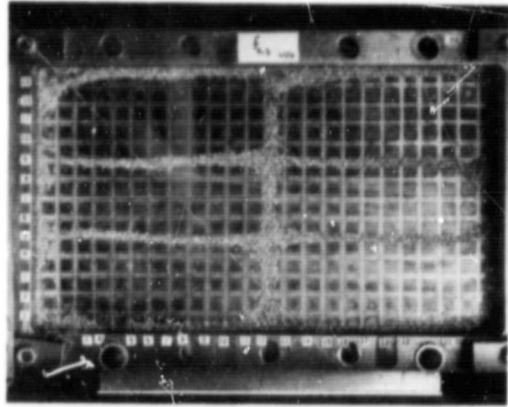
Mode (2,3)
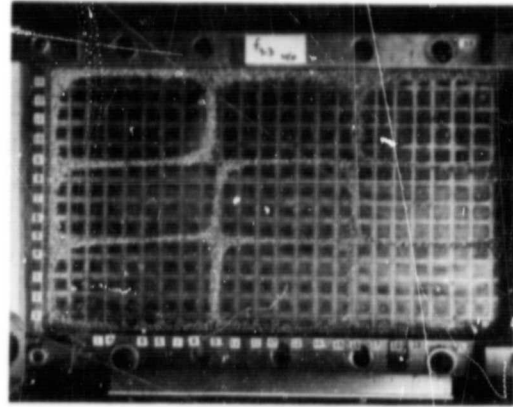
Mode (3,3)
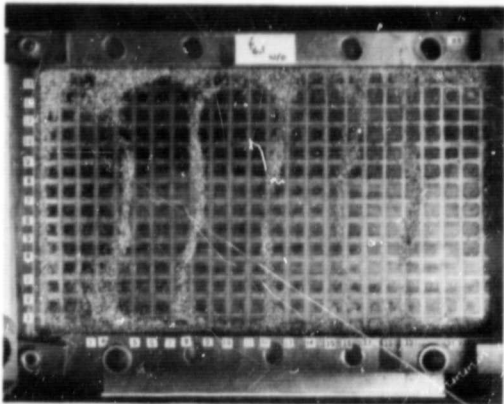
Mode (6,1)
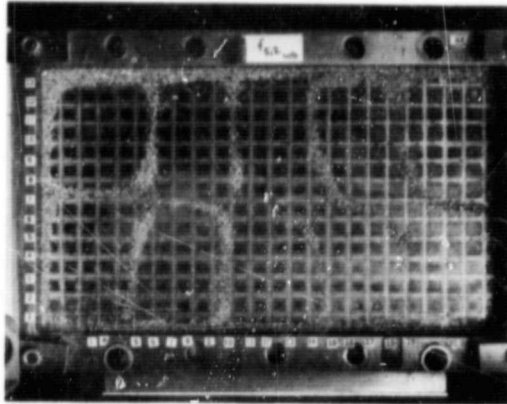
Mode (5,2)
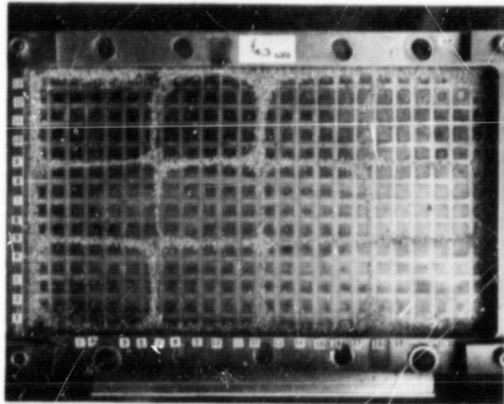
Mode (4,3)
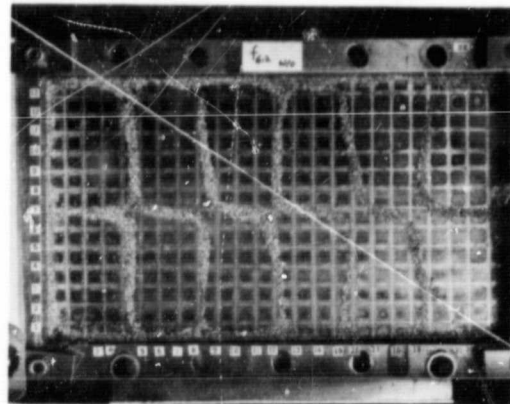
Mode (6,2)
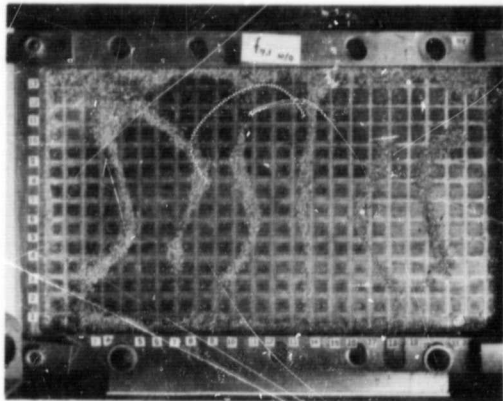
Mode (7,1)
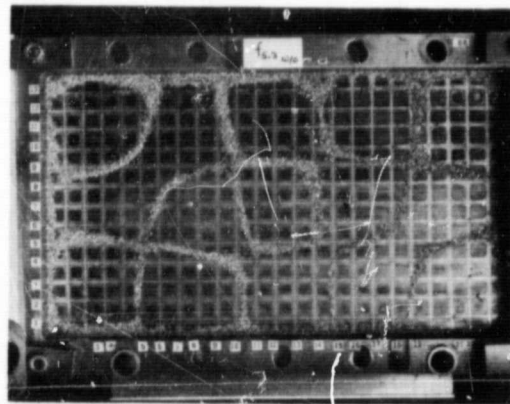
Mode (5,3)

FIGURE 14.—CONCLUDED
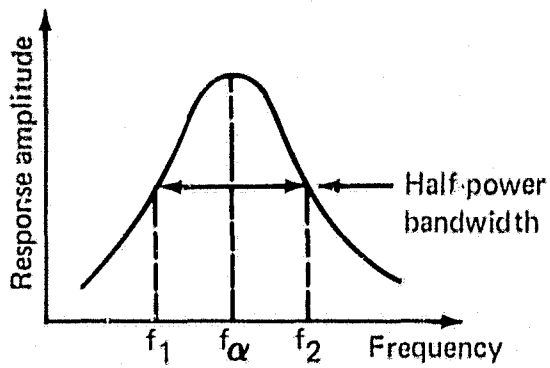
$$\zeta_\alpha = \frac{f_2 - f_1}{2f_\alpha}$$

(a) Response Amplitude Plot
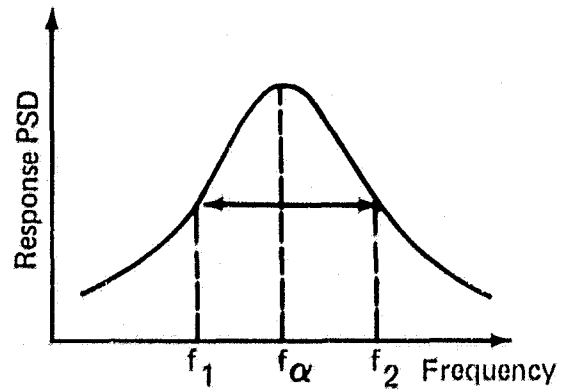
(d) Response PSD
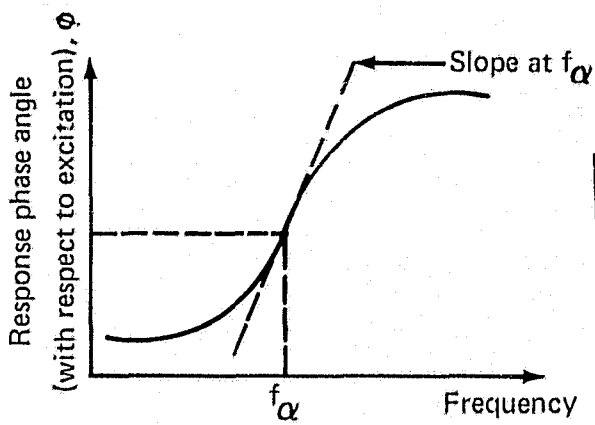
$$\zeta_\alpha = \frac{1}{f_\alpha \dfrac{\partial \alpha}{\partial f}\Big|_{\text{at } f_\alpha}}$$

(b) Phase Angle Plot
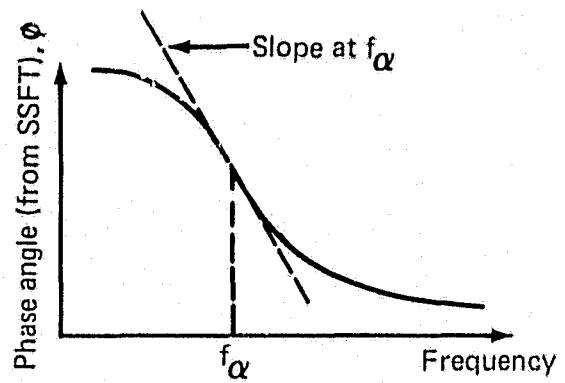
(e) Phase Angle Plot of SSFT
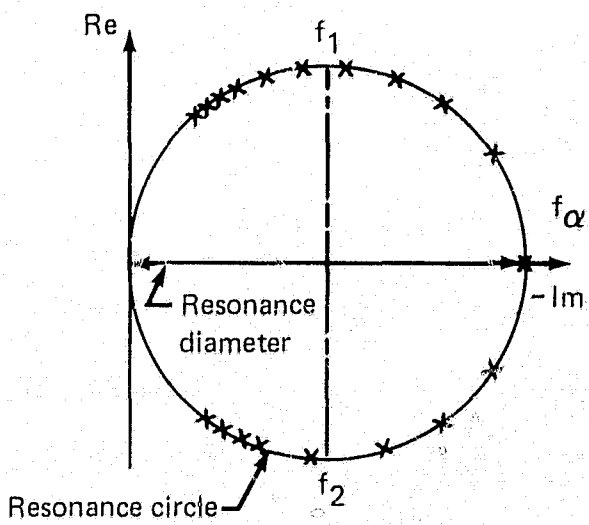
$$\zeta_\alpha = \frac{f_2 - f_1}{2f_\alpha}$$

(c) Kennedy-Pancu Vector Diagram
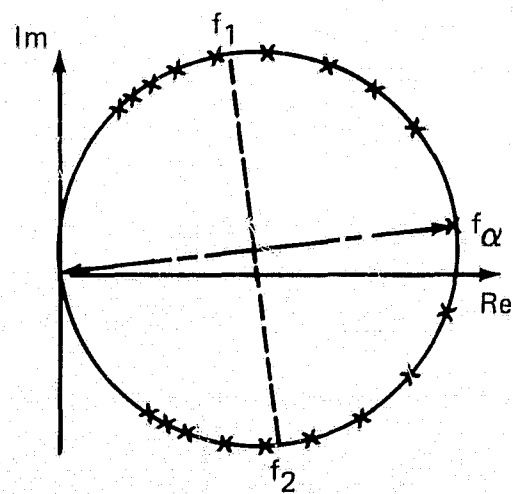
(f) Vector Diagram of SSFT

Figure 15.—Three Schemes for Calculating Damping Factor
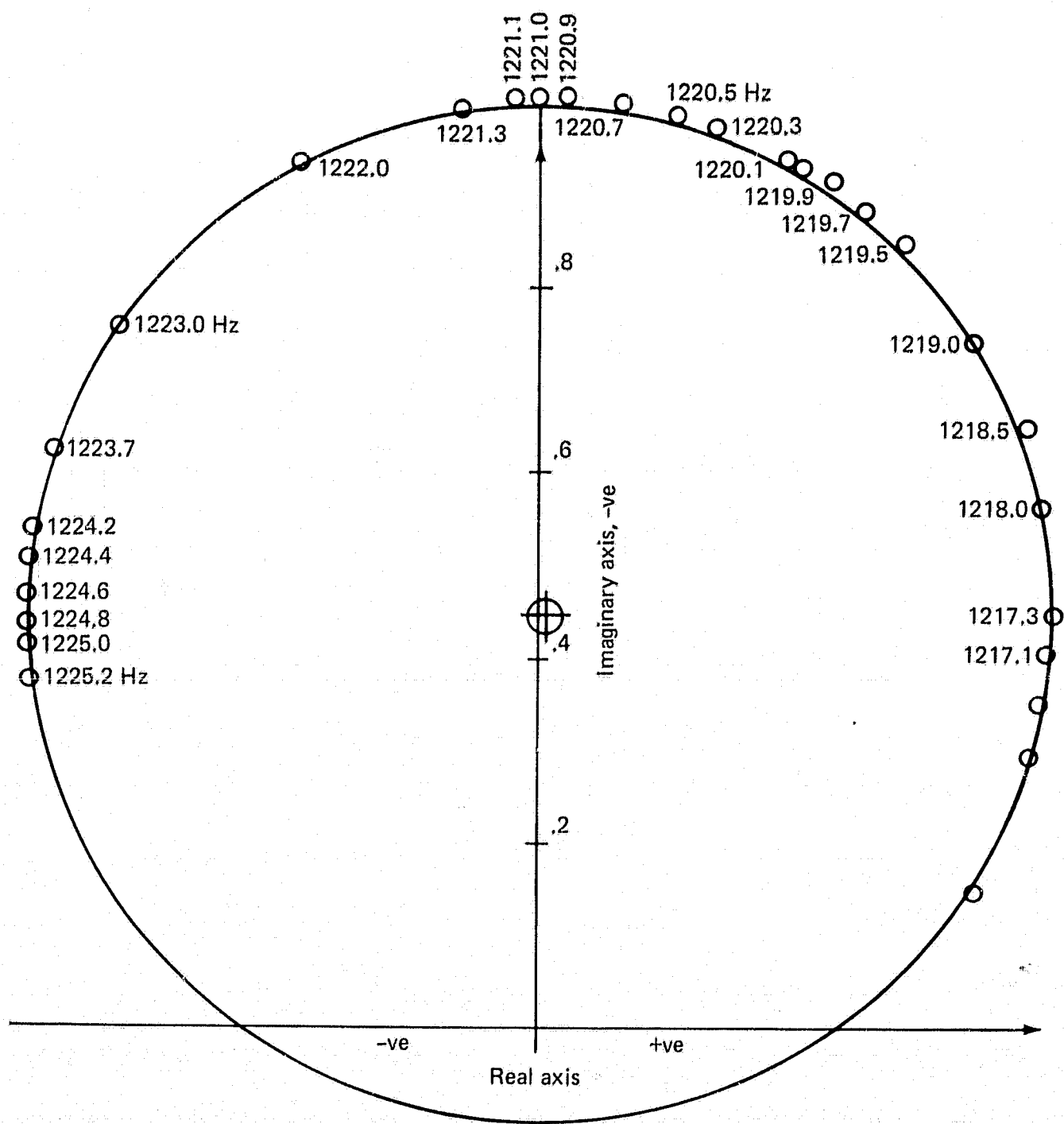
Figure 16.—Vector Diagram for Mode (2,3), Low Damping
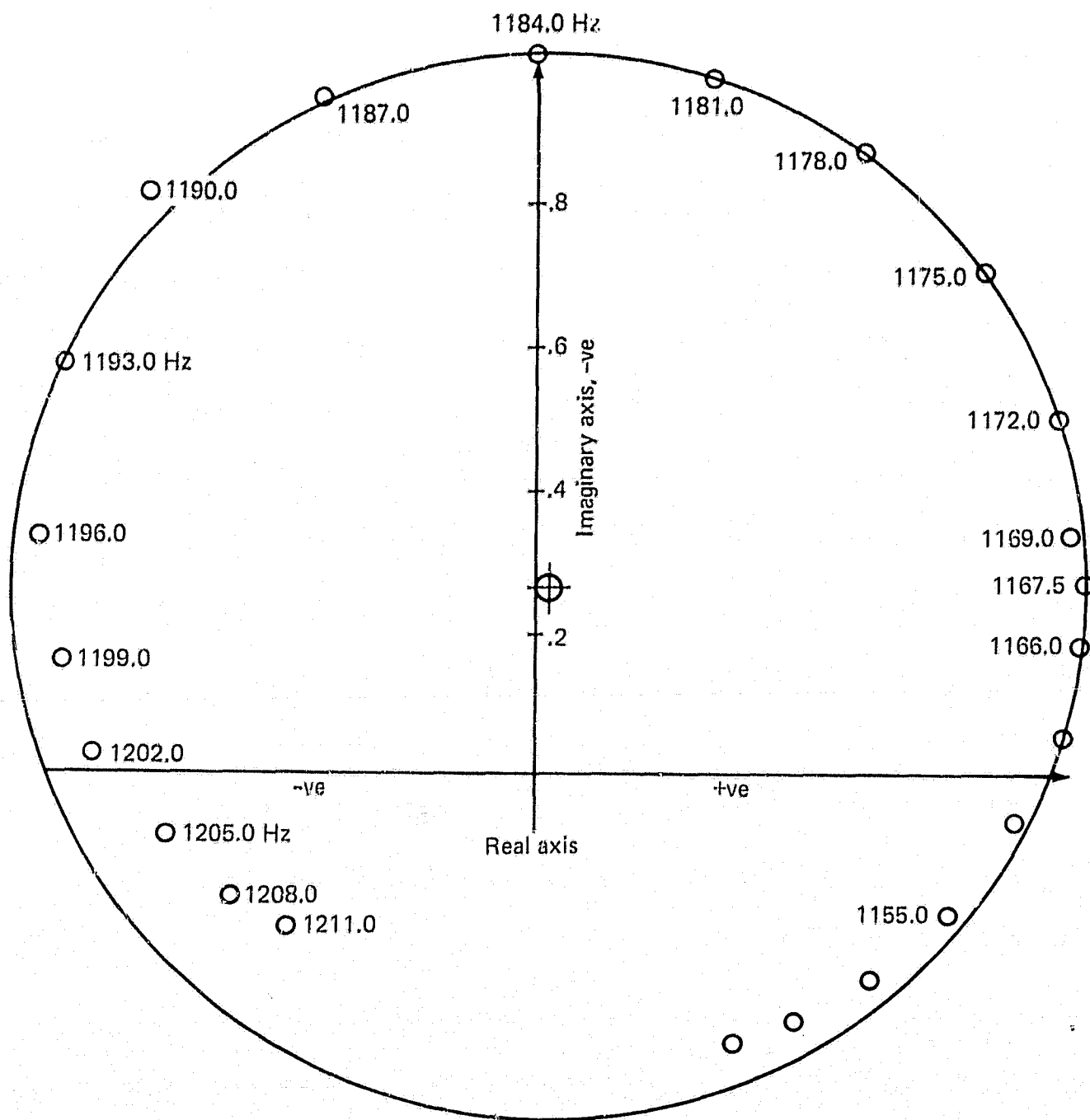
Figure 17.—Vector Diagram for Mode (2,3), High Damping
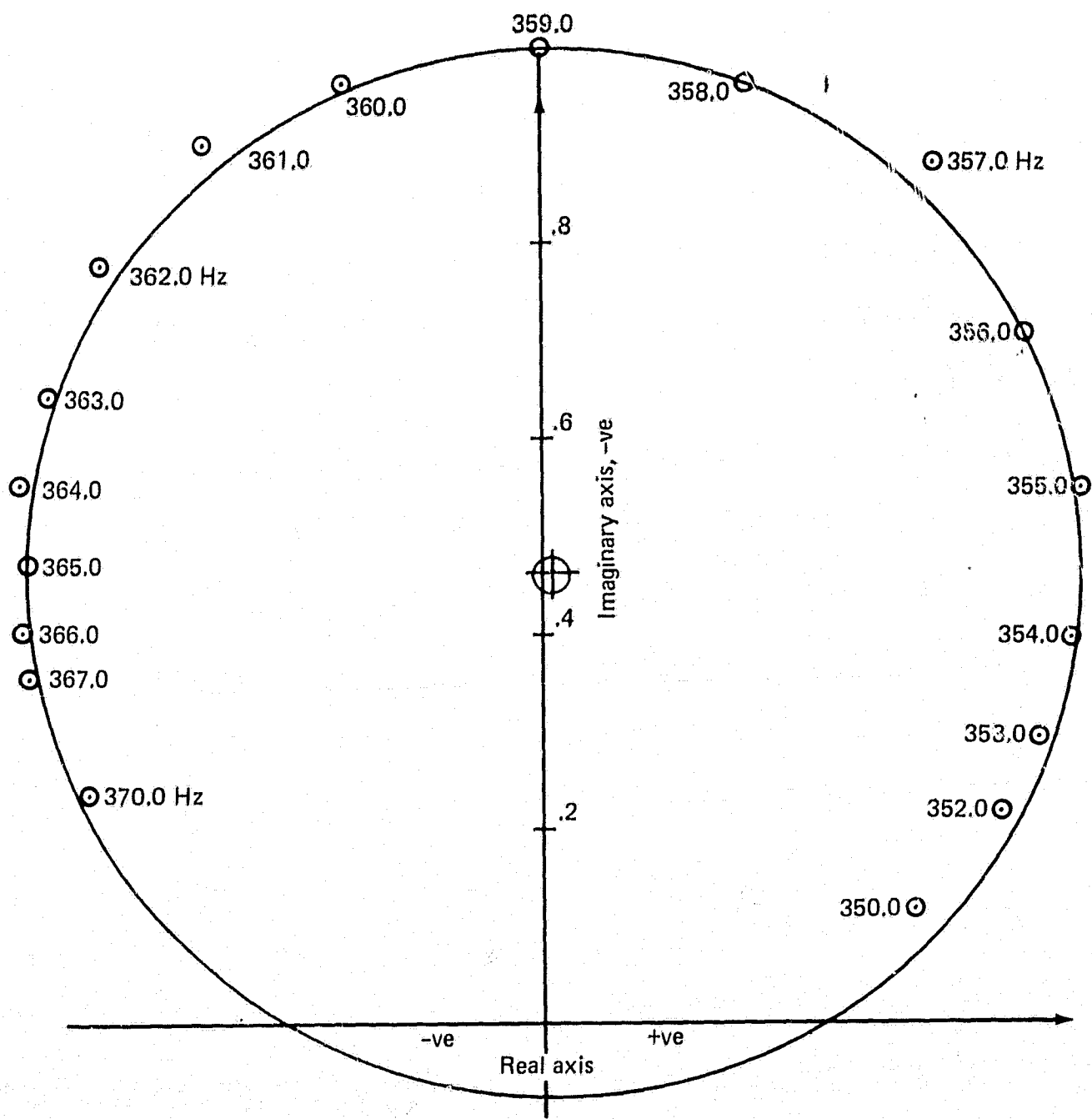
Figure 18.—Vector Diagram for Mode (2,1), High Damping
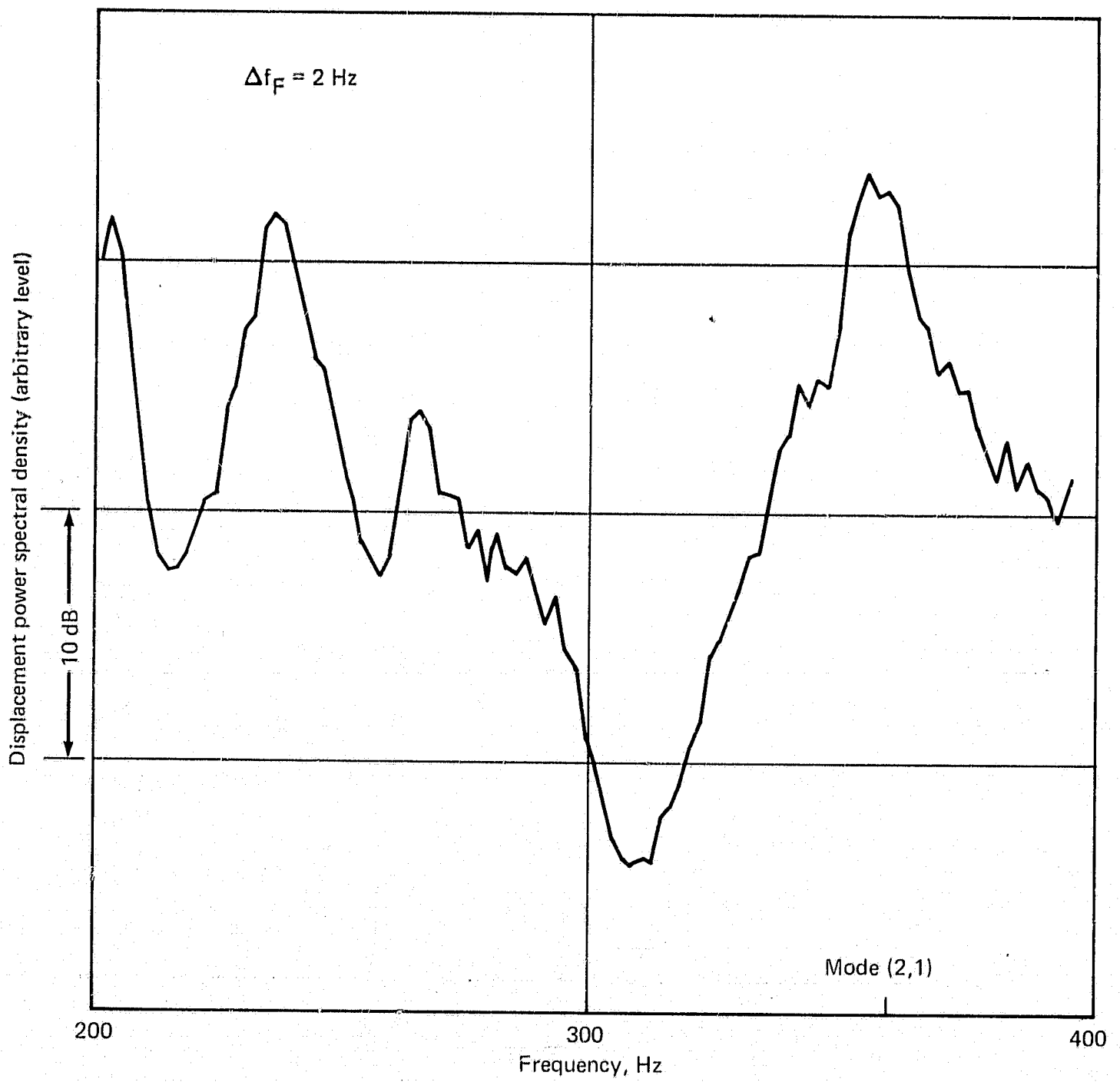
Figure 19.—Displacement Power Spectral Density for Run 2B, High Damping
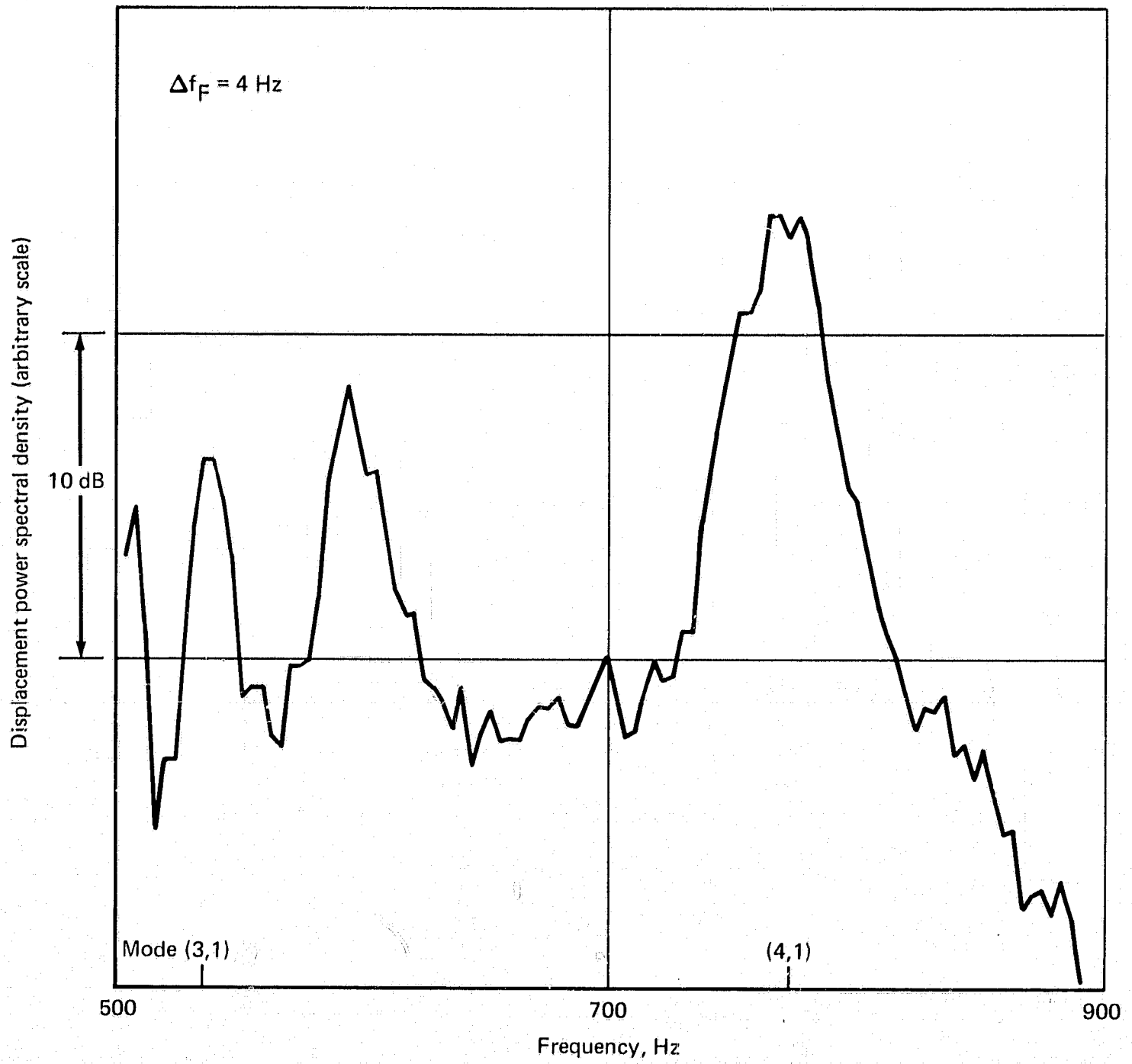
Figure 20.—Displacement Power Spectral Density for Run 4B, High Damping
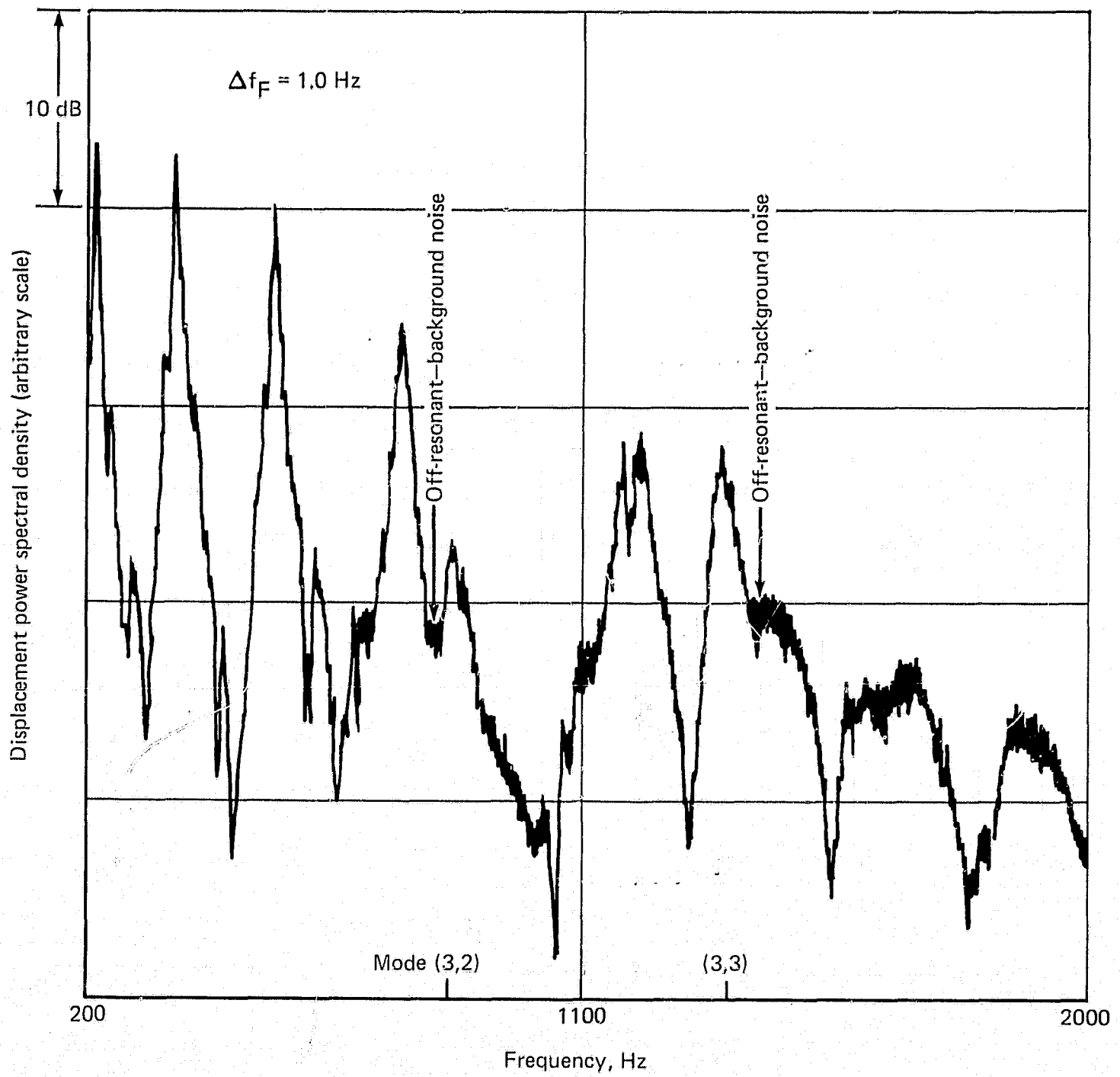
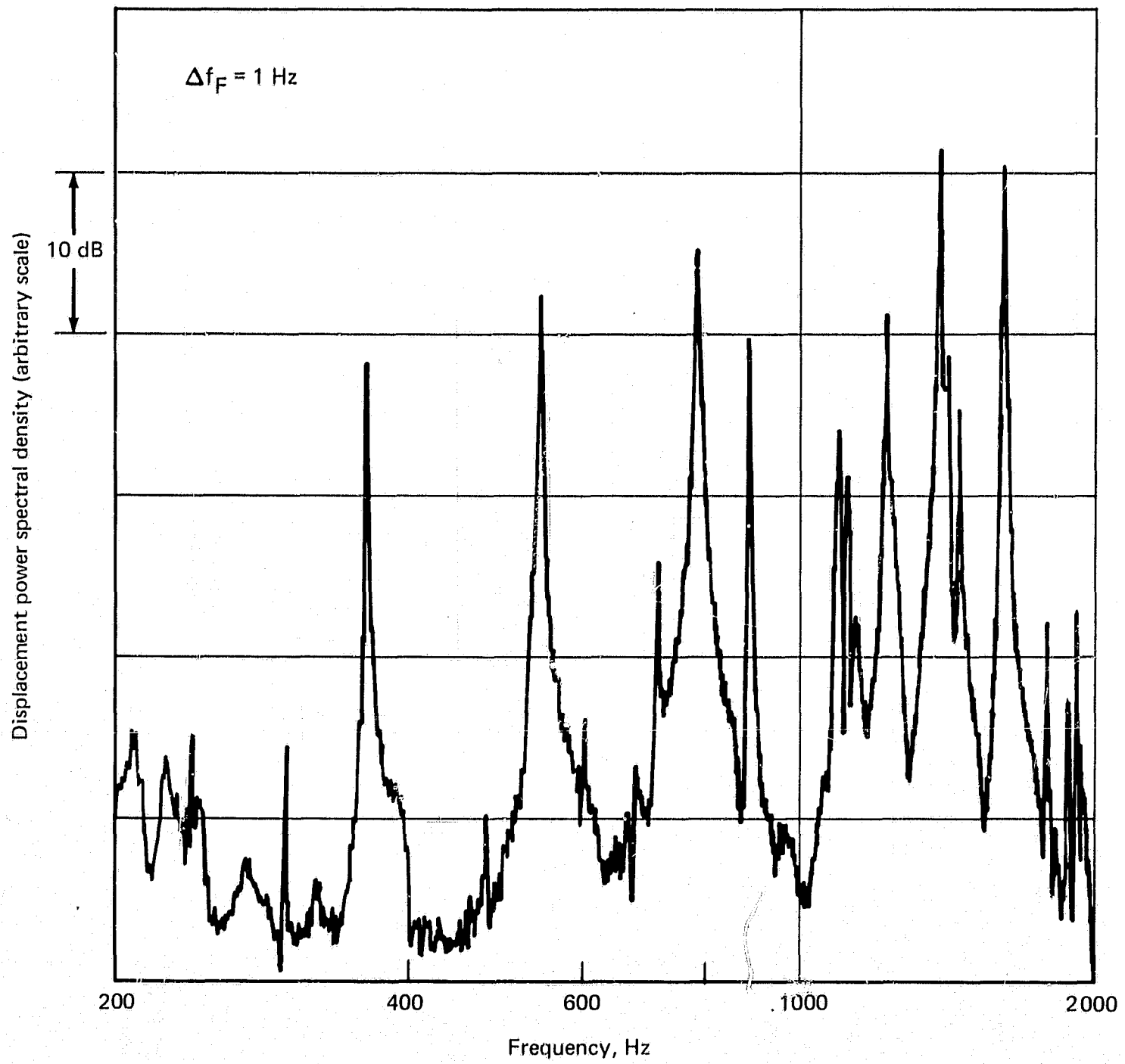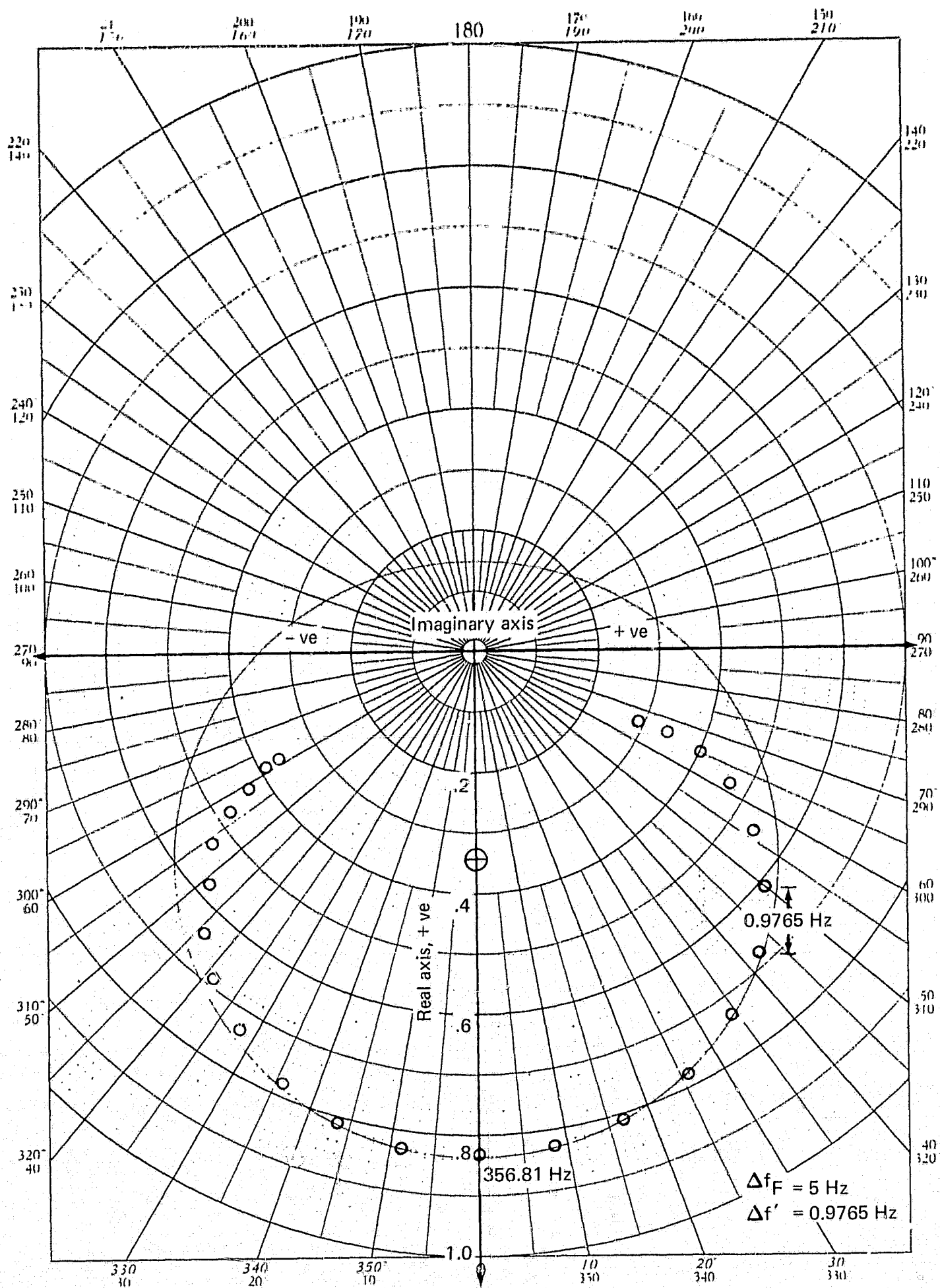Figure 21.—Displacement Power Spectral Density for Run 9B, High Damping
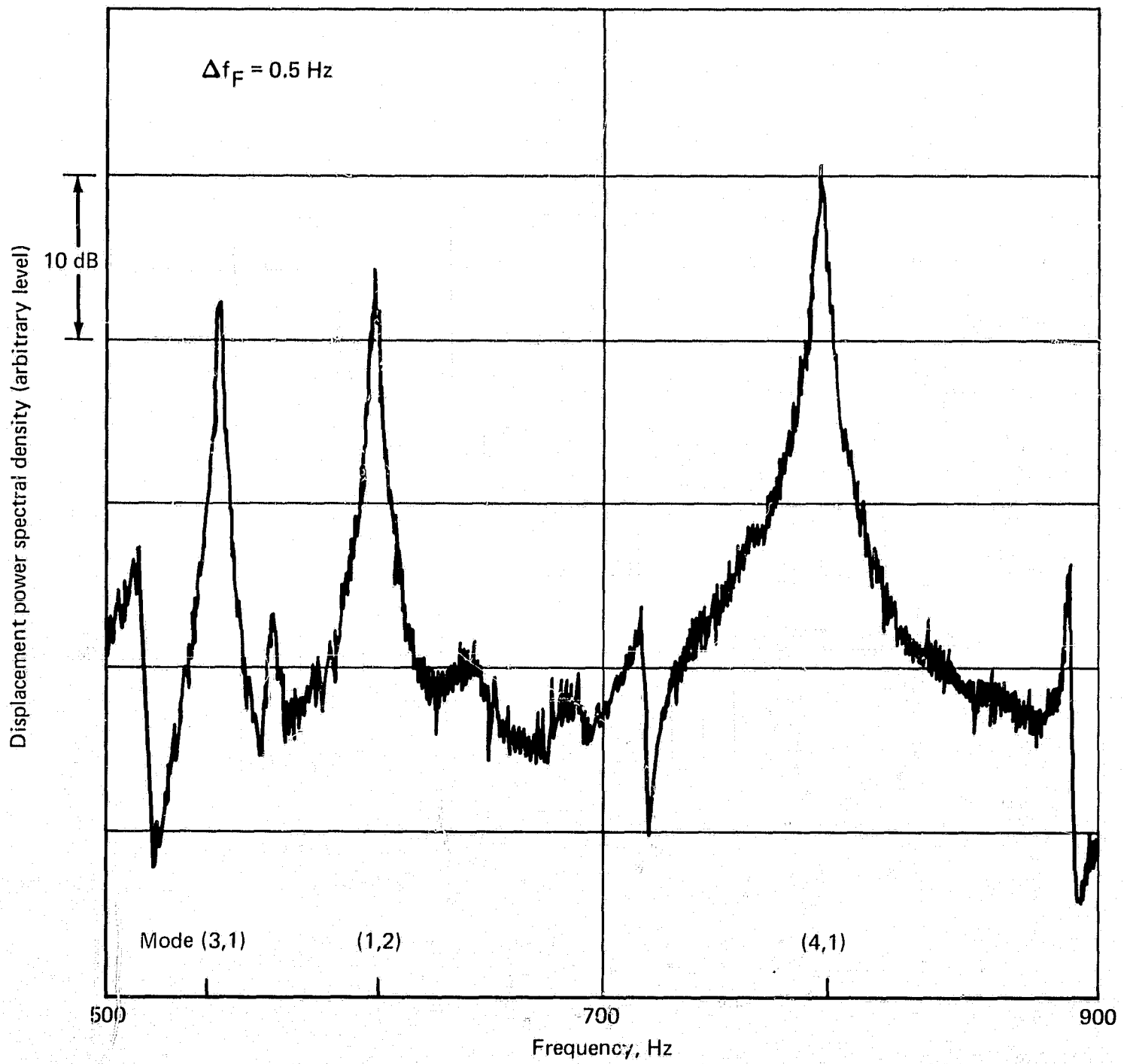
Figure 22.—Displacement Power Spectral Density for Run 4B, Low Damping
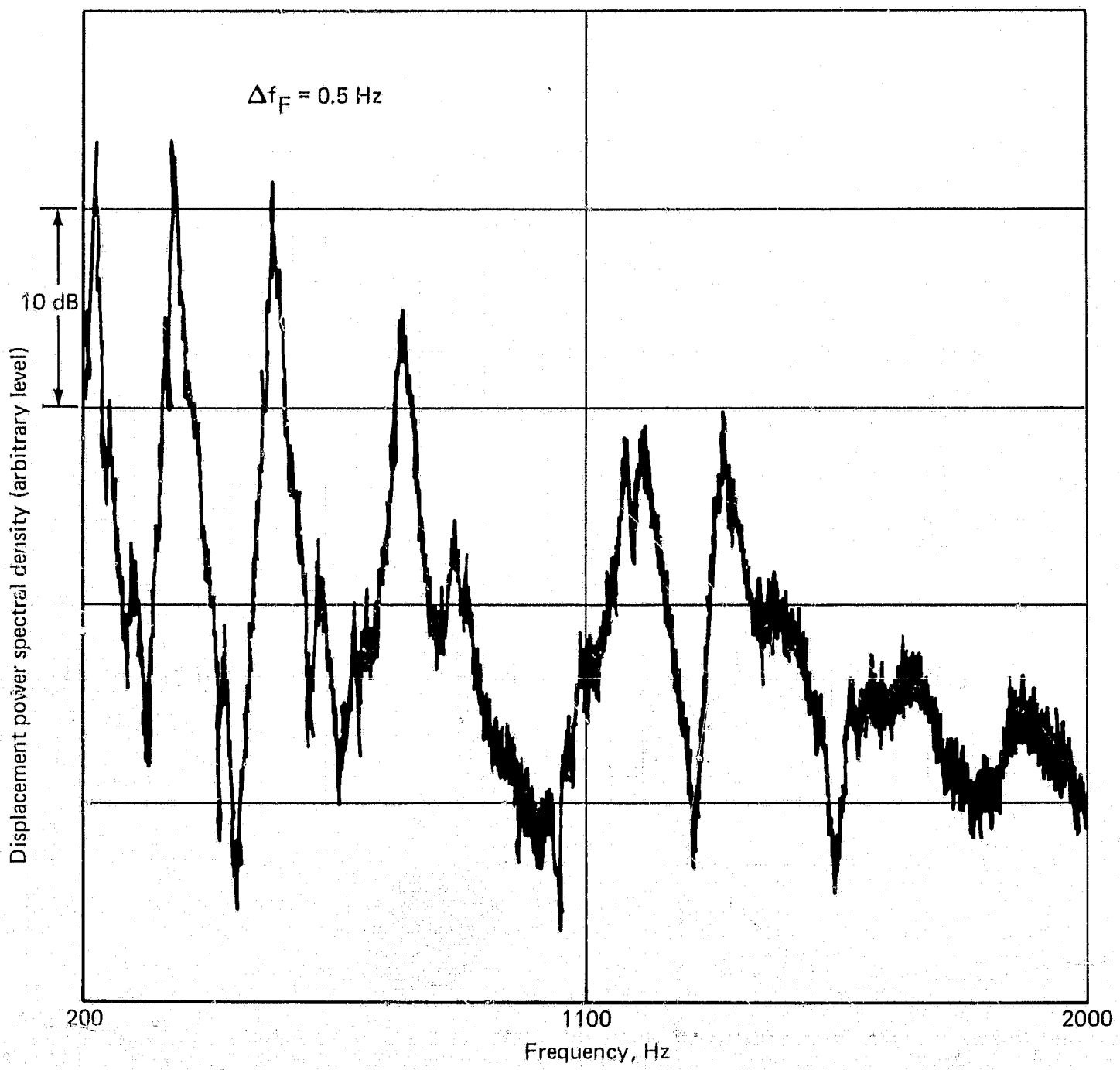
Figure 23.—Displacement Power Spectral Density for Run 9B, Low Damping

Figure 24.—Displacement Power Spectral Density for Run 8B, Low Damping

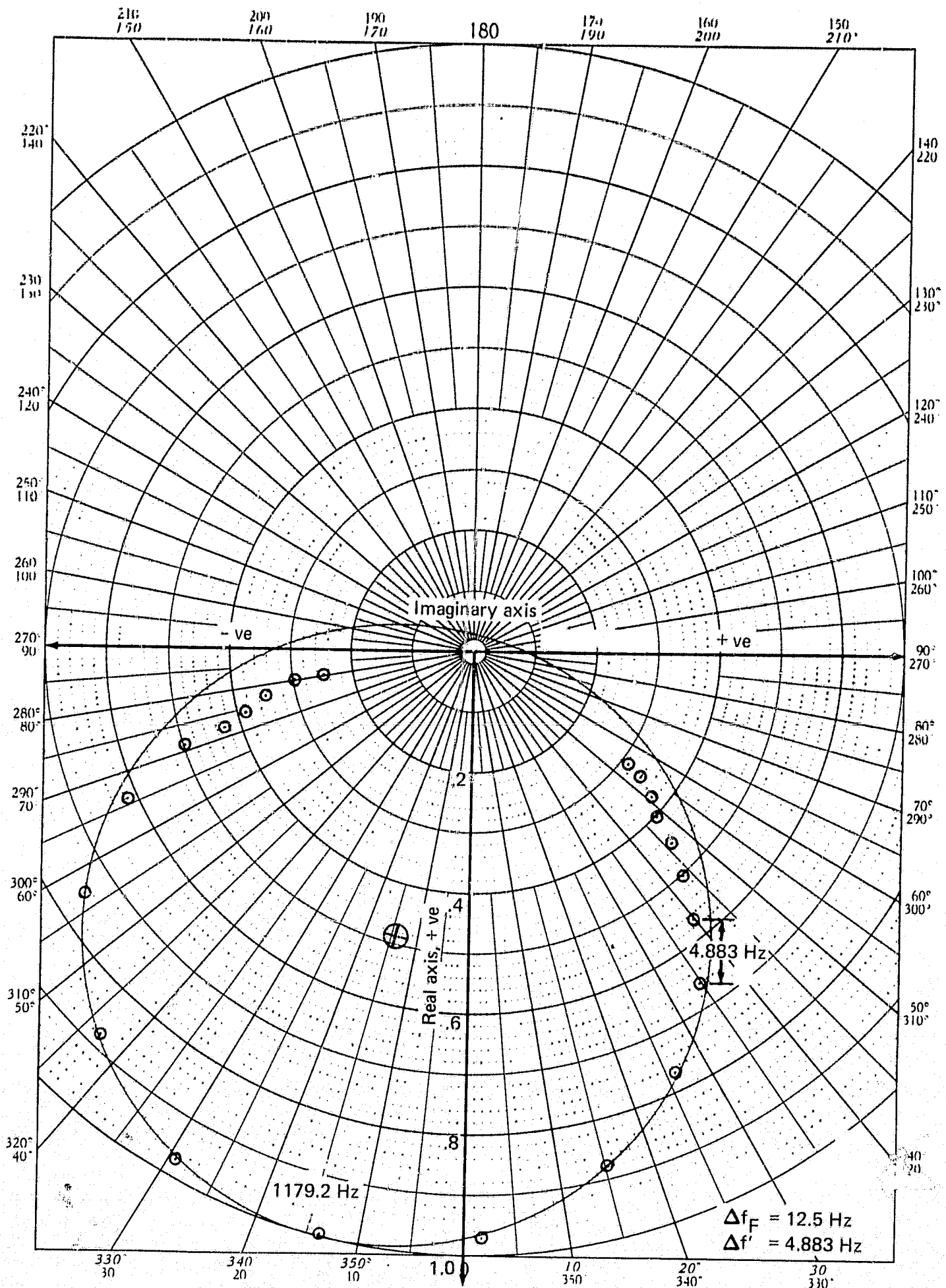Figure 25.—Vector Diagram of $F_W(\omega)$ for Mode (2,1), Run 9B, High Damping

110

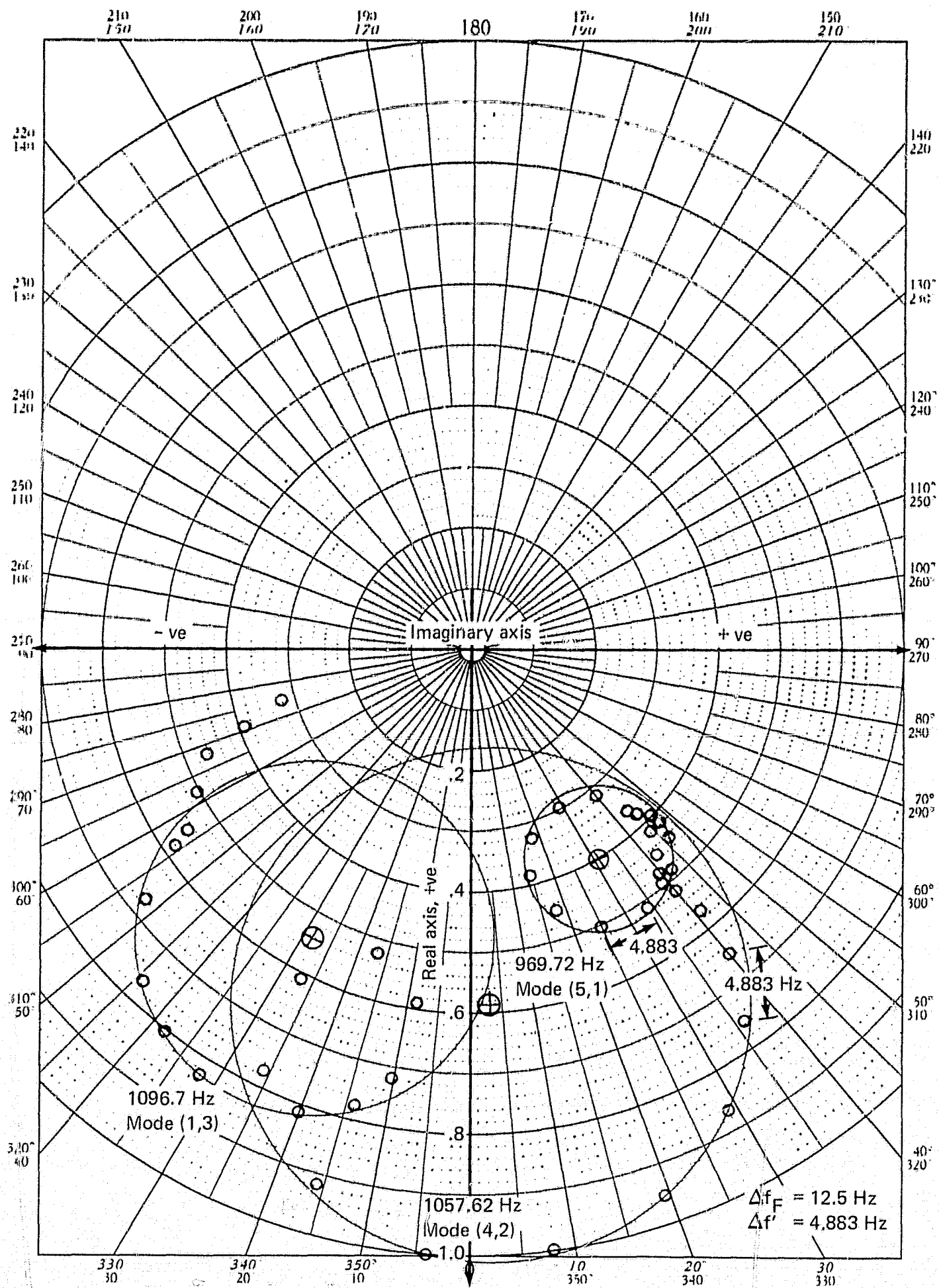Figure 26.—Vector Diagram of $F_w(\omega)$ for Mode (2,3), Run 7B, High Damping

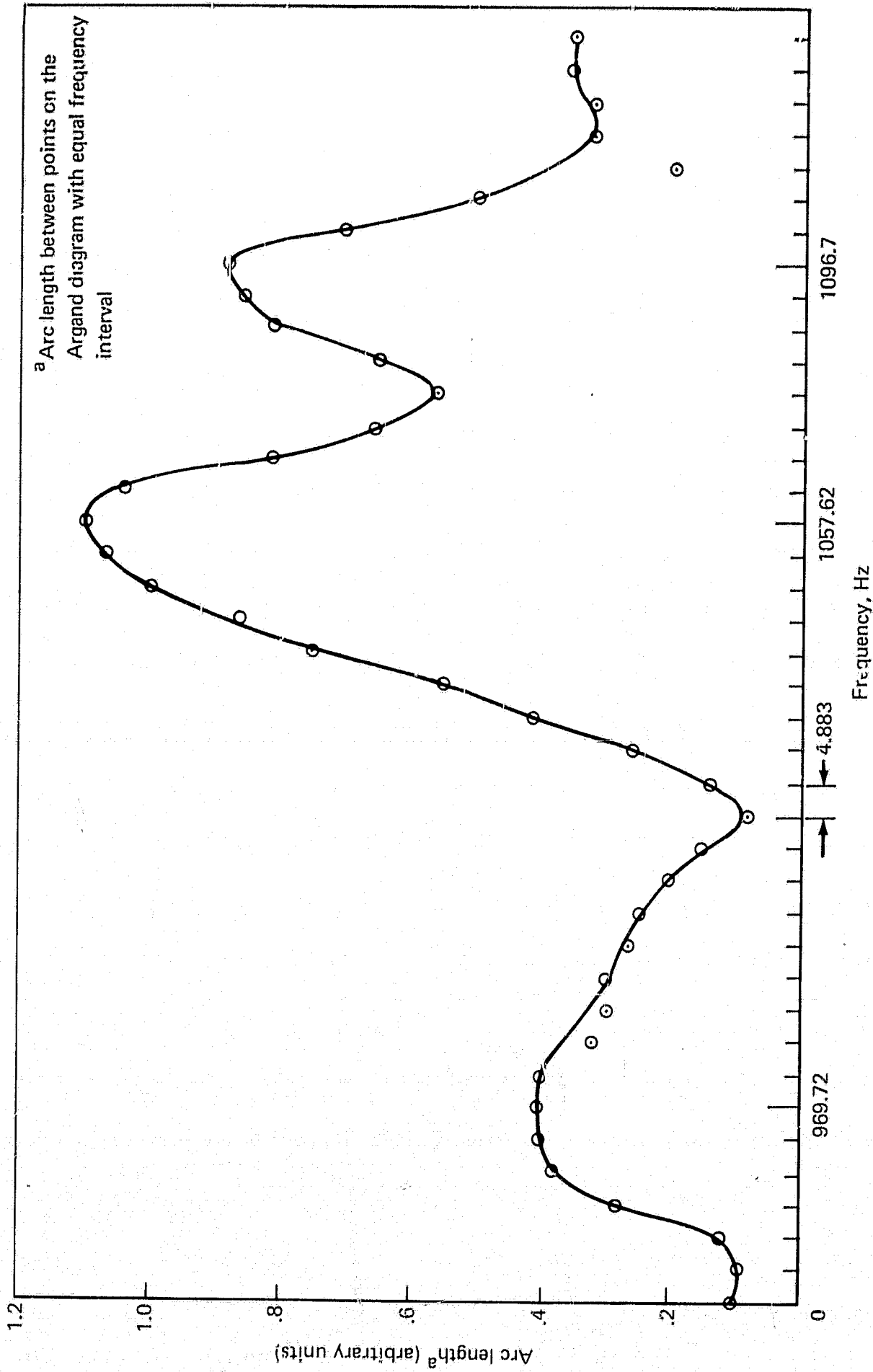Figure 27.—Vector Diagram of $F_w(\omega)$ for Modes (5,1), (4,2), and (1,3), Run 7A, High Damping

Figure 28.—Change in Arc Length With Frequency